TRANSIENT ANALYSIS OF SELF-EXCITED INDUCTION GENERATOR (SEIG) WITH ELECTRONIC LOAD CONTROLLER (ELC) SUPPLYING STATIC AND DYNAMIC LOADS

A DISSERTATION

Submitted in partial fulfillment of the
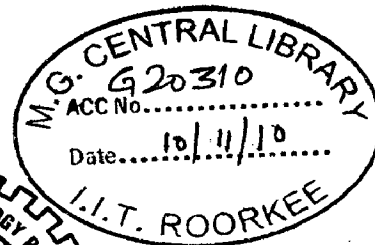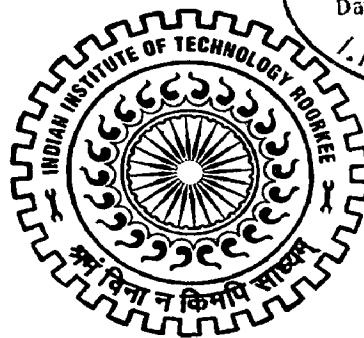*requirements for the award of the degree*
of
MASTER OF TECHNOLOGY
in
ALTERNATE HYDRO ENERGY SYSTEMS

By

ANURAG CHAUHAN

ALTERNATE HYDRO ENERGY CENTRE
INDIAN INSTITUTE OF TECHNOLOGY ROORKEE
ROORKEE-247 667 (INDIA)
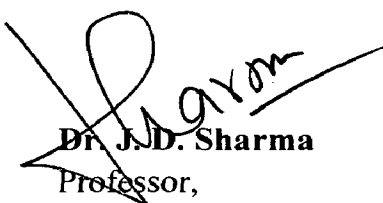JUNE, 2010

CANDIDATE'S DECLARATION

I hereby declare that the report which is being presented in this dissertation work "**TRANSIENT ANALYSIS OF SELF-EXCITED INDUCTION GENERATOR (SEIG) WITH ELECTRONIC LOAD CONTROLLER (ELC) SUPPLYING STATIC AND DYNAMIC LOADS**" in partial fulfillment of the requirements for the award of the degree of **Master of Technology** with specialization in **Alternate Hydro Energy Systems**, submitted in **Alternate Hydro Energy Centre, Indian Institute of Technology Roorkee** is an authentic record of my own work carried out during a period from July 2009 to June 2010 under the supervision of **Dr. J. D. Sharma**, Professor, Electrical Engg. Department, Indian Institute of Technology Roorkee and **Dr. D. K. Khatod**, Assistant Professor, Alternate Hydro Energy Centre, Indian Institute of Technology Roorkee.

I have not submitted the matter embodied in this report for the award of any other degree or diploma.

Date: 29 June, 2010   (ANURAG CHAUHAN)

This is to certify that the above statement made by the candidate is correct to the best of my knowledge.

Dr. J. D. Sharma   Dr. D. K. Khatod
Professor,   Assistant Professor,
Department of Electrical Engineering,   Alternate Hydro Energy Centre,
Indian Institute of Technology Roorkee,   Indian Institute of Technology Roorkee,
Roorkee-247667 (Uttarakhand)   Roorkee-247667 (Uttarakhand)

i

ABSTRACT

Small scale power generation near consumer's premises has received greater attention in recent years for use in remote and rural communities due to the cost and complexity involved in the grid extension. Thus, suitable stand-alone systems using locally available energy sources have become a preferred option. With increased emphasis on eco-friendly technologies the use of renewable sources such as small hydro, wind and biomass is being explored. Subject to availability, small hydro systems with minimal civil works to electrify local communities are considered as an attractive option.

This report focuses on transient analysis of three phase self-excited induction generator (SEIG) with electronic load controller (ELC). All components of the considered system are modeled and simulated for transient analysis of the system. This transient analysis includes process of self-excitation, voltage build up, faults, unbalanced loading, unbalanced excitation and switching of resistive and dynamic loads. The performed study may help in determining insulation strength, suitability of winding, shaft strength, value of capacitor and devising the protection strategy for the SEIG. This system stability can further be extended to interconnected system with necessary modifications in mathematical modelling.

ACKNOWLEDGEMENT

I would like to express my sincere gratitude to my supervisors **Dr. J. D. Sharma**, Professor, Department of Electrical Engineering, Indian Institute of Technology, Roorkee and **Dr. D. K. Khatod**, Assistant Professor, AHEC, Indian Institute of Technology, Roorkee for their valuable guidance, support, encouragement and immense help.

I also express my deep and sincere sense of gratitude to Dr. Arun Kumar, Head, AHEC, Indian Institute of Technology, Roorkee for his motivation and full cooperation during the work of dissertation.

I am also grateful to all faculty members and staff of Alternate Hydro Energy Centre, Indian Institute of Technology, Roorkee.

I extend my thanks to all my friends who have helped directly or indirectly for the completion of this dissertation.

Finally, I would like to express my deepest gratitude to the Almighty for showering blessings on me. I gratefully acknowledge my heartiest thanks to all my family members for their inspirational impetus and moral support during the course of work.

Date:2 9June, 2010

(ANURAG CHAUHAN)

TABLE OF CONTENTS

NOTATIONS USED

v	Direct and quadrature axis voltage matrix of SEIG
i	Direct and quadrature axis current matrix of SEIG
R	Stator and rotor resistance diagonal matrix of SEIG
L	Inductance matrix of SEIG
G	Speed inductance matrix of SEIG
v_{ds}	Direct axis component of stator voltage
v_{qs}	Quadrature axis component of stator voltage
v_{dr}	Direct axis component of rotor voltage
v_{qr}	Quadrature axis component of rotor voltage
i_{ds}	Direct axis component of stator current
i_{qs}	Quadrature axis component of stator current
i_{dr}	Direct axis component of rotor current
i_{qr}	Quadrature axis component of rotor current
I_m	Magnetizing current
R_s	Stator resistance
R_r	Rotor resistance
L_{ss}	Stator self inductance
L_{rr}	Rotor self inductance
L_m	Mutual inductance
P	Number of poles of SEIG
ω_g	Rotor speed of SEIG
T_e	Electromagnetic torque of SEIG
T_{shaft}	Input torque
J	Moment of inertia of SEIG
p	$\left[\dfrac{d}{dt}\right]$
i_{ga}, i_{gb}, i_{gc}	Line currents of induction generator
i_a, i_b, i_c	Phase currents of induction generator

v_a, v_b, v_c	Voltages at induction generator terminals
C_a, C_b, C_c	Values of delta connected capacitors
i_{ca}, i_{cb}, i_{cc}	Line currents of capacitor bank
i_{aL}, i_{bL}, i_{cL}	Line currents of load
i_{Da}, i_{Db}, i_{Dc}	Line currents of dump load
v_M	Direct and quadrature axis voltage matrix of induction motor load
i_M	Direct and quadrature axis current matrix of induction motor load
R_M	Stator and rotor resistance diagonal matrix of induction motor load
L_M	Inductance matrix of induction motor load
G_M	Speed inductance matrix of induction motor load
ω_M	Rotor speed of induction motor load
T_{eM}	Electromagnetic torque of induction motor load
T_L	Load torque
J_M	Moment of inertia of induction motor load
P_M	Number of poles of induction motor load
L_{mM}	Mutual inductance of induction motor load
$_{dsM}$	Direct axis component of stator voltage of induction motor load
i_{qsM}	Quadrature axis component of stator voltage of induction motor load
i_{drM}	Direct axis component of rotor current of induction motor load
i_{qrM}	Quadrature axis component of rotor current of induction motor load
R_{La}, R_{Lb}, R_{Lc}	Value of resistances of three phase resistive load

LIST OF FIGURES

LIST OF TABLES

1.1   GENERAL

The increasing concern for the environment and fast depletion of fossil fuels have motivated the world towards rationalizing the use of conventional energy resources and exploring the non-conventional energy sources like wind, biomass, solar and small hydro to meet the ever-increasing energy demand. Mini/Micro/Small hydro schemes can easily be developed for power generation in hilly areas having perennial sources of water and can be catered to meet the electricity demand of the nearby villages. Such schemes generally employ self-excited induction generator (SEIG) with electronic load controller (ELC). Hence, the idea of studying a mini/micro hydro system in isolated configuration has mooted out. This may necessarily help in providing better operation and control of isolated mini/micro hydro plants [1].

1.2   SMALL HYDRO POWER

Among various renewable energy sources, small hydro is considered as an attractive option due to minimum civil works, short gestation period and inexpensive operation and maintenance. An estimated potential of about more 15,000 MW of small hydro power (SHP) projects exists in India [2]. World installed capacity of small hydro today is around 50,000 MW against an estimated potential of 180,000 MW. A general scenario of small hydro installed capacity worldwide is shown in Table 1.1.

Table 1.1: Small Hydro Installed Capacity Worldwide [2]

COUNTRY	INSTALLED CAPACITY (MW)
India	2,181
Japan	3,900
China	15,000
Rest of Asia	400
Europe	9,000
Rest of the world	20,000
Total	**50,000**

Table 1.2: International Definition of Small Hydro [3]

COUNTRY	PLANT CAPACITY (MW)
UK (NFFO)	Less than 5
UNIDO	< 10
Sweden	<15
Colombia	<20
Australia	<20
India	<25
China	<25
United States	<30
Brazil	<30
Philippines	<50
New Zealand	<50

There is a general tendency all over the world to define small hydro by power output. Different Countries have different norms keeping the upper limit ranging from 5 to 50 MW as shown in Table 1.2. In India, small hydro schemes are further classified on the basis of station capacity as shown in Table 1.3. A classification of SHP on the basis of head is presented in Table 1.4.

Table 1.3: Classification of Small Hydro Schemes [3]

TYPE	STATION CAPACITY	UNIT CAPACITY
Micro Hydro	Up to 100 kW	Up to 100 kW
Mini Hydro	101 kW to 2000 kW	101 kW to 1000 kW
Small Hydro	2001 kW to 25000 kW	1001 kW to 5000 kW

Table 1.4 Classification of SHP based on head [3]

TYPE	HEAD
Ultra Low Head	Below 3 m
Low Head	3 to 40 m
Medium/ High Head	Above 40 m

Micro hydro is the subset of small hydro with capacity up to 100 kW [3]. There is huge potential available in the micro hydro range ready to be harnessed. The current concern on the global environment has imposed a new constraint on the production of electricity. The emphasis is put on the development of environmental friendly form of

2

energy to promote the sustainable social development. In these circumstances, Micro hydro is an answer to the rural electrification in the remote, hilly and unelectrified areas where potential exists. A rural population is scattered and unaware of the technological developments. For such areas, the isolated micro-hydro power plants are the least cost options for electricity supply because the other options such as grid extension, diesel power etc. are more expensive and complex.

1.3 INDUCTION GENERATOR

Induction machine (IM) is quite popular with isolated micro-hydro power plants. It is a singly-excited ac machine. Stator winding of a 3-phase IM is connected to a 3-phase ac source and rotor winding receives its energy from stator by means of electro-magnetic induction. Balanced 3-phase currents in 3-phase stator winding produce a rotating magneto motive force (m.m.f.) of constant amplitude. Both the m.m.f. waves and produced by stator and rotor rotate in the air gap in the same direction at synchronous speed. These two m.m.f. waves are thus stationary with respect to each other. Consequently, the steady electromagnetic torque is developed. Based on the slip value, an IM works in motor and generator mode as:

a) In motoring mode (0 < slip < 1), rotor rotates in the direction of rotating field produced by the stator currents. The slip varies from '1' at stand still to '0' at synchronous speed.

b) In generating mode (-1 < slip < 0), stator terminals are connected to a constant frequency voltage source and rotor is driven at above synchronous speed by a prime mover.

The induction generator (IG) has very similar construction as induction motor with some possible improvements in efficiency. As the speed during induction generator operation is not synchronous, it is also called an asynchronous generator.

1.3.1 Merits and Demerits of Induction Generator

IGs offer several advantages to hydro and wind power plants because of following merits associated [1]:

> brushless and rugged construction,

3

> ➤ Low cost,

> ➤ Maintenance and operational simplicity,

> ➤ Self-protection against faults,

> ➤ Good dynamic response,

> ➤ Capability to generate power at varying speed.

Despite of several advantages, IG has some disadvantages as given below [4]:

> ➤ Poor voltage regulation,

> ➤ Poor frequency regulation,

> ➤ Low power factor,

> ➤ Excessive heating, insulation stress, winding stress, and shaft vibrations due to unbalanced operation.

1.3.2   Classification of Induction Generators

IG has a wide range of applications in different areas and hence, it has many classifications [1].

1.3.2.1   Classification of IG on the basis of excitation process

As IG needs reactive power support from some external source, IGs are classified depending on the mode of excitation as:

(A)   Grid Connected Induction Generator
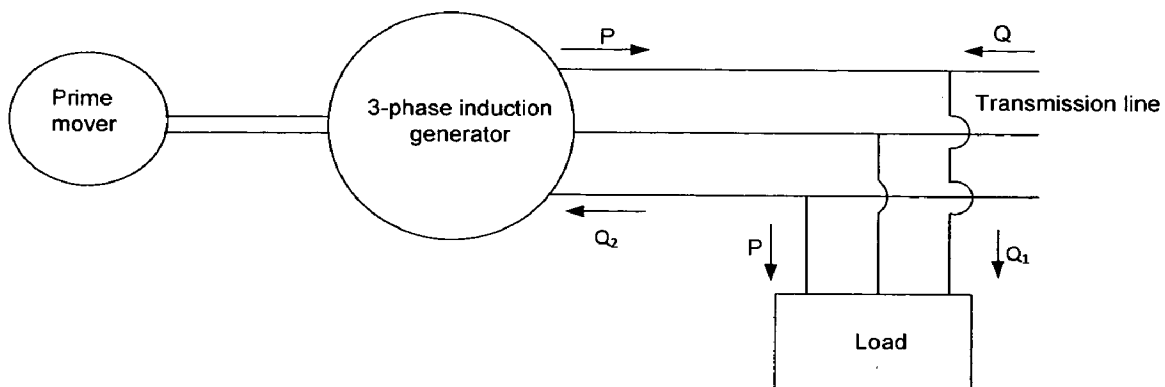
Fig. 1.1: Grid connected induction generator

4

The grid connected IG takes its reactive power for excitation process from the grid supply, so it is called grid connected induction generator. It is also called autonomous system. In this system generator is driven by a prime mover above its synchronous speed and hence the slip is negative in case of grid connected induction generator. Fig. 1.1 shows a grid connected induction generator. The power factor of the grid connected induction generator is fixed by its slip and its equivalent circuit parameters and not affected by the load [1].

(B) Self-excited Induction Generator

Self-excited induction generator (SEIG) employs cage rotor construction with shunt capacitors connected at its terminals for excitation. The shunt capacitors may be either constant or variable. In Fig. 1.2, a capacitor bank is connected across the stator terminals of a 3-phase IG in order to supply the reactive power for self excitement process [1].
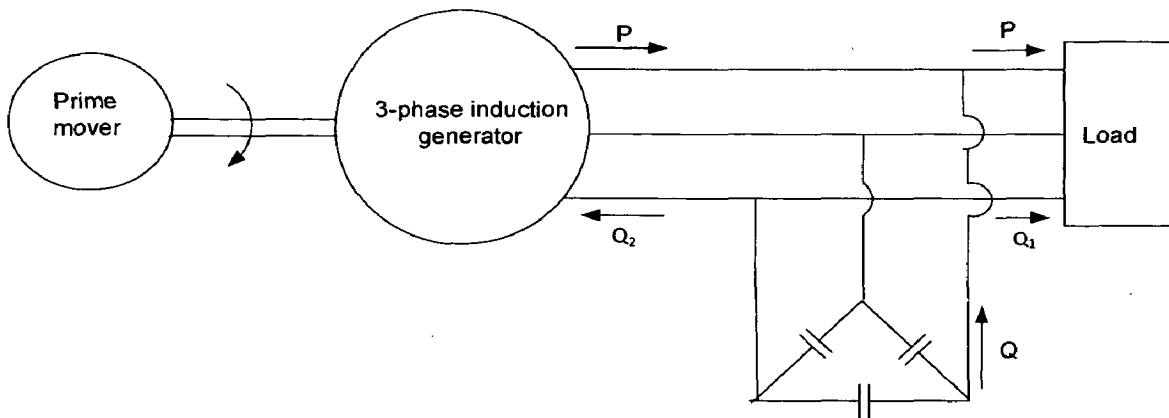
Fig. 1.2: Self-excited induction generator

1.3.2.2   Classification of IG on the basis of prime mover used

Depending upon the prime movers used and their locations, generating schemes can be broadly classified as:

(A) Constant Speed Constant Frequency

In this scheme, the prime mover speed is held constant by electronic load controller (ELC) in case of micro hydro and by adjustment of blade pitch in case of wind turbines [1].

(B) Variable Speed Constant Frequency

Popular schemes to obtain constant frequency output from variable speed are as:

(i) AC–DC–AC Link

The ac output of the three-phase IG is rectified by using a bridge rectifier and then converted back to ac using line commutated inverters. As the frequency is automatically fixed by the power line, these inverters are also known as synchronous inverters [1].

(ii) Double Output Induction Generator

The DOIG consists of a three-phase wound rotor IG mechanically coupled to either a wind or hydro turbine and stator terminals connected to a constant voltage and constant frequency utility grid [1]. The variable frequency output is fed into the ac supply by an ac–dc–ac link converter consisting of either a full-wave diode bridge rectifier and thyristor inverter combination or current source inverter (CSI)-thyristor converter link. The outstanding advantage of double output induction generator (DOIG) is that it is the only scheme in which the generated power is more than the rating of the machine. However, due to operational disadvantages, DOIG scheme could not be used extensively. The maintenance requirements are high, the power factor is low, and reliability is poor under dusty and abnormal conditions because of the sliding mechanical contacts in the rotor. This scheme is not suitable for isolated power generations because it needs grid supply to maintain excitation.

(C) Variable-Speed Variable Frequency

For variable speed corresponding to the changing derived speed, SEIG can be conveniently used for resistive heating loads, which are essentially frequency insensitive.

This scheme is gaining importance for stand-alone applications [1]. The shunt capacitors may be constant or may be varied through power electronics devices [4].

1.3.2.3 Classification of IG on the basis of rotor construction

IGs can also be classified on the basis of rotor construction as

(A) Wound Rotor Induction Generator

The wound rotor consists of slotted armature. Insulated conductors are put in the slots and connected to form a three-phase double layer distributed winding similar to the stator winding. The rotor windings are connected in star. The open ends of the star circuit are bought outside the rotor and connected to three insulated slip rings. The slip rings are mounted on the shaft with brushes resting on them.

(B) Squirrel Cage Induction Generator

In cage IG, each slot contains an uninsulated bar conductor of aluminium or copper. At each end of the rotor, the rotor bar conductors are short-circuited by heavy end rings of the same material. The conductors and the end rings form a cage of the tyre which was commonly used for keeping squirrels.

1.4 ELECTRONIC LOAD CONTROLLER

In small hydro power scheme, the hydraulic governor costs a significant fraction upto 30% of the total system cost. In addition to this, the hydraulic governor is technically complicated and requires skilled maintenance. In small hydel applications (upto 500 kW), the provision of low cost stand-alone generation is of great interest. Cost reduction may be obtained by utilizing electronic load controller (ELC) to regulate the supply frequency. As the turbine operates at constant flow, no hydraulic stability problem exists and no mechanical speed governing is required.

The aim of an ELC is to reduce the cost of a small hydro installation by replacing the hydraulic governor with an electronic circuit. Water flow to the turbine remains constant at a rate required to produce optimum power from the generator. No attempt is made to adjust this flow once the initial setting has been done.

7

The basic principle of an ELC is that the electrical load on the generator must be constant even though the consumer load may vary in an unpredictable manner from zero to full rated load of the system. In the event of change of consumer load, a ballast load is adjusted so that the total load on the generator remains constant as:

$$P_{out} = P_c + P_d$$

where P_{out} is the generated power of the generator (which should be constant), P_c is the consumer power and P_d is the dump load power. This dump power (P_d) may be used for space heating, water heating, battery charging, cooking, baking etc.

1.5 TRANSIENT ANALYSIS OF SEIG

Transient analysis of SEIG involves its behavior under initial excitation, sudden load application/removal, switching of another machine for parallel operation, switching on/off the excitation capacitors and symmetrical/unsymmetrical faults in the system. The operation of a SEIG under unbalanced operating conditions causes additional loss, excessive heating, large insulation, winding stress, and shaft vibrations [1], hence its Transient analysis is vey important which helps in determining the following [1]:

> Insulation strength,

> Suitability of winding,

> Shaft strength,

> Value of capacitor,

> Devising the protection strategy.

1.6 SCOPE OF THE WORK

The transient values of voltages, currents and torque are needed for the design of insulation level of generator windings, capacitor rating and shaft sturdiness. The developed mathematical model used for steady state analysis of the SEIG cannot directly be used for calculating the transient performances such as voltage dips, current surge and de-excitation during dynamic cases such as load perturbation, short circuit etc.

Therefore, in this work, a SEIG-ELC system consisting of a SEIG, capacitor bank, consumer load and ELC has been considered for analysing its transient performance. A composite mathematical model of entire system has been developed

under MATLAB/SIMULINK environment by combining the models of prime mover, SEIG, ELC and load. The developed model has been successfully simulated for different conditions.

1.7 ORGANISATION OF REPORT

A brief description of each chapter contained in this thesis is as follows:

Chapter 1 presents the overview of small hydro, SEIG, ELC and the scope of the work done.

Chapter 2 presents the literature review on self-excitation, transient analysis, steady state analysis, voltage and frequency control strategy of SEIG.

Chapter 3 covers the modeling of the different components of the considered isolated SEIG based system.

Chapter 4 deals with algorithm and data used for simulation. This chapter also covers the simulation results of the considered isolated SEIG based system.

Chapter 5 presents the conclusion of the work and scope for the future work

2.1 GENERAL

This chapter presents an overview of the literature related with self-excitation and voltage build up, transient analysis, steady state analysis, voltage and frequency control strategy and parallel operation of 3-phase SEIG based system.

2.2 LITERATURE REVIEW

The literature review is given with the help of following subheadings:

(A) SELF EXCITATION PROCESS AND VOLTAGE BUILD UP IN SEIG

The process of voltage build up in an induction generator is very much similar to that of a dc generator. There must be a suitable value of residual magnetism in the rotor of SEIG to ease the process of excitation. Many researchers have determined the minimum capacitor for self-excited induction generator [5-11]. Ahmed *et al.* [5] presented the minimum capacitance required for self excitation for variable speed prime mover using a nodal admittance approach. Seyoum *et al.* [6] analyzed the behavior of SEIG as a function its magnetizing inductance. They found the value of magnetizing inductance at very low terminal voltage as the key factors for self excitation. They also investigated the effect of magnetizing inductance on self-excitation and presented the loading analysis of an isolated induction generator.

Malik and Mazi [7] proposed an analytical method to compute minimum capacitance required for self excitation under no load condition of SEIG. They concluded that this minimum capacitance required is inversely proportional to the square of the speed and the maximum saturated magnetizing reactance. Based on first-order eigen value sensitivity method, Wang and Su [8] presented a simple and direct approach to determine both maximum and minimum values of capacitance required for an isolated SEIG under different loading conditions.

Singh *et al.* [9] performed a study on 6-phase induction generator using self excitation. Bhattacharya and Woodward [10] proposed an unbalanced excitation scheme

for SEIG in order to maximize the power output from it. Using nodal analysis, Eltamaly [11] proposed an expression to obtain the minimum capacitance required for induction generator operation at different load and speed conditions.

(B)   TRANSIENT ANALYSIS OF SEIG

Various dynamic models have been proposed to study the dynamic and transient behavior of SEIG [12-19]. Wang [12] presented an algorithm to evaluate dynamic performance of SEIG under unbalanced excitation capacitor. Mahto et al. [13] analysed the transient behavior of a single phase self regulated SEIG using a 3-phase SEIG feeding dynamic load. Considering the effect of main and cross flux saturation, Jain et al. [14] demonstrated the transient performance of a three phase SEIG during balanced and unbalanced load, balanced and unbalanced capacitor configuration and balanced and unbalanced fault conditions. They found that the dynamic model of SEIG is able to handle any capacitor and/or load configuration while maintaining the integrity and generalized nature of the model. They also concluded that the excessive high torque during short circuit and the sustained pulsating torque during imbalance may be taken into account in order to design the appropriate shaft.

Shridhar et al. [15] performed the transient analysis of SEIG feeding an induction motor (IM) load for overloading, load perturbation and short circuit at SEIG terminals. They concluded that SEIG can withstand starting transients of an IM having 60% of SEIG rating and withstand load perturbation as long as the load on IM does not exceed the maximum power limit as given by the steady-state load characteristic. They proposed that the capacitance should be applied in two steps: first to self-excite the generator, and second, to run IM. They observed that for IM loads with low starting torque less than 20% rating of SEIG, a single capacitance can be used for both starting and running operation.

Bhim Singh et al. [16] proposed an ELC employing a 24-pulse rectifier with 14 diodes and a chopper for SEIG. They designed and developed a polygon wound autotransformer with reduced kVA rating for 24-pulse ac–dc converter for harmonic current reduction to meet the power quality requirements. They carried out the comparative study of two topologies of bridge-rectifier-base ELC, conventional six-pulse

11

and 24-pulse ELC. They concluded that the 24-pulse ELC results in the improved voltage and frequency regulation of SEIG with negligible harmonic distortion in the generated voltage and current at varying consumer loads.

Wang *et al*. [17] presented a comparative study on dynamic performance of long-shunt and short-shunt configurations of an isolated SEIG feeding an IM load. They observed that when IM load is suddenly connected to the SEIG with the long-shunt configuration, this configuration may lead to unwanted rotor oscillations and the generated voltage distorts significantly. When IM load is suddenly connected to the SEIG with the short-shunt configuration, the short-shunt connection maintains better voltage profile.

Wang *et al*. [18] presented the dynamic performances of an isolated SEIG under different power-factor loading conditions. They investigated the characteristics of both terminal voltage and magnetizing reactance of the SEIG subject to sudden connection and disconnection of various power-factor loads. They observed significant voltage drop with sudden connection of the both purely resistive and inductive loads and very less voltage drop with sudden connection of capacitive load. They also observed that when both purely resistive and inductive loads are suddenly disconnected from SEIG, terminal voltage quickly reaches its new steady-state value.

Kasal *et al*. [19] proposed a decoupled controller for an isolated asynchronous generator feeding constant power three-phase four-wire loads to control the voltage and frequency at the generator terminal independently. They used decoupled controller as a combination of a static synchronous compensator (STATCOM) for regulating the voltage and an ELC for controlling the power to maintain the constant system frequency. They realized the STATCOM using a 4-leg insulated gate bipolar transistor (IGBT)-based current controlled voltage-sourced converter (CC-VSC) and a self-supporting dc bus, while ELC using a three-phase diode bridge rectifier, a chopper switch and a dump load. They aimed the minimal harmonic distortion while feeding balanced, unbalanced, linear and nonlinear loads.

(C)   STEADY STATE ANALYSIS

The analysis of steady state performance of SEIG is important for ensuring good quality power and assessing the suitability of the configuration for a particular application. A number of research papers are available on the steady state analysis of SEIG [20-22].

Shridhar et al. [20] presented an algorithm, based upon per phase equivalent circuit of SEIG, to find the unknown values of magnetizing reactance and frequency after solving two non linear equations.

Chan [21] proposed an iterative technique for the steady state analysis of SEIG. First, he assumed the suitable initial values for frequency and magnetizing reactance and then solved the steady state equations to get the new values considering a small increment until the result is converged.

Alolah and Alkanhal [22] investigated an optimization based approach for steady state analysis of SEIG. They formulated the problem as a multidimensional optimization problem in order to minimize the cost function of the total impedance or admittance of the circuit of SEIG. They used a constrained optimizer to obtain the frequency and other performance of the machine.

(D)   VOLTAGE AND FREQUENCY CONTROL STRATEGY

The induction generator having mainly two drawbacks one is need of reactive power support and second is poor voltage regulation. The voltage regulation can be improved by using additional series capacitors in its short and long shunt configurations. Different controllers are used to improve the frequency and voltage regulation. A considerable amount of work has been directed towards the design and the analysis of voltage and frequency regulators [23-29].

Singh et al. [23] presented the analysis and design of an ELC for three-phase SEIG suitable for stand-alone pico-hydro power generation with constant input power. They optimized the required capacitances and presented the parameters for different rating of SEIG. They also calculated the voltage and current rating for three phase rectifier and chopper, dump load and dc filtering capacitor rating.

13

Ahmed *et al.* [24] proposed an impedance based approach for voltage and frequency regulation. They demonstrated a proportional–integral (PI) closed-loop feedback voltage regulation of the three-phase SEIG driven by the variable speed prime mover. On the basis of the static VAR compensator (SVC) composed of the thyristor phase-controlled reactor in parallel with the thyristor switched capacitor and the fixed-excitation capacitor bank, they designed a power conditioner for the wind generation. With the simulation analysis and experimental results, they demonstrated the practical effectiveness of the additional SVC with the PI-controller-based feedback loop in steady-state operation in terms of high performance with low cost.

Chtchetinin [25] aimed to overcome the problem of terminal voltage stabilization for SEIG in stand-alone mode by implementing different designs of control schemes. He proposed an optimization technique for tuning of digital control block based on direct modeling of transients in the system using space vector theory.

Singh *et al.* [26] proposed an analysis of SEIG operating with an ELC for regulating its voltage and frequency under varying load condition. The proposed ELC consists of a rectifier and a chopper circuit whose operation generates harmonics on AC side of the SEIG system. They presented the complete description of the AC current harmonics generated in ELC operation and their effects on the performance of SEIG.

Joshi *et al.* [27] presented a genetic algorithm based approach for constant voltage and constant frequency operation. Singh *et al.* [28] proposed the use of damping resistors across series capacitors to damp out the starting transients and for the stable operation. They used simulated annealing based approach to solve voltage regulation optimization problem.

Palwalia *et al.* [29] demonstrated the digital design and implementation of a new digital signal processor-based load controller to regulate the voltage and frequency of a single-phase SEIG suitable for stand-alone operation with an unregulated turbine and constant excitation. They implemented a sinusoidal pulse-width-modulated AC chopper control technique to regulate the random consumer load so as to maintain a constant load on the generator.

14

(E) PARALLEL OPERATION OF SEIGs

SEIGs can be operated in parallel. Few researchers have made the study of parallel operation of SEIGs [30-32].

Chakraborty *et al.* [30] presented an iterative solution technique for the problems related to steady state performance of SEIGs operating in parallel. Based on voltage and current balance equations, they derived a model for steady state equivalent circuit of induction machine considering the non-linearity in the magnetization characteristics. This proposed method can be applied for analysis of any number of parallel connected machines.

Wang *et al.* [31] demonstrated a novel approach, based on eigen value and its sensitivity analyses, to predict both minimum and maximum values of capacitance required for self-excitation of parallel operated three-phase induction generators.

Al-Bahrani [32] described two methods of analysis to control the common bus voltage of any number of parallel SEIGs under steady state balanced conditions. The proposed methods are general and can be used for a single or a group of SEIGs employing similar or different machines with equal or unequal prime movers speeds.

15

MATHEMATICAL MODELING

3.1   GENERAL

This chapter describes the dynamic modelling of various components of a 3-phase SEIG-ELC based micro hydropower plant. The considered SEIG-ELC system consists of an induction generator (IG), capacitor bank, consumer loads (static as well as dynamic loads) and ELC with control circuit and is shown in Fig. 3.1.
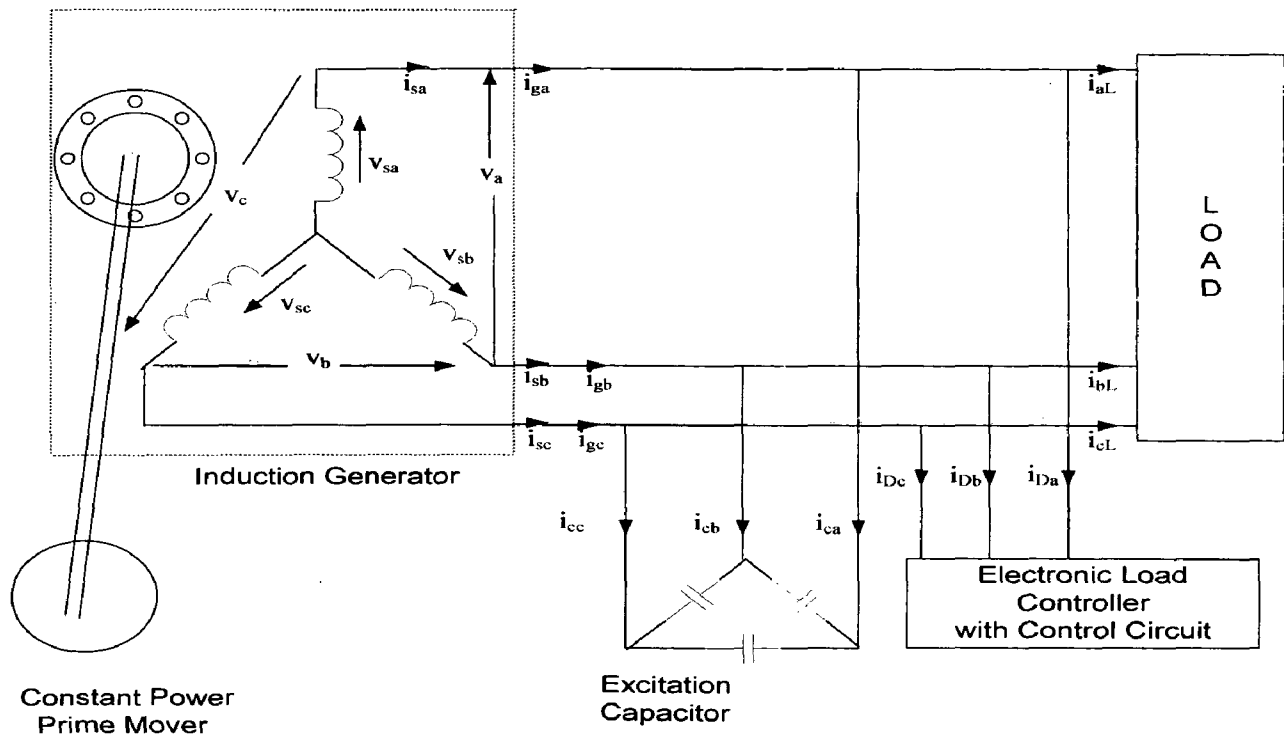

Fig. 3.1: Schematic diagram of three-phase SEIG with ELC and Load

3.2   MODELING OF PRIME MOVER

In constant power applications such as micro-hydro, an uncontrolled turbine is used. The shaft torque, T_{shaft} of prime-mover and speed is represented by a linear curve and given in (3.1).

16

$$T_{shaft} = k_1 - k_2 \, \omega_r \qquad\qquad\qquad (3.1)$$

where, T_{shaft} is the shaft torque which shows the drooping characteristics of prime-mover, ω_r is the speed of rotor in rad/s and k_1 and k_2 are constants.

3.3   MODELING OF SEIG

The dynamic models of symmetrical three-phase induction machine are derived considering the following assumptions [33]:

(1) The change in resistance due to the change in frequency and temperature is neglected.

(2) The MMF space and time harmonics are neglected.

(3) The core loss is neglected.
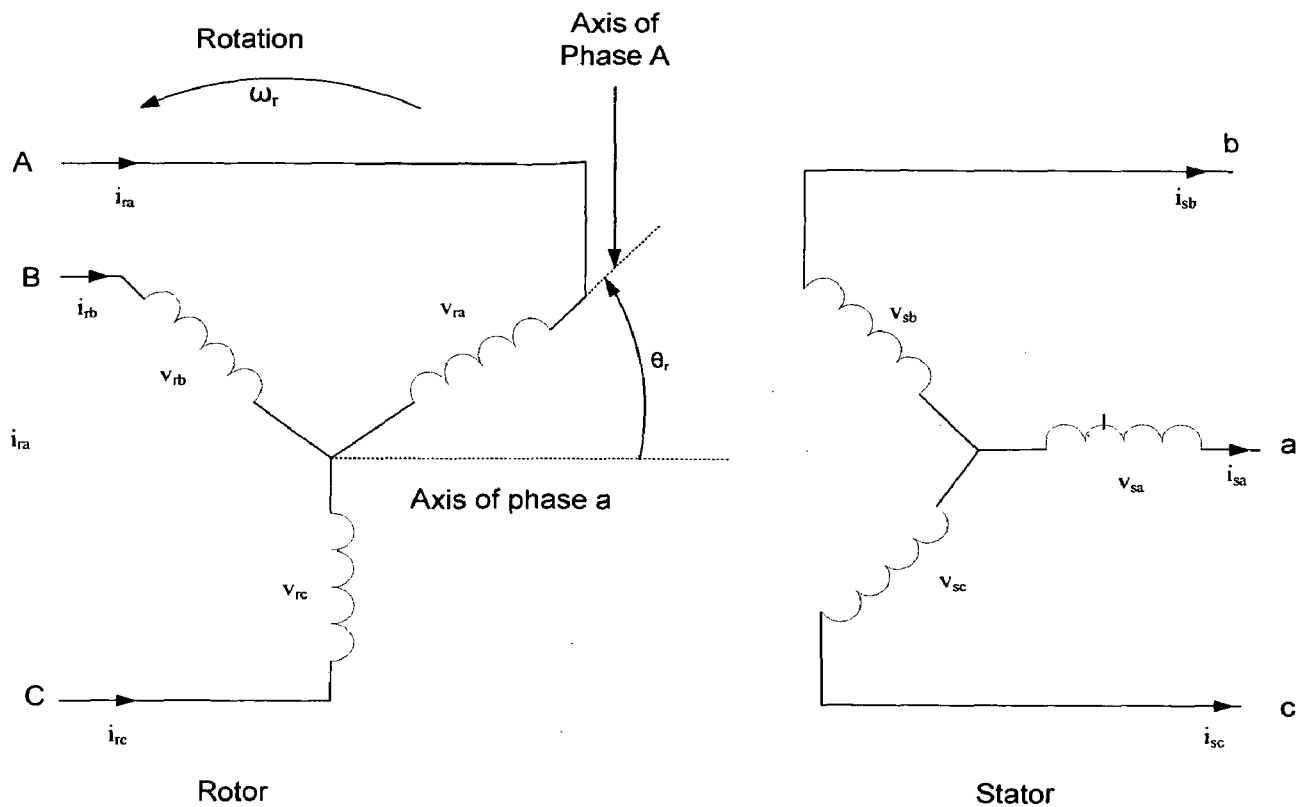

Fig. 3.2: Stator and rotor circuits of a 3-phase induction machine in a-b-c phase

Fig. 3.2 shows the stator and rotor circuits of a 3-phase induction machine in *a-b-c* phase. The voltage and flux linkage in phase variables can be expressed as [34]:

$$[v_{abcs}] = [R_s][i_{abcs}] + p[\lambda_{abcs}] \qquad (3.2)$$

$$[v_{abcr}] = [R_r][i_{abcr}] + p[\lambda_{abcr}] \qquad (3.3)$$

$$[\lambda_{abcs}] = [L_s][i_{abcs}] + [L_{sr}][i_{abcr}] \qquad (3.4)$$

$$[\lambda_{abcr}] = [L_{sr}]^T[i_{abcs}] + [L_r][i_{abcr}] \qquad (3.5)$$

where,

$$[v_{abcs}] = [v_{sa} \ v_{sb} \ v_{sc}]^T, \qquad\qquad [v_{abcr}] = [v_{ra} \ v_{rb} \ v_{rc}]^T$$

$$[i_{abcs}] = [i_{sa} \ i_{sb} \ i_{sc}]^T, \qquad\qquad [i_{abcr}] = [i_{ra} \ i_{rb} \ i_{rc}]^T$$

$$[\lambda_{abcs}] = [\lambda_{sa} \ \lambda_{sb} \ \lambda_{sc}]^T, \qquad\qquad [\lambda_{abcr}] = [\lambda_{ra} \ \lambda_{rb} \ \lambda_{rc}]$$

$$[R_s] = diag[R_s], \qquad\qquad [R_r] = diag[R_r]$$

$$[L_s] = \begin{bmatrix} L_{ls} + L_{ms} & -\frac{1}{2}L_{ms} & -\frac{1}{2}L_{ms} \\ -\frac{1}{2}L_{ms} & L_{ls} + L_{ms} & -\frac{1}{2}L_{ms} \\ -\frac{1}{2}L_{ms} & -\frac{1}{2}L_{ms} & L_{ls} + L_{ms} \end{bmatrix}$$

$$[L_r] = \begin{bmatrix} L_{lr} + L_{mr} & -\frac{1}{2}L_{mr} & -\frac{1}{2}L_{mr} \\ -\frac{1}{2}L_{mr} & L_{lr} + L_{mr} & -\frac{1}{2}L_{mr} \\ -\frac{1}{2}L_{mr} & -\frac{1}{2}L_{mr} & L_{lr} + L_{mr} \end{bmatrix}$$

$$[L_{sr}] = \begin{bmatrix} L_{sr}\cos\theta_r & L_{sr}\cos(\theta_r + 120°) & L_{sr}\cos(\theta_r - 120°) \\ L_{sr}\cos(\theta_r - 120°) & L_{sr}\cos\theta_r & L_{sr}\cos(\theta_r + 120°) \\ L_{sr}\cos(\theta_r + 120°) & L_{sr}\cos(\theta_r - 120°) & L_{sr}\cos\theta_r \end{bmatrix}$$

Since, the magnetizing and mutual inductances are associated with same magnetic flux path, it can be shown that

$$L_{mr} = \left(\frac{N_r}{N_s}\right)^2 L_{ms} \quad \text{and} \quad L_{sr} = \left(\frac{N_s N_r}{N_s}\right) L_{ms}$$

If $N_s = N_r$, then $L_{mr} = L_{ms}$ and $L_{sr} = L_{ms}$

The equations, given by (3.2) to (3.5), contain inductance terms, which vary with angle θ_r, which in turn varies with time. This suggests the transformation of a-b-c phase quantities into d-q-o variables as shown in Fig. 3.3.

The q-axis lags the d-axes by 90°. In the d-q model, coils DS and QS replace the stator phase coils, while coils DR and QR replace the rotor phase coils. Although the d-q-o axes can rotate at any arbitrary speed, there is no relative speed between the four coils DS, QS, DR and QR.

Fig. 3.3: D-Q axes superimposed onto a three-phase induction machine and Q-axes lags D-axes by 90° [34]

The transformation of a-b-c phase variables $[F_{abc}]$ to d-q-o variables $[F_{dqo}]$ may be expressed as:

For stator circuit

$$[F_{dqos}] = [K_s][F_{abcs}]$$
(3.6)

for rotor circuit

$$[F_{dqor}] = [K_r][F_{abcr}] \qquad (3.7)$$

where, $[F_{dqos}] = [f_{ds} \; f_{qs} \; f_{os}]^T$ and $[F_{abcs}]^T = [f_{sa} \; f_{sb} \; f_{sc}]^T$

$[F_{dqor}] = [f_{dr} \; f_{qr} \; f_{or}]^T$ and $[F_{abcr}]^T = [f_{ra} \; f_{rb} \; f_{rc}]^T$

In the above equations, 'f' can represent either voltage or current or flux linkage or electric charge. The superscript 'T' represents the transpose of a matrix.

$$[K_s] = \begin{bmatrix} \cos\theta & \cos(\theta - 120°) & \cos(\theta + 120°) \\ \sin\theta & \sin(\theta - 120°) & \sin(\theta - 120°) \\ \dfrac{1}{2} & \dfrac{1}{2} & \dfrac{1}{2} \end{bmatrix}$$

$$[K_r] = \frac{2}{3}\begin{bmatrix} \cos\beta & \cos(\beta - 120°) & \cos(\beta + 120°) \\ \sin\beta & \sin(\beta - 120°) & \sin(\beta + 120°) \\ \dfrac{1}{2} & \dfrac{1}{2} & \dfrac{1}{2} \end{bmatrix}$$
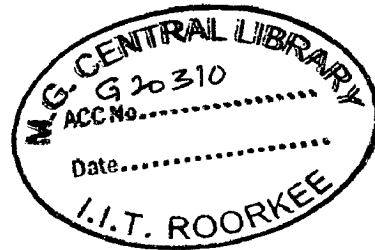
Changing the a-b-c variables, given by (3.2)-(3.3), into d-q-o variables by the transformation relation given by (3.6) and (3.7), we get

$$[v_{dqos}] = [R_s][i_{dqos}] + [K_s]p[K_s]^{-1}[\lambda_{dqos}] + [K_s][K_s]^{-1}p[\lambda_{dqos}] \qquad (3.8)$$

$$[v_{dqor}] = [R_r][i_{dqor}] + [K_r]p[K_r]^{-1}[\lambda_{dqor}] + [K_r][K_r]^{-1}p[\lambda_{dqor}] \qquad (3.9)$$

Hence,

$$[v_{dqos}] = [R_s][i_{dqos}] + \begin{bmatrix} 0 & 0 & p\theta \\ 0 & -p\theta & 0 \\ 0 & 0 & 0 \end{bmatrix}[\lambda_{dqos}] + p[\lambda_{dqos}] \qquad (3.10)$$

$$[v_{dqor}] = [R_r][i_{dqor}] + \begin{bmatrix} 0 & 0 & p\beta \\ 0 & -p\beta & 0 \\ 0 & 0 & 0 \end{bmatrix}[\lambda_{dqor}] + p[\lambda_{dqor}] \qquad (3.11)$$

In stationary reference frame

$$\omega = p\theta = 0 \qquad \text{and} \qquad \beta = \theta - \theta_r$$

So, $\qquad p\beta = -p\theta_r = -\omega_r$

20

Changing the *a-b-c* variables, given by (3.4)-(3.5), into *d-q-o* variables by the transformation relation given by (3.6) and (3.7), we obtain

$$[\lambda_{dqos}] = [K_s][L_s][K_s]^{-1}[i_{dqos}] + [K_s][L_{sr}][K_r]^{-1}[i_{dqor}] \tag{3.12}$$

$$[\lambda_{dqor}] = [K_r][L_{sr}]T[K_s]^{-1}[i_{dqos}] + [K_r][L_r][K_r]^{-1}[i_{dqor}] \tag{3.13}$$

It can be shown by simple matrix exercise that

$$[K_s][L_s][K_s]^{-1} = \begin{bmatrix} L_{ls} + L_m & 0 & 0 \\ 0 & L_{ls} + L_m & 0 \\ 0 & 0 & L_{ls} \end{bmatrix}, \quad [K_r][L_r][K_r]^{-1} = \begin{bmatrix} L_{lr} + L_m & 0 & 0 \\ 0 & L_{lr} + L_m & 0 \\ 0 & 0 & L_{lr} \end{bmatrix}$$

$$[K_s][L_{sr}][K_r]^{-1} = \begin{bmatrix} L_m & 0 & 0 \\ 0 & L_m & 0 \\ 0 & 0 & 0 \end{bmatrix}, \quad [K_r][L_{sr}][K_s]^{-1} = \begin{bmatrix} L_m & 0 & 0 \\ 0 & L_m & 0 \\ 0 & 0 & 0 \end{bmatrix}$$

where,

$$L_m = \frac{3}{2} L_{ms}$$

Since, variables corresponding to *o* axis are related arithmetically to the *a-b-c* variables and not to the arbitrary reference frame, the equations for *o* axis variables may be eliminated. Here onwards, *o* axis variables are not shown in the *d-q* equations.

Substituting the flux linkage equations, given by (3.12) and (3.13), in voltage equations, given by (3.10) and (3.11) and simplifying the result, we have

$$[v] = [R][i] + [L]p[i] + \omega_r[G][i] \tag{3.14}$$

where

$$[v] = [v_{ds} \; v_{qs} \; v_{dr} \; v_{qr}]^T, \qquad [i] = [i_{ds} \; i_{qs} \; i_{dr} \; i_{qr}]^T$$

$$[R] = \begin{bmatrix} R_{ss} & 0 & 0 & 0 \\ 0 & R_{ss} & 0 & 0 \\ 0 & 0 & R_{rr} & 0 \\ 0 & 0 & 0 & R_{rr} \end{bmatrix}, \quad [L] = \begin{bmatrix} L_{ls} + L_m & 0 & L_m & 0 \\ 0 & L_{ls} + L_m & 0 & L_m \\ L_m & 0 & L_{lr} + L_m & 0 \\ 0 & L_m & 0 & L_{lr} + L_m \end{bmatrix}$$

$$[G] = \begin{bmatrix} 0 & 0 & 0 & 0 \\ 0 & 0 & 0 & 0 \\ 0 & -L_m & 0 & -(L_{lr} + L_m) \\ L_m & 0 & L_{lr} + L_m & 0 \end{bmatrix}$$

21

The electromagnetic torque in Newton-meters (N-m) is given by

$$T_e = \left(\frac{P}{2}\right) [i_{abcs}]^T \frac{\partial}{\partial \theta_r} [L_{sr}][i_{abcr}]$$ (3.15)

Using transformation equations, we have

$$T_e = \left(\frac{P}{2}\right) [K_s]^{-1}[i_{dqos}]^T \frac{\partial}{\partial \theta_r} [L_{sr}][K_r]^{-1}[i_{dqor}]$$

In terms of current, this can be written as:

$$T_e = \left(\frac{3}{2}\right)\left(\frac{P}{2}\right) Lm (i_{dr}i_{qs} - i_{qr}i_{ds})$$ (3.16)

Torque balance equation is:

$$T_{shaft} = T_e + J\left(\frac{2}{P}\right) p\omega_g$$ (3.17)

The derivative of the rotor speed from (3.17) can be expressed as:

$$p\omega_g = \left(\frac{P}{2}\right) \frac{(T_{shaft} - T_e)}{J}$$ (3.18)

Here, T_{shaft} is the input torque to SEIG from the prime mover, J is moment of inertia and P is number of poles.

The SEIG operates in the saturation region and its magnetizing characteristic is non-linear in nature. So, the magnetizing current should be calculated in every step of integration in terms of stator and rotor d-q currents as

$$I_m = \frac{\left\{(i_{ds}+i_{dr})^2 + (i_{qs}+i_{qr})^2\right\}^{1/2}}{\sqrt{2}}$$ (3.19)

The magnetizing inductance (L_m) is calculated from the magnetizing characteristic as

$$L_m = a + b \times I_m + c \times I_m^2 + d \times I_m^3$$ (3.20)

Further, following equations can be given for the excitation capacitors of SEIG as shown in Fig. 3.1.

$$C_a pv_a - C_c pv_c = i_{ca} = i_{ga} - (i_{aL} + i_{Da})$$ (3.21)

$$C_b pv_b - C_a pv_a = i_{cb} = i_{gb} - (i_{bL} + i_{Db})$$ (3.22)

$$C_c pv_c - C_b pv_b = i_{cc} = i_{gc} - (i_{cL} + i_{Dc})$$ (3.23)

The currents i_{aL}, i_{bL} and i_{cL} are line currents of the load and i_{Da}, i_{Db} and i_{Dc} are the ac currents of the ELC as shown in Fig. 3.1. Voltages v_a, v_b and v_c are line voltages and hence,

$$v_a + v_b + v_c = 0$$ (3.24 a)

22

Substitution of (3.24 a) into (3.21)–(3.22) results in following two equations as:

$$(C_a + C_c)pv_a + C_c pv_b = i_{ca} \tag{3.24}$$

$$C_a pv_a + C_b pv_b = i_{ca} \tag{3.25}$$

Solving (3.24) and (3.25), the voltage derivatives are

$$pv_a = \left\{ \frac{\{C_a i_{ca} + C_c i_{cb}\}}{K_{eq}} \right\} \tag{3.26}$$

$$pv_b = \left\{ \frac{\{C_a i_{ca} + (C_a + C_c) i_{cb}\}}{K_{eq}} \right\} \tag{3.27}$$

with $K_{eq} = C_a C_b + C_b C_c + C_c C_a$

3.4   MODELING OF CONSUMER LOADS:

Practical consumer loads consisting of induction motor and resistive load are modeled as follows [35]:

3.4.1   DYNAMIC LOAD:

The dynamic model of the three-phase squirrel cage induction motor (IM) is similar to the induction generator. A schematic of three phase induction motor load is shown in Fig. 3.4.

Star connected three-phase
Induction motor

Delta connected three-phase
Induction motor

Fig. 3.4: Three phase induction motor load

23

The volt ampere equations in *d-q* stationary reference frame are:

$$[v_M]=[R_M][i_M]+[L_M]p[i_M]+\omega_M[G_M][i_M] \tag{3.28}$$

From which, the current derivative can be expressed as:

$$p[i_M]=[\,L_M]^{-1}\{[v_M]-[\,R_M][\,i_M]-\omega_M[G_M][\,i_M]\} \tag{3.29}$$

Developed electromagnetic torque of the motor is:

$$T_{eM} = \left(\tfrac{3P_M}{4}\right)L_{mM}\,(i_{qsM}\,i_{drM} - i_{dsM}\,i_{qrM}) \tag{3.30}$$

Torque balance equation:

$$T_L = T_{eM} + \left(\tfrac{2J_M}{P_M}\right)p\omega_M \tag{3.31}$$

From (3.39), The derivative of the speed of the motor can be expressed as:

$$p\omega_M = \left(\tfrac{P_M}{2}\right)\frac{(T_L - T_{eM})}{J_M} \tag{3.32}$$

where T_L, J_M and P_M denote load torque, moment of inertia and number of poles of IM, respectively.

3.4.2 STATIC LOAD:

A schematic of three phase resistive load is shown in Fig. 3.4.

Fig. 3.5: Three phase resistive load

The volt ampere equations in *d-q* stationary reference frame are:

$$[v_M]=[R_M][i_M]+[L_M]p[i_M]+\omega_M[G_M][i_M]$$

(3.28)

From which, the current derivative can be expressed as:

$$p[i_M]=[L_M]^{-1}\{[v_M]-[R_M][i_M]-\omega_M[G_M][i_M]\}$$

(3.29)

Developed electromagnetic torque of the motor is:

$$T_{eM} = \left(\tfrac{3P_M}{4}\right)L_{mM} (i_{qsM}\ i_{drM} - i_{dsM}\ i_{qrM})$$

(3.30)

Torque balance equation:

$$T_L = T_{eM} + \left(\tfrac{2J_M}{P_M}\right)p\omega_M$$

(3.31)

From (3.39), The derivative of the speed of the motor can be expressed as:

$$p\omega_M = \left(\tfrac{P_M}{2}\right)\frac{(T_L - T_{eM})}{J_M}$$

(3.32)

where T_L, J_M and P_M denote load torque, moment of inertia and number of poles of IM, respectively.

3.4.2 STATIC LOAD:

A schematic of three phase resistive load is shown in Fig. 3.4.

Fig. 3.5: Three phase resistive load

For the three-phase delta connected resistive load as shown in Fig. 3.4, the line currents are given by the following relations:

$$i_{aL} = i_{pa} - i_{pc} = \left(\frac{v_a}{R_{La}}\right) - \left(\frac{v_c}{R_{Lc}}\right) \tag{3.33}$$

$$i_{bL} = i_{pb} - i_{pa} = \left(\frac{v_b}{R_{Lb}}\right) - \left(\frac{v_a}{R_{La}}\right) \tag{3.34}$$

$$i_{cL} = i_{pc} - i_{pb} = \left(\frac{v_c}{R_{Lc}}\right) - \left(\frac{v_b}{R_{Lb}}\right) \tag{3.35}$$

3.5   MODELING OF ELC:

The considered ELC consists of an uncontrolled diode rectifier bridge, a control circuit, a solid-state switch (IGBT) operating as a chopper and the dump load (resistors) as shown in Fig. 3.5. The stator voltage is fed to the ELC circuit through a small value of source inductance (L_f) and resistance (R_f). A filtering capacitor (C) is connected across the rectifier output to filter out the ac ripples of the dc voltage [35].

The volt–current relation of the complete load controller system is

$$v_{max} = 2R_f i_d + 2L_f p i_d + v_d \tag{3.36}$$

from which the derivative of ELC current (i_d) is defined as

$$p i_d = \frac{(v_{max} - v_d - 2R_f i_d)}{2L_f} \tag{3.37}$$

where, v_{max} is the maximum value of ac line voltages (v_a, v_b, v_c, $-v_a$, $-v_b$ and $-v_c$) depending on which diode pair is conducting and v_d is the dc-link voltage. The ac dump load currents in the three phases (i_{Da}, i_{Db} and i_{Dc}) are obtained by using the magnitude of i_d and direction (sign) corresponding to conducting pairs of diodes.

25
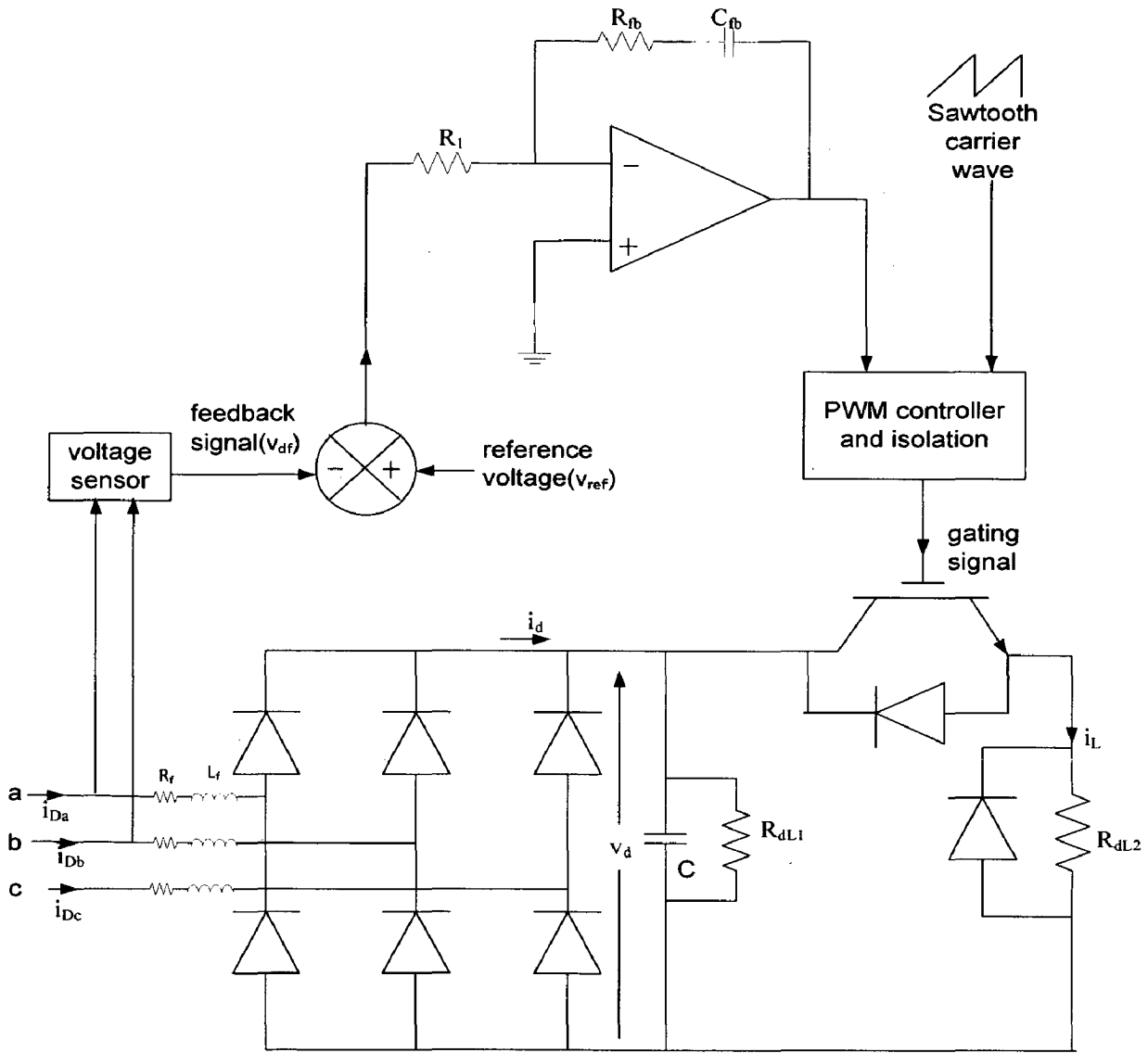
Fig. 3.6: Schematic diagram of ELC with Control circuit [35]

Charging and discharging of the filter capacitor is expressed as

$$pv_d = \frac{(i_d - i_L)}{C} \qquad\qquad (3.38)$$

with $i_L = \frac{v_d}{R_{dL1}} + S\frac{v_d}{R_{dL2}}$

where, S is the switching function indicating the switching status of the IGBT switch. When the switch is closed, then S = 1 and when the switch is opened, then S = 0.

The switching states of the IGBT chopper (S = 1 or 0) depend on the output of Pulse Width Modulation (PWM) wave with the varying duty cycle which compares the output of Proportional Integral (PI) voltage controller with the sawtooth carrier wave as shown in Fig. 3.5 .

3.6   MODELING OF CONTROL SCHEME OF ELC

The closed-loop control is the heart of ELC and it plays a vital role in keeping the terminal voltage of the SEIG constant. The SEIG output voltage is sensed using a step-down transformer and converted to dc through a single-phase rectifier circuit for the feedback signal, as shown in Fig. 3.6. A small capacitor (C_s) is used to filter the ripples out from the rectified voltage to be used as the feedback signal (v_{df}) and it is compared with the reference voltage (v_{ref}) [36].

The error voltage is fed to a PI voltage controller. The output of controller is compared with the sawtooth carrier waveform to result in the PWM signal to alter the duty cycle of the chopper. The single-phase rectifier circuit used in this feedback loop is modeled as

$$v_f = R_{ff}i_{df} + L_{ff}pi_{df} + Kv_{df} \qquad (3.39)$$

Here, v_f is the absolute value of the instantaneous value of the ac output voltage of the step-down transformer corresponding to the SEIG voltage (v_a or $-v_a$) depending on which diode pair is conducting and v_{df} is the dc voltage. R_{ff} and L_{ff} are the resistance and leakage inductance of the step-down transformer, respectively. K is a constant depending upon the tapping of the potentiometer.

From (3.47), the derivative of current (i_{df}) is given as

$$pi_{df} = \frac{(v_f - Kv_{df} - R_{ff}i_{df})}{L_{ff}} \qquad (3.40)$$
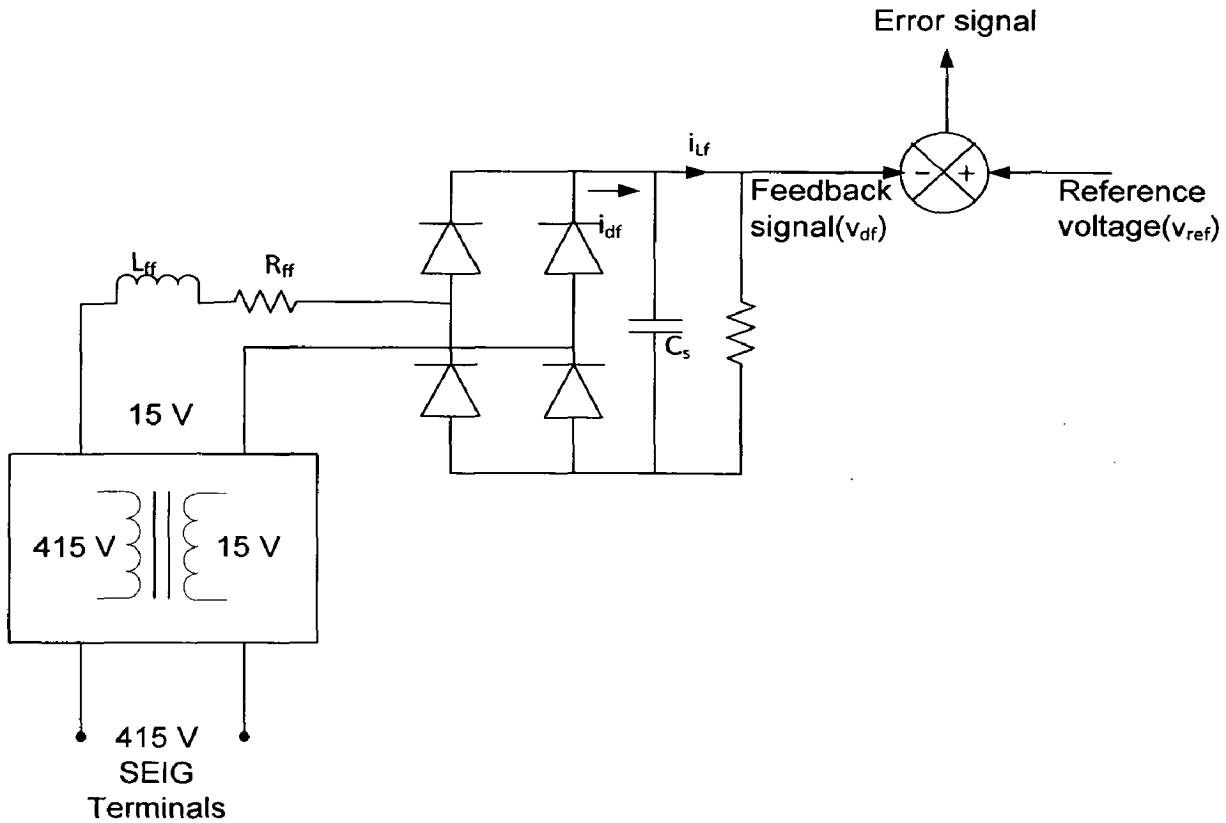
Fig. 3.7: Voltage Sensing Circuit [36]

Charging and discharging of the filtering capacitor (C_s) at the output of the single-phase uncontrolled rectifier is as follows:

$$pv_d = \frac{i_{df} - R_{ff}\, i_{df}}{C_s K}$$

(3.41)

Voltage v_{df} is used as the feedback voltage signal and compared with the reference signal. The resulting error is fed to the PI voltage controller. The analog PI voltage controller modeled as

$$pv_{01} = K_1 \frac{v_{ref} - v_{df}}{T_{cc}}$$

(3.42)

$$v_{02} = K\,(v_{ref} - v_{df})$$

(3.43)

The output signal of the PI controller (v_0) is

$$v_0 = v_{01} + v_{02}$$

(3.44)

where v_{ref} is the reference voltage, $K_1 = R_{fb}/R_1 = 34.55$ and $T_{cc} = R_{fb}f_b = 0.1935$ as $R_{fb} = 194 \text{ k}\Omega$, $R_1 = 5.6 \text{ k}\Omega$, $C_{fb} = 1 \text{ }\mu\text{F}$. R1, R_{fb} and R_1 are the input resistance, feedback resistance, and feedback capacitance used in the analog PI controller.

The output of the PI controller (v_0) is compared with the saw-tooth PWM carrier waveform. The sawtooth waveform is defined as

$$v_{st} = \frac{A_m t}{T_p} \tag{3.45}$$

where A_m is an amplitude of the sawtooth carrier waveform (2.38 V), t is time in microseconds, and T_p is a time period (200μs) of the sawtooth PWM carrier wave.

The PI controller output voltage (v_0) is compared with the sawtooth carrier waveform and output is fed to the gate of the chopper switch (IGBT), whuich is operated as:

S = 1, when $v_{st} > v_o$, and S = 0, when $v_{st} < 0$,

where S is the switching function used for generating the gating signal of the IGBT of the chopper of the ELC.

The PWM signal is fed to an opto-isolator, which isolates the power circuit and the control circuit. The opto-isolator inverts the signal at its output and hence a single stage transistor amplifier is used at its output, which again inverts the signal to regain the original signal. This signal is then fed to a push-pull amplifier, which drives the IGBT chopper with the appropriate duty cycle.

DATA AND SIMULATION RESULTS

This chapter deals with simulation of SEIG-ELC based micro hydro power plant using the mathematical modelling of different components of it presented in the previous chapter. In this chapter, various data used for simulation purpose, algorithm for simulation and results obtained after simulation are presented.

4.1 DATA

The data for various components of SEIG-ELC based micro hydro system, simulated in this dissertation work, are given below:

(A)   Parameters of SEIG [23]:

For simulating SEIG, an Induction machine rated as 3.7 kW, 3-phase, 4-pole, 50 Hz, 415 V, 7.4 A, Y connected induction machine is used with following parameters:

$$R_s = 1.433 \ \Omega, \quad R_r = 1.606 \ \Omega, \quad X_{ls} = 3.1626 \ \Omega, \quad X_{lr} = 3.1626 \ \Omega$$

The magnetizing inductance L_m is related to the magnetizing current as

$$
\begin{aligned}
L_m &= 1.0 & \text{for} \quad I_m &\leq 0.36 \\
&= 1.12 - 0.3437 I_m + 0.042 I_m^2 - 0.00164 I_m^3 & \text{for} \quad 3.6 &\leq I_m \leq 3.2 \\
&= 0.4 & \text{for} \quad I_m &\geq 3.2
\end{aligned}
$$

The moment of inertia of the induction machine including the prime mover coupled on its shaft is 0.0966 kg-m^2.

(B)   Parameters of Prime-mover Characteristics

The following parameters are used for simulating the characteristics of prime mover:

$$k_1 = 600 \text{ and } k_2 = 3.5$$

(C)   Parameters of Electronic Load Controller and Control Circuit [37]

For ELC and its control circuit, values of different parameters are as follows:

$$R_{DL} = 84 \ \Omega, \quad C_{dc} = 380 \ \mu F, \quad R_f = 1 \ \Omega, \quad L_f = 0.001 \text{ H}$$

R_{fb} =194 k Ω, R_1= 5.6k Ω, C_{fb} = 1 μF

R_{ff}= 1 Ω, L_{ff}=0.0085 H

Cs= 40 μF, R_{Lf}=40 k Ω

(D)   Parameters of Induction Motor Loads [37]:

To Simulate dynamic load, 735 W, 3-phase, 4-pole, 50 Hz, 230 V,Y connected induction motor is considered with

$$R_s = 8.38\ \Omega, \quad R_r = 10.58\ \Omega, \quad X_{ls} = 50.77\ \Omega, \quad Xl_r = 50.77\ \Omega$$
$$X_{lm} = 84.466\ \Omega, \quad J=0.0018\ Kg\text{-}m^2$$

4.2   ALGORITHM FOR SIMULATION

The algorithm used for simulation is shown in Fig. 4.1 with the help of a flow-chart.

```
                    ( Start )
                        |
                        v
            +-----------------------+
            |    Read input data    |
            +-----------------------+
                        |
                        v
            +-----------------------+
            | Calculate system      |
            |     parameters        |
            +-----------------------+
                        |
                        v
        +-------------------------------+
        | Find out system initial       |
        |         conditions            |
        +-------------------------------+
                        |
                        v
                      ( A )
```

31
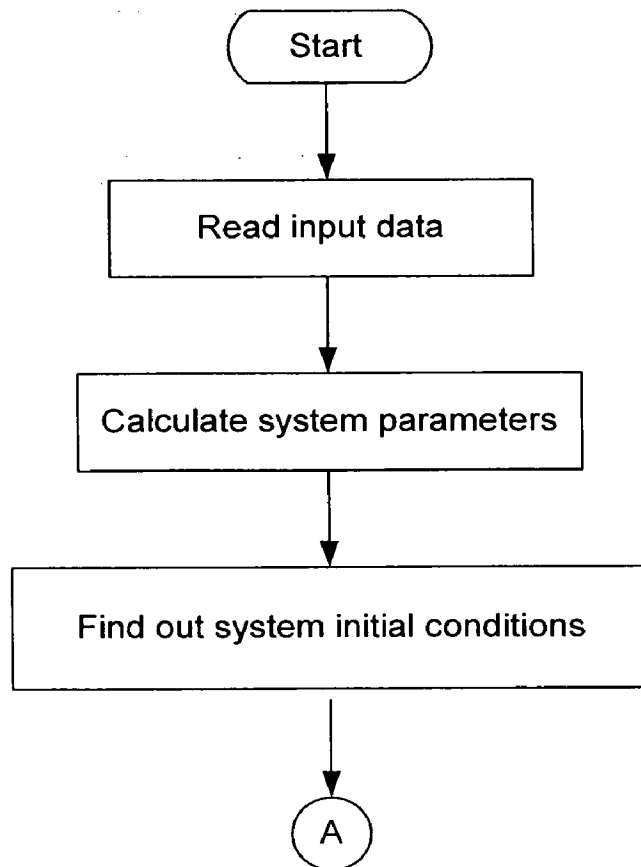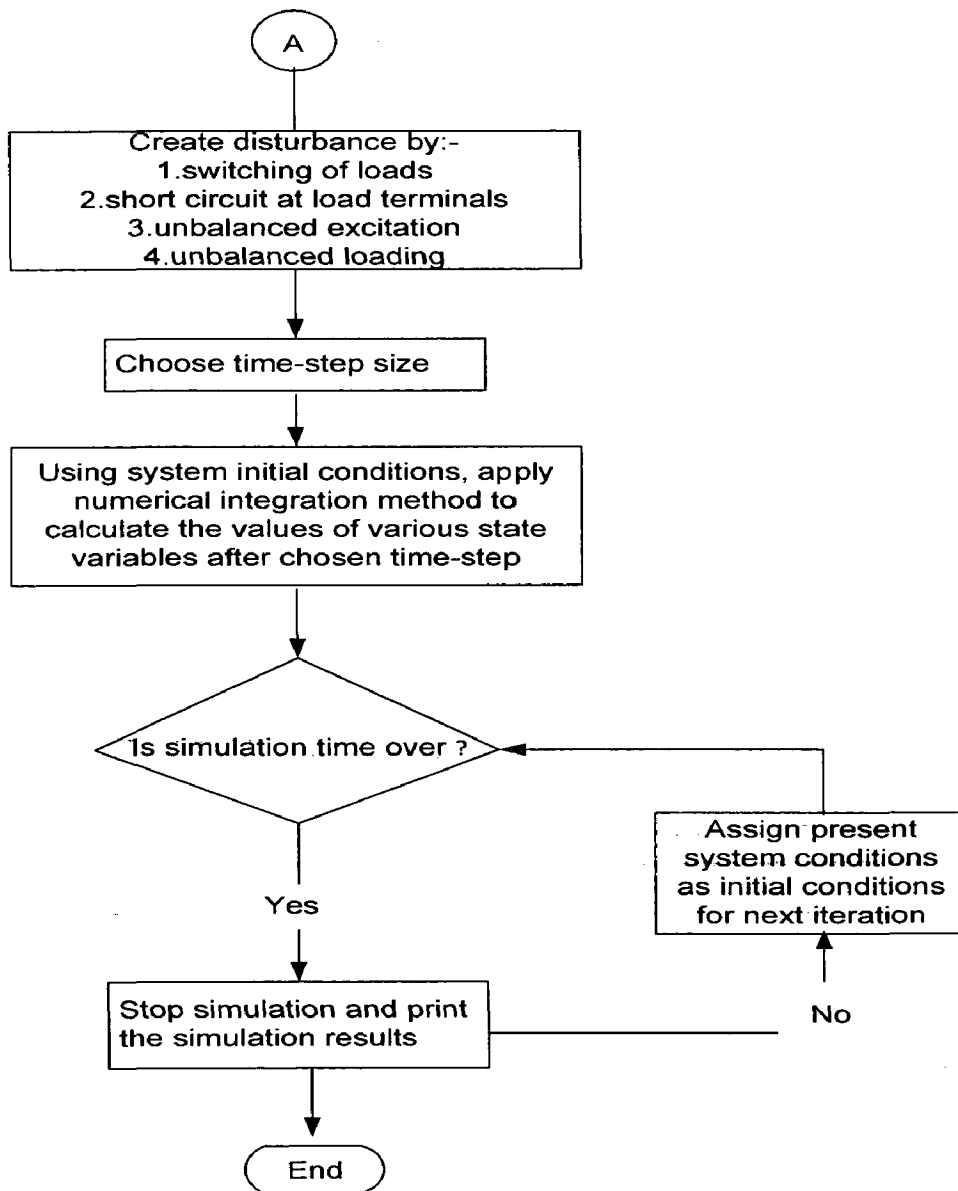
Fig. 4.1: Flow chart for simulation

4.3 SIMULATION RESULTS

The objective of the work is to simulate a self excited induction generator (SEIG) with electronic load controller (ELC) under various transient conditions. The complete

MATLAB Simulink model is developed with the help of SimPower systems block sets and shown in Appendix-A.

Following cases are taken for study:

1. Process of Self-excitation and Voltage build up,
2. Sudden application and removal of resistive load,
3. Sudden application and removal of IM load,
4. Faults,
5. Unbalanced Loading,
6. Unbalanced Excitation.

4.2.1 Process of Self-excitation and Voltage Build up

In this case, SEIG is started at no load with excitation capacitors of 200μF per phase. Figs. 4.2 to 4.5 show voltage build up for all three lines at SEIG terminals, capacitor currents, Electromagnetic torque, Rotor speed and frequency of generated voltage, respectively..

Time(sec.)
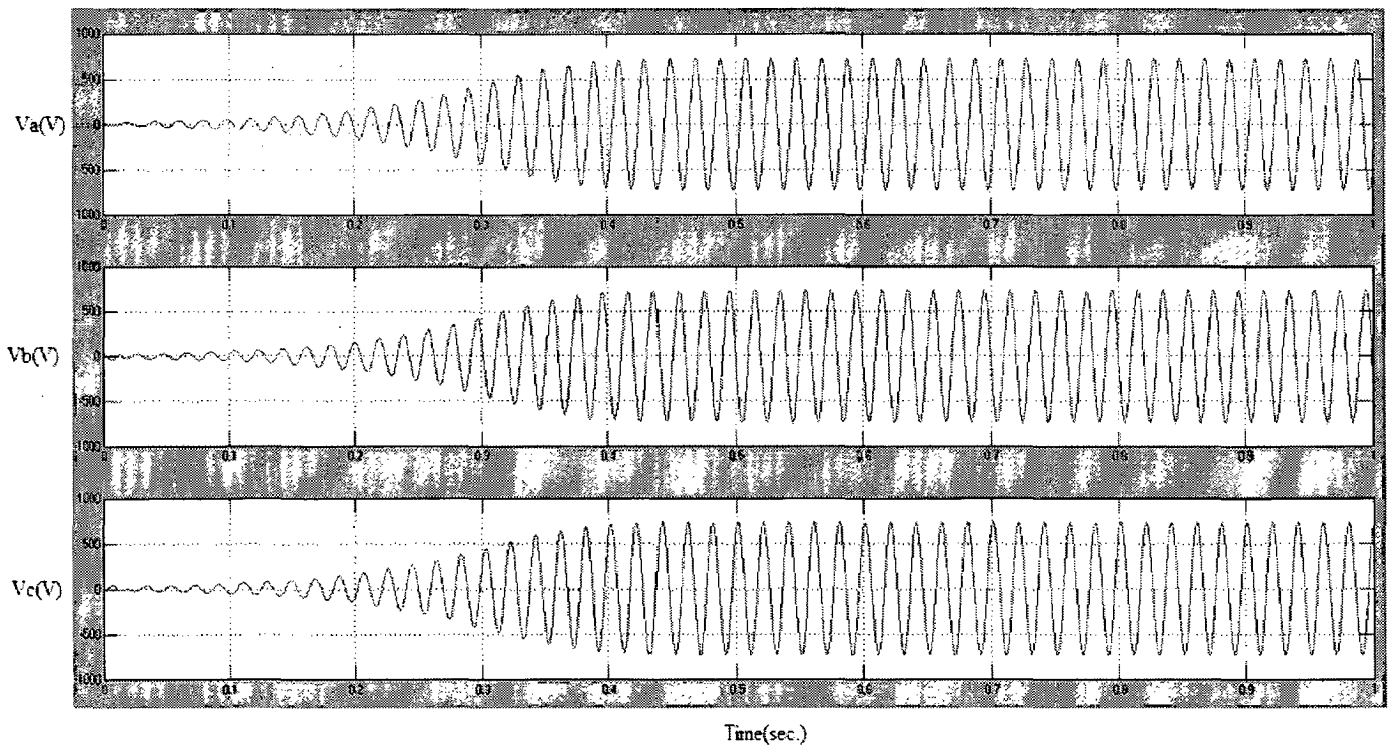
Fig. 4.2: Three line voltages build up at SEIG terminals

33
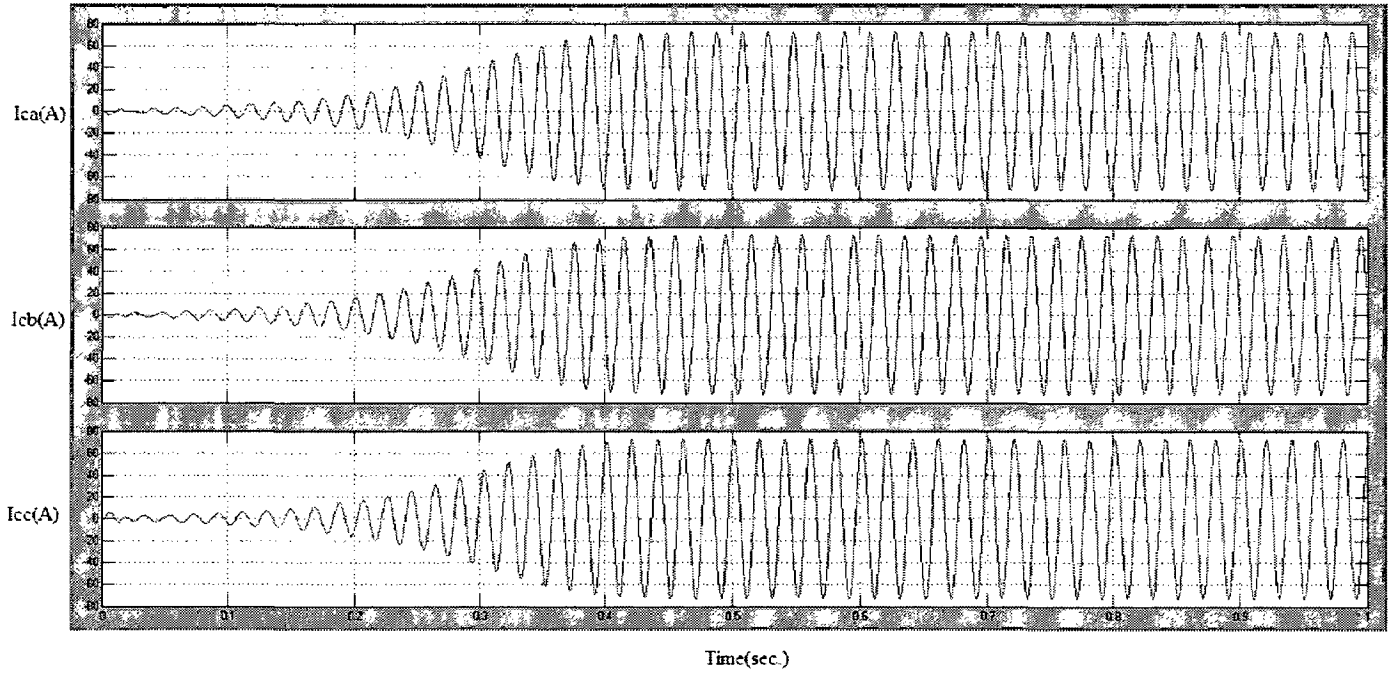
Fig. 4.3: Three line capacitor currents
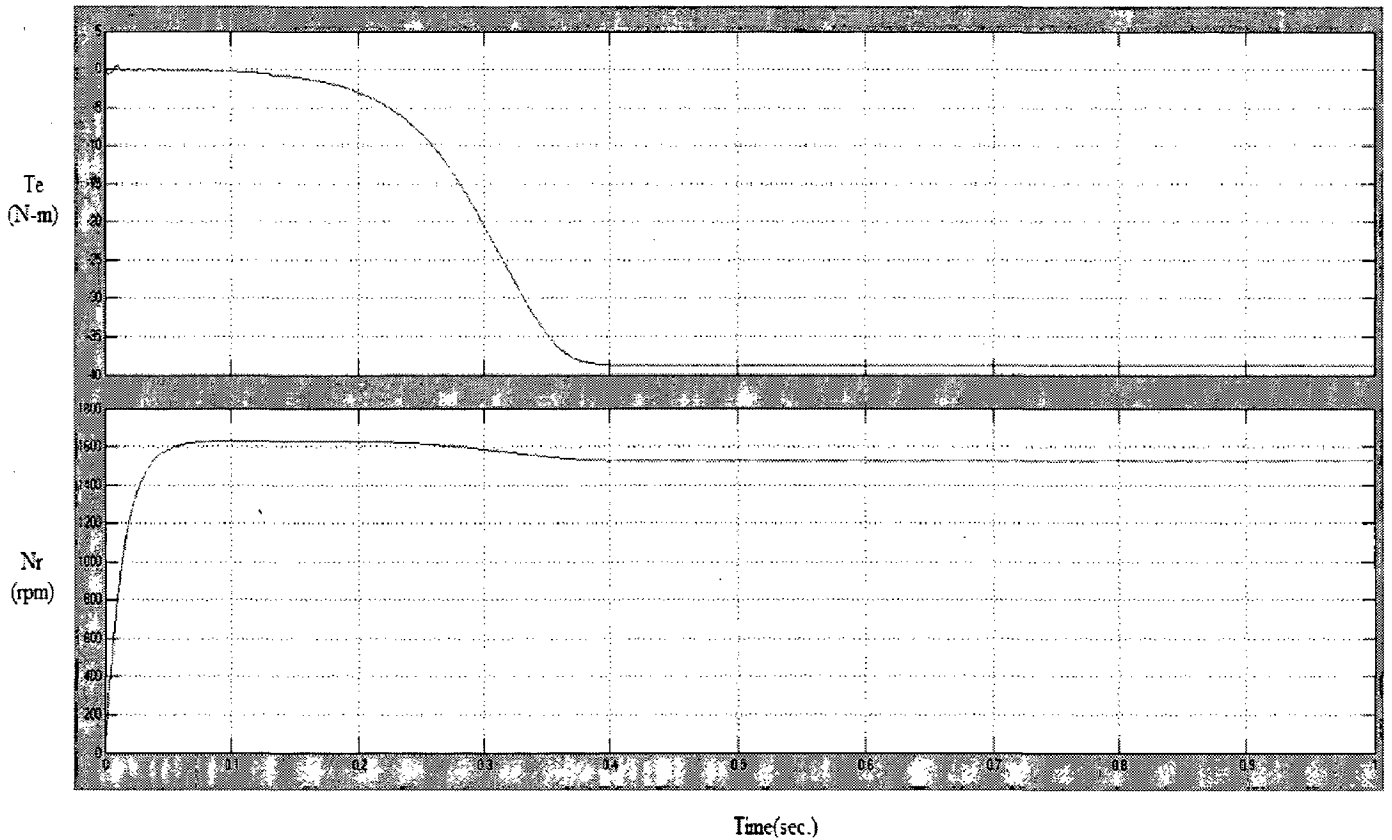
Fig. 4.4: Electromagnetic torque and rotor speed developed in SEIG

34
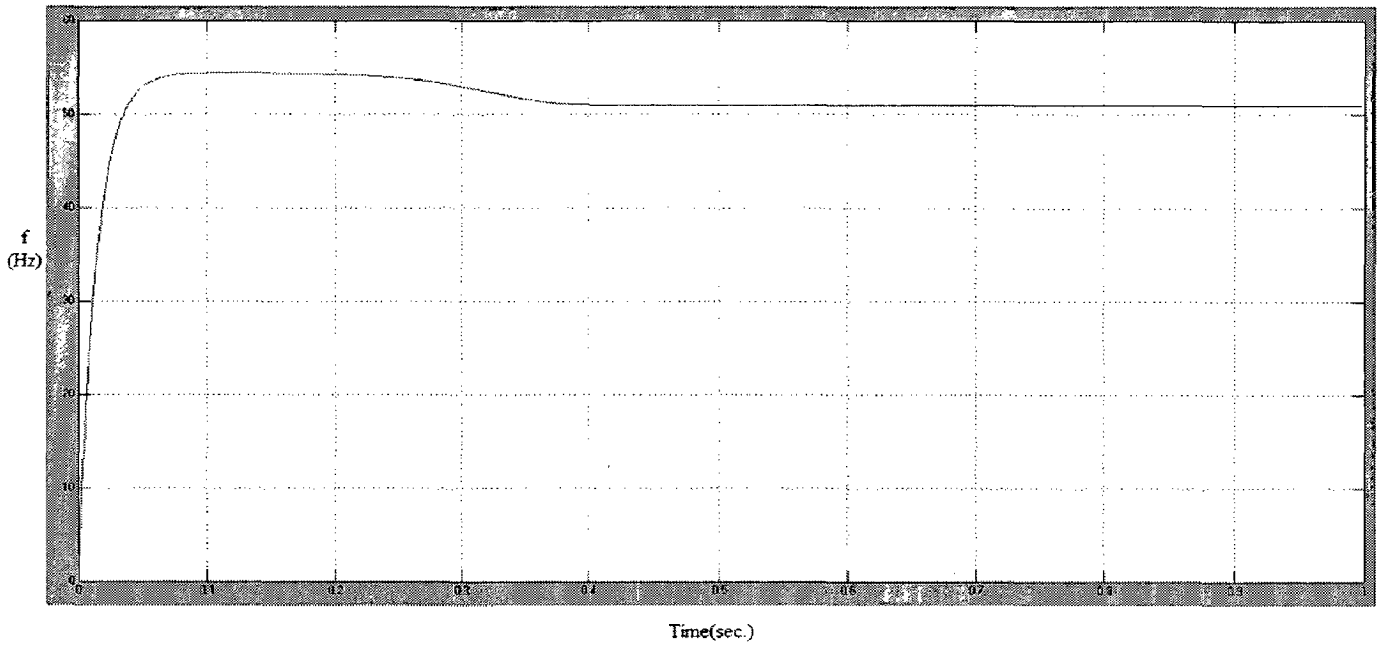
Fig. 4.5: Frequency of generated voltage

4.2.2 Sudden Application And Removal Of Resistive Load

Schematic diagram of 3-phase SEIG with ELC feeding static load (resistive load) is shown in the Fig. 4.6. Two cases, sudden application and sudden removal of resistive load of 1500 W are considered.
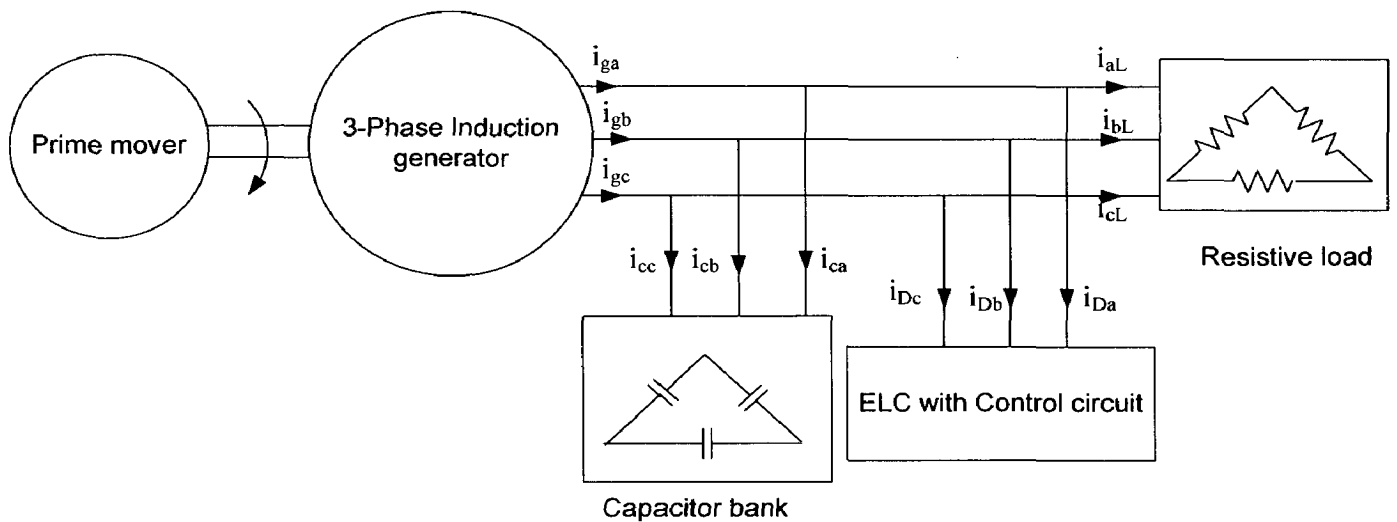
Fig. 4.6: Schematic diagram of SEIG feeding resistive Load

(i)   Sudden Application

Initially SEIG is operated at no load. At t = 1 sec., ELC is connected at SEIG terminals and consume rated power. At t = 1.5 sec., a resistive load of 1500 W is suddenly connected to the SEIG terminals. Figs. 4.7-4.12 illustrate the sudden application of resistive load.

Figs. 4.7 and 4.8 show the waveforms of the voltage and current of line-A at SEIG terminals and three line capacitor currents, respectively. Figs. 4.9 and 4.10 represent the main load current and ELC current of line-A, respectively. Figs. 4.11 and 4.12 show the variation in electromagnetic torque, rotor speed and frequency due to switching of resistive load, respectively.

It is found that the line-A voltage and frequency of generated voltage at SEIG terminals remain almost unchanged.

Time(sec.)
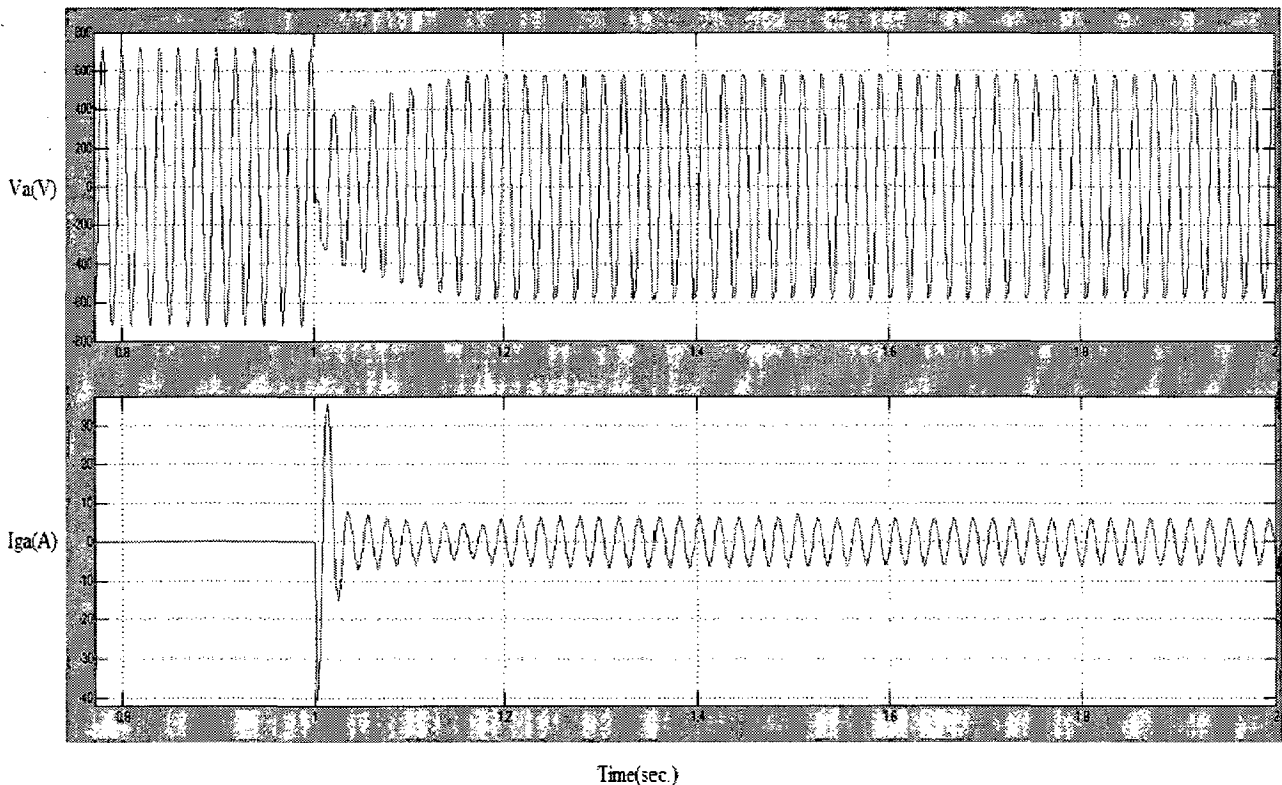
Fig. 4.7: Voltage and current waveforms of line-A at the SEIG terminals due to sudden application of resistive load

36

Time(sec.)
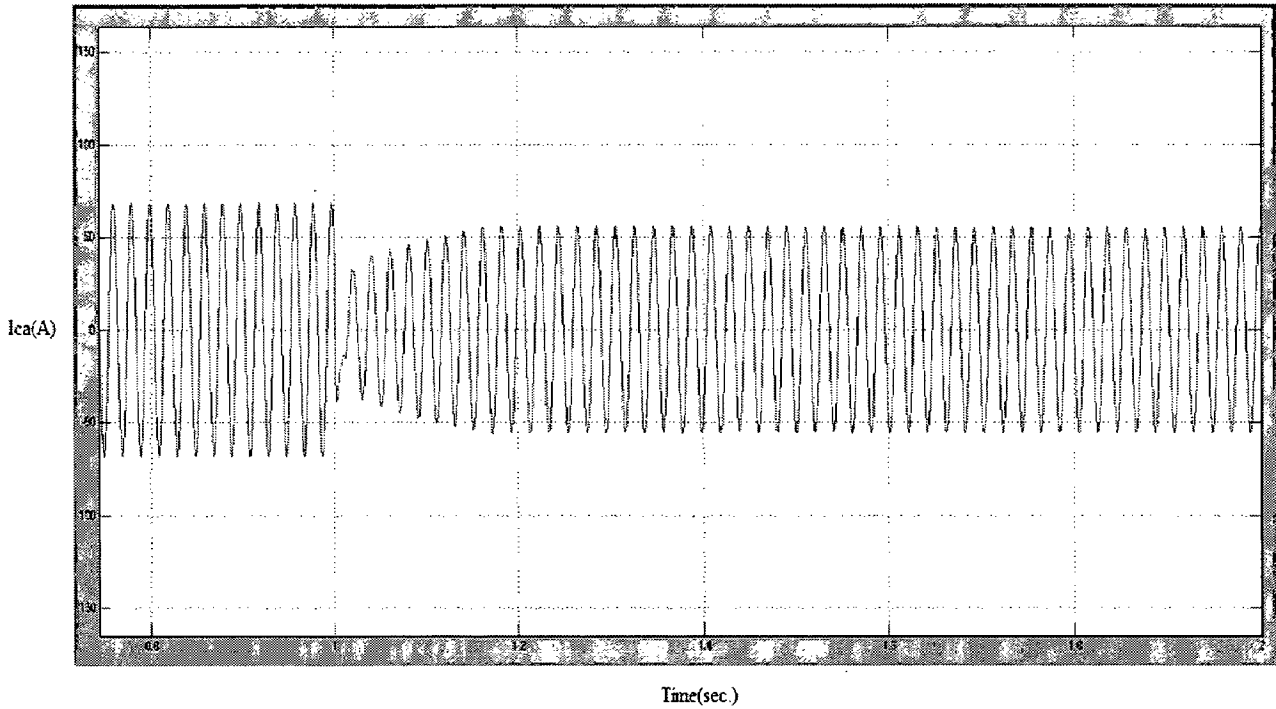
Fig. 4.8: Capacitor current of line-A due to sudden application of resistive load
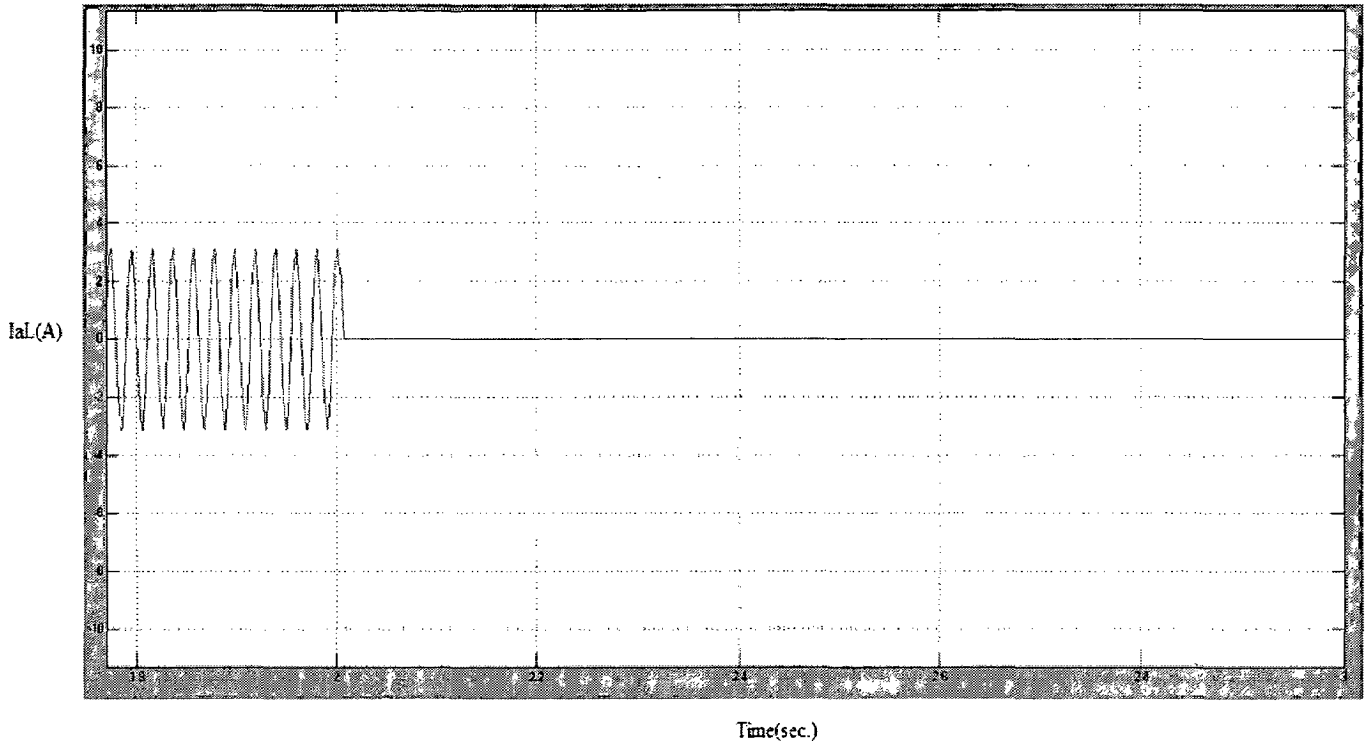

Time(sec.)
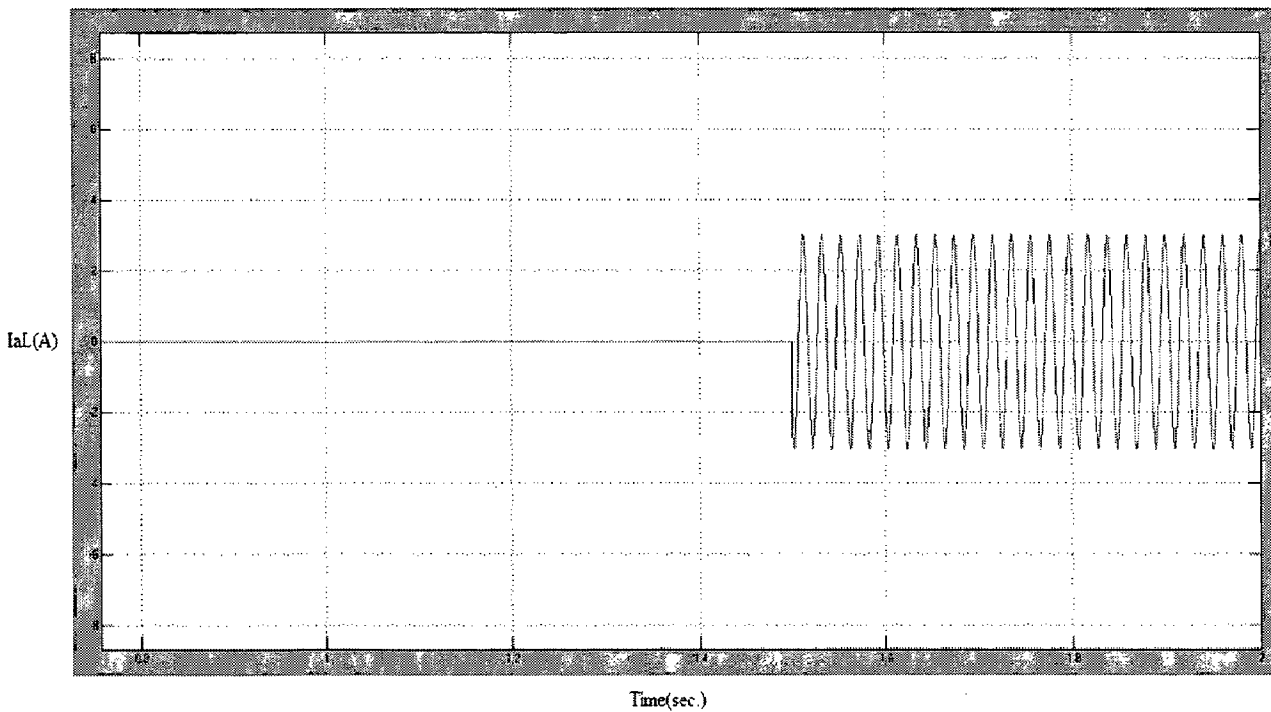
Fig. 4.9: Waveforms of main load current of line-A due to sudden application of resistive load

37
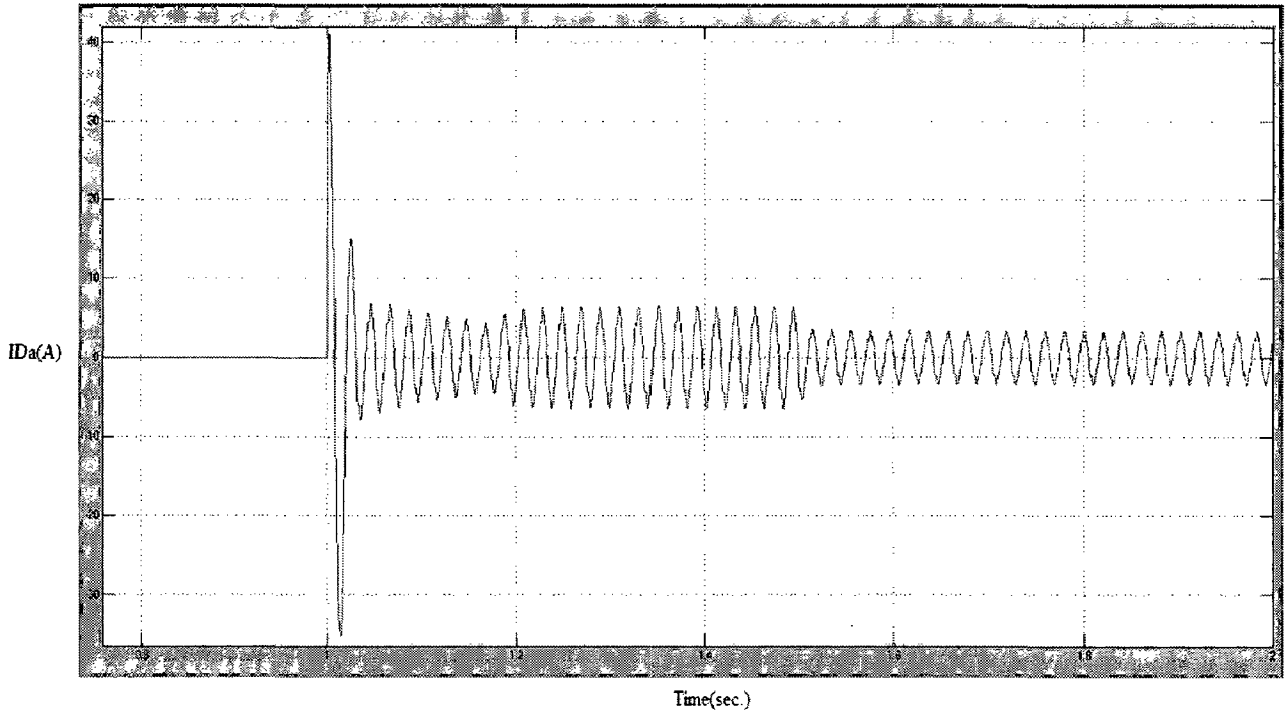
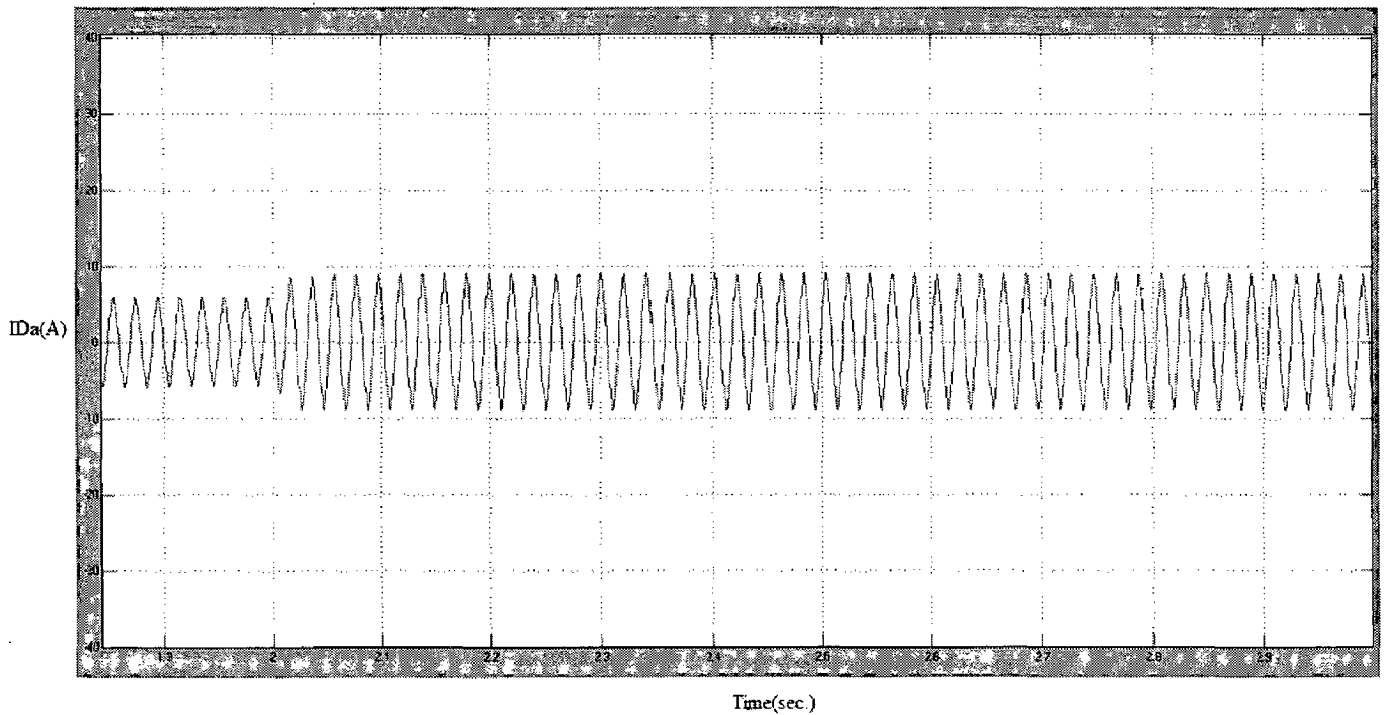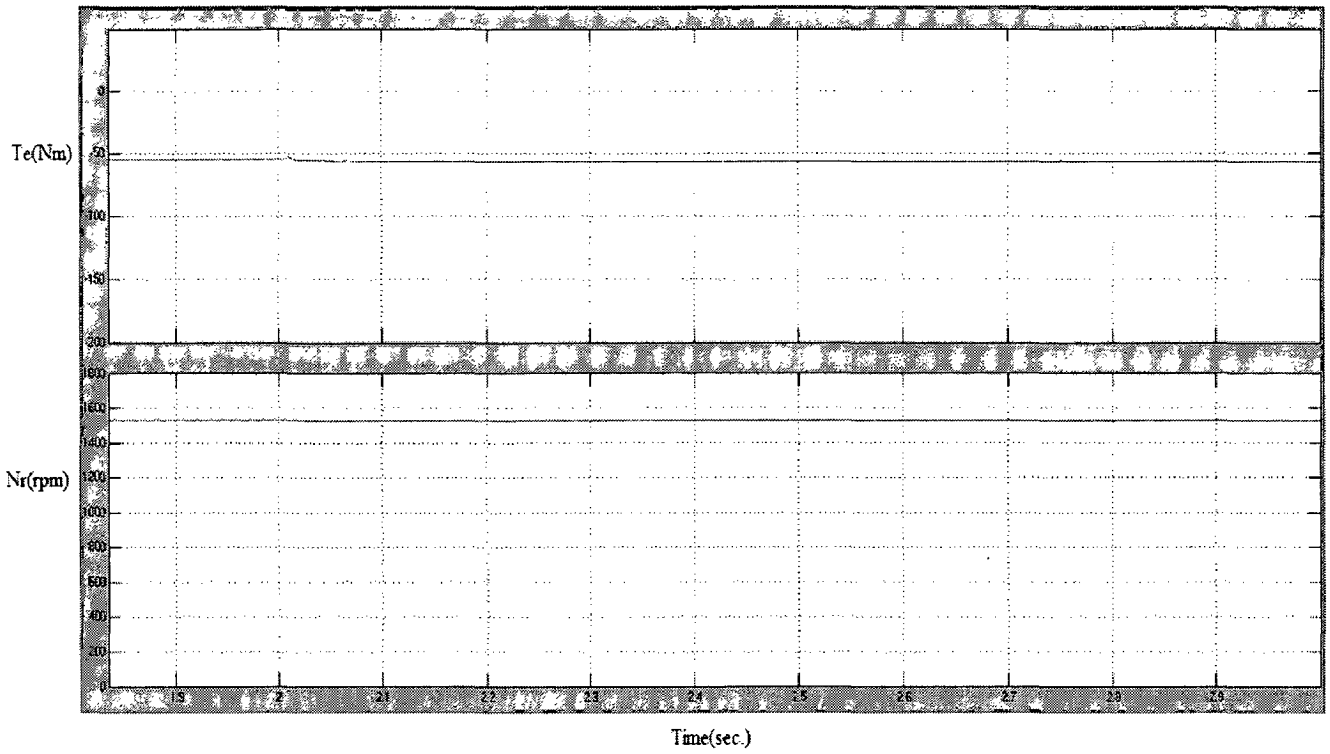**Fig. 4.10: Waveforms of ELC current of line-A due to sudden application of resistive load**
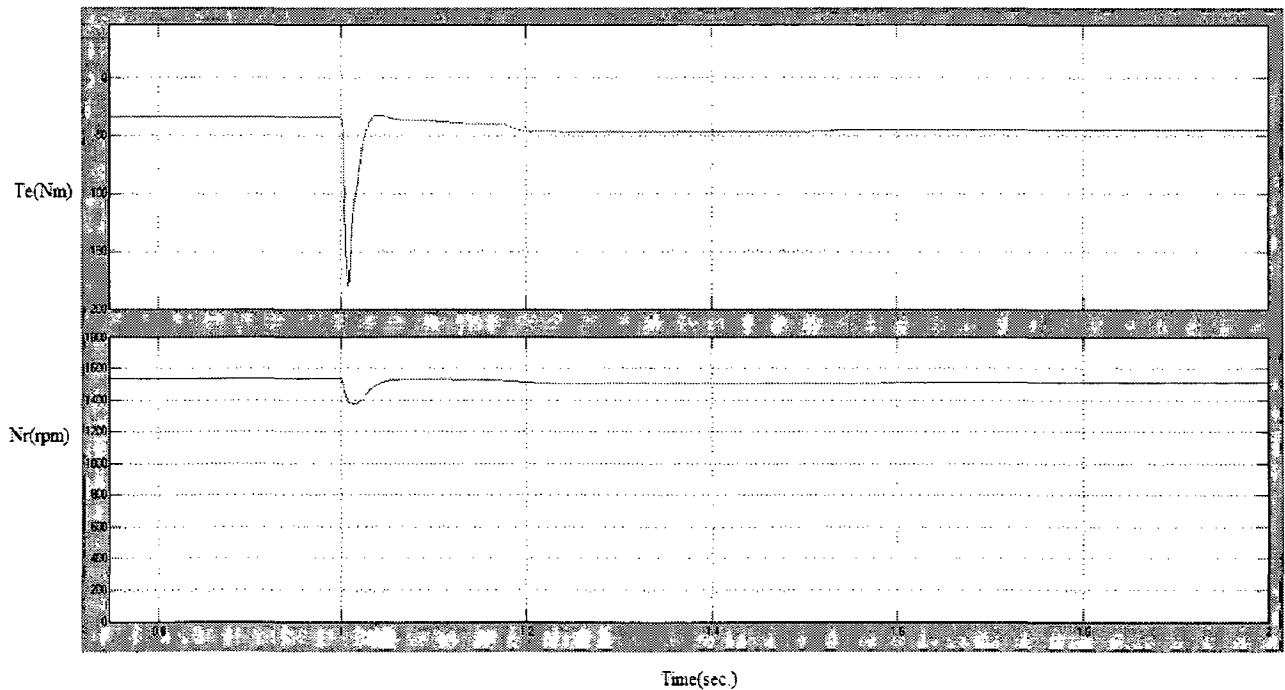
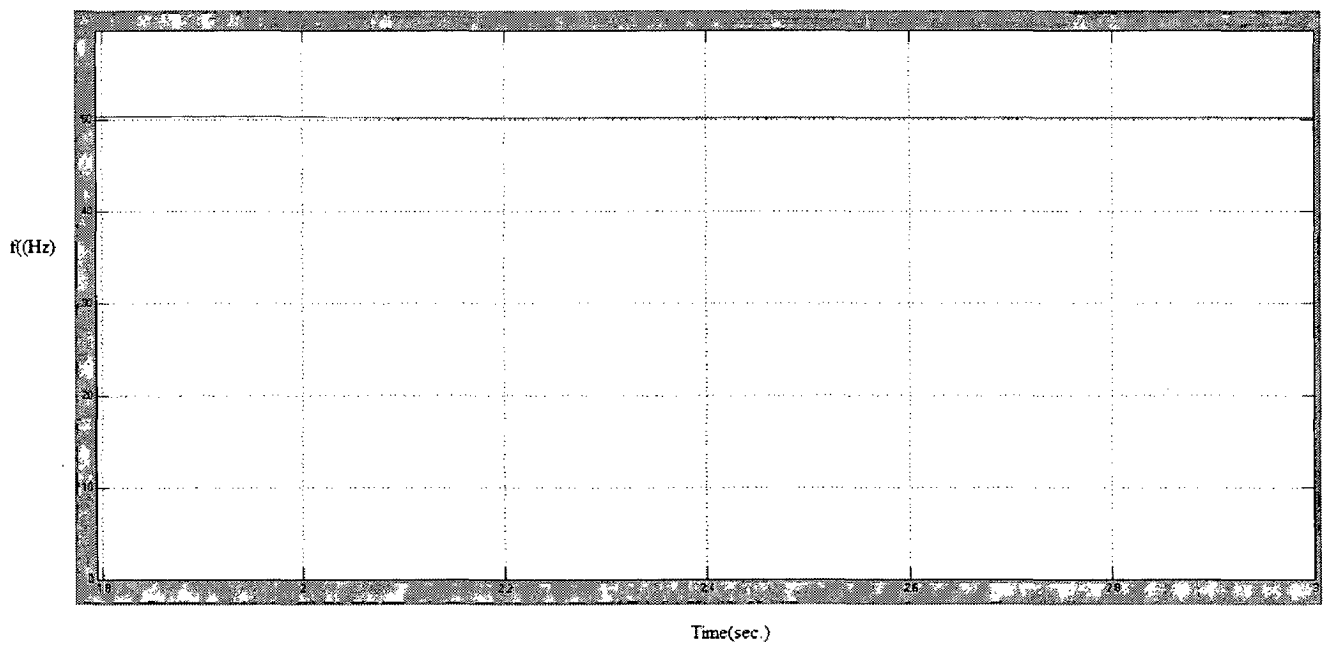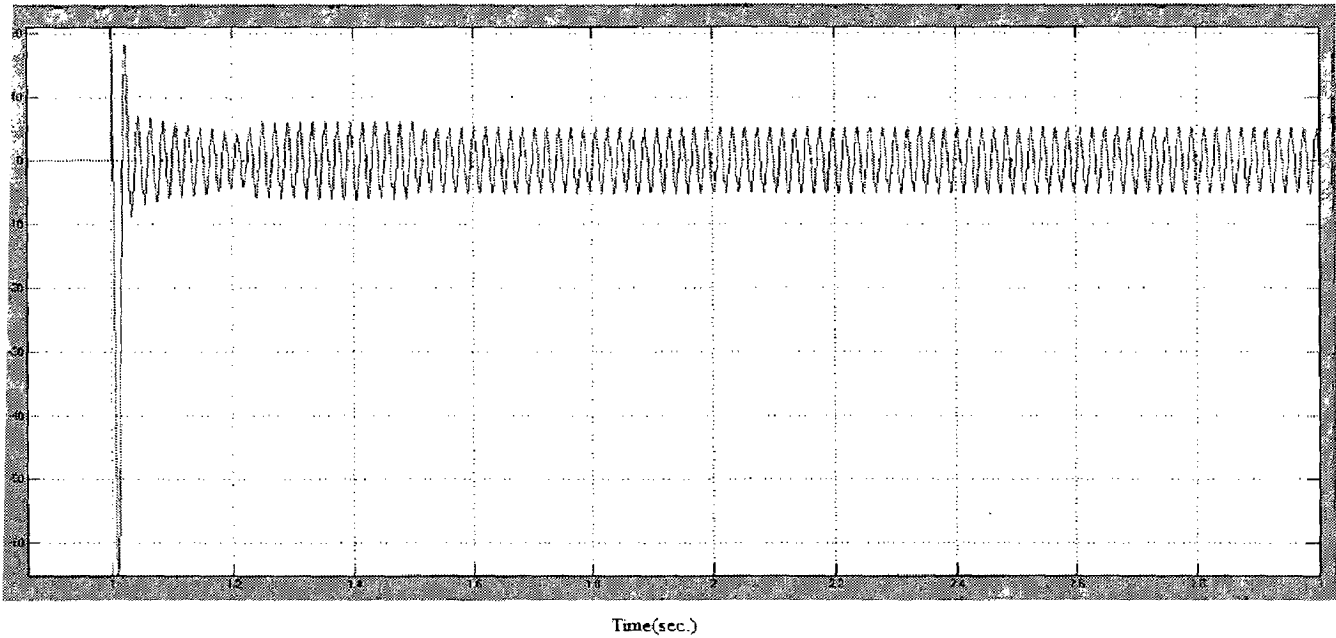**Fig. 4.11: Electromagnetic torque and rotor speed in SEIG due to sudden application of resistive load**

38
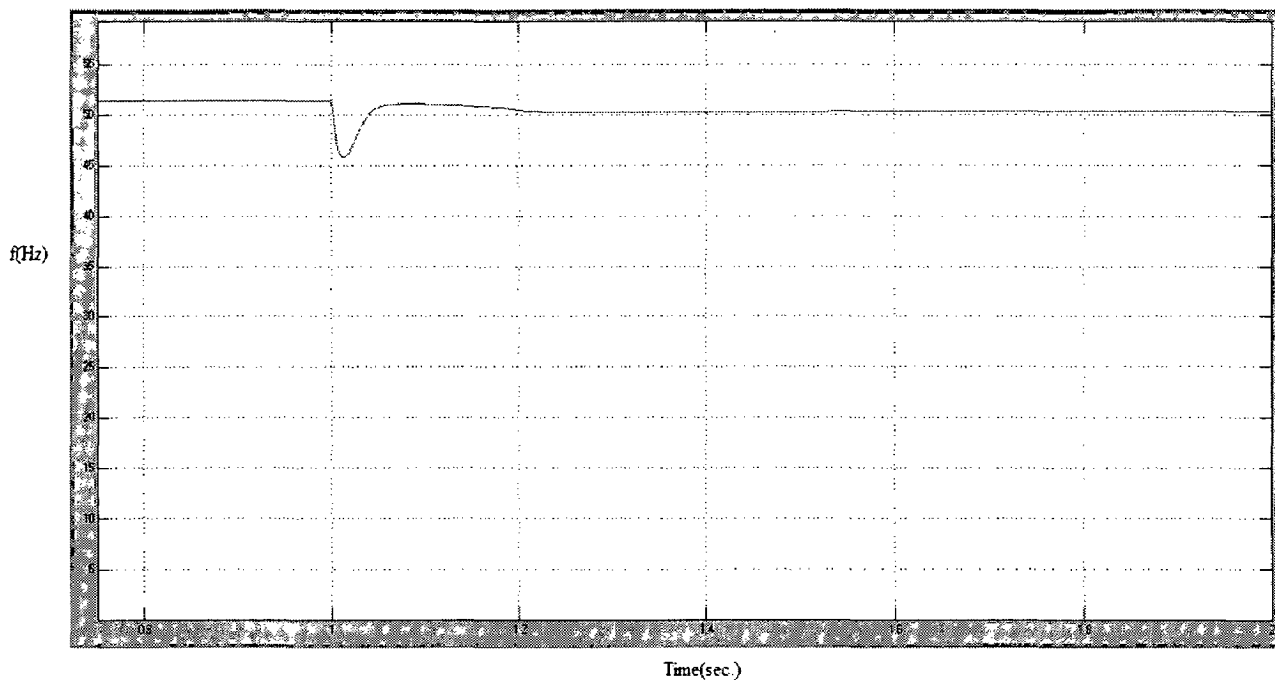
Fig. 4.12: Frequency of generated voltage due to sudden application of resistive load

(ii)   Sudden Removal

Initially SEIG-ELC system is operated with 1500 W resistive load. Suddenly resistive load of 1500 W is removed at t= 2 sec from the SEIG terminals.

The waveforms due to the removal of resistive load of 1500 W at t=2 sec. are shown in Figs. 4.13 to 4.18. In this case, the line voltages and currents and the output voltage of the SEIG remain same after removal of resistive load.

When a resistive load of 1500 W is suddenly removed across the SEIG terminals, it is seen that peak value of the ELC input current of line-A increases. Fig. 4.16 shows ELC current of line-A. The duty cycle of the chopper switch is increased. This indicates that the power is transferred from main load to the dump load and accordingly, the total power supplied by the SEIG remains unchanged. Thus the terminal voltage of the SEIG is maintained constant.
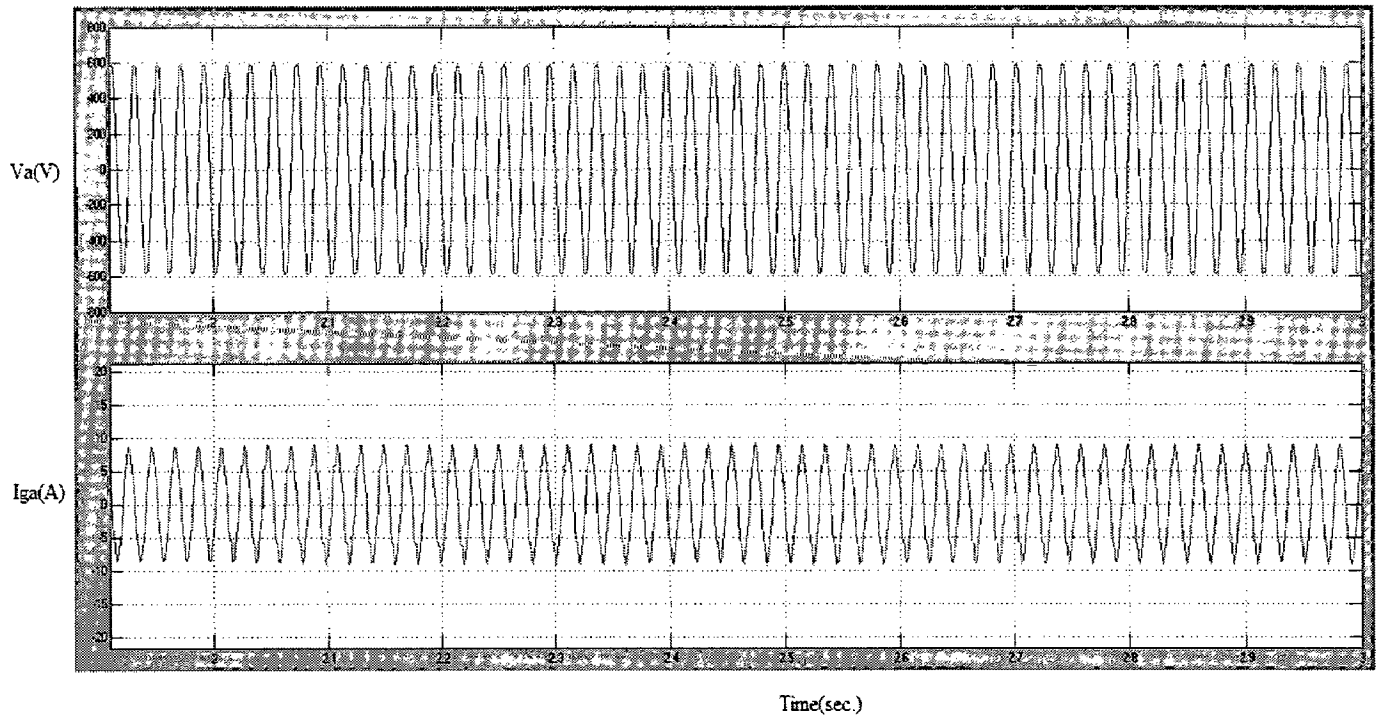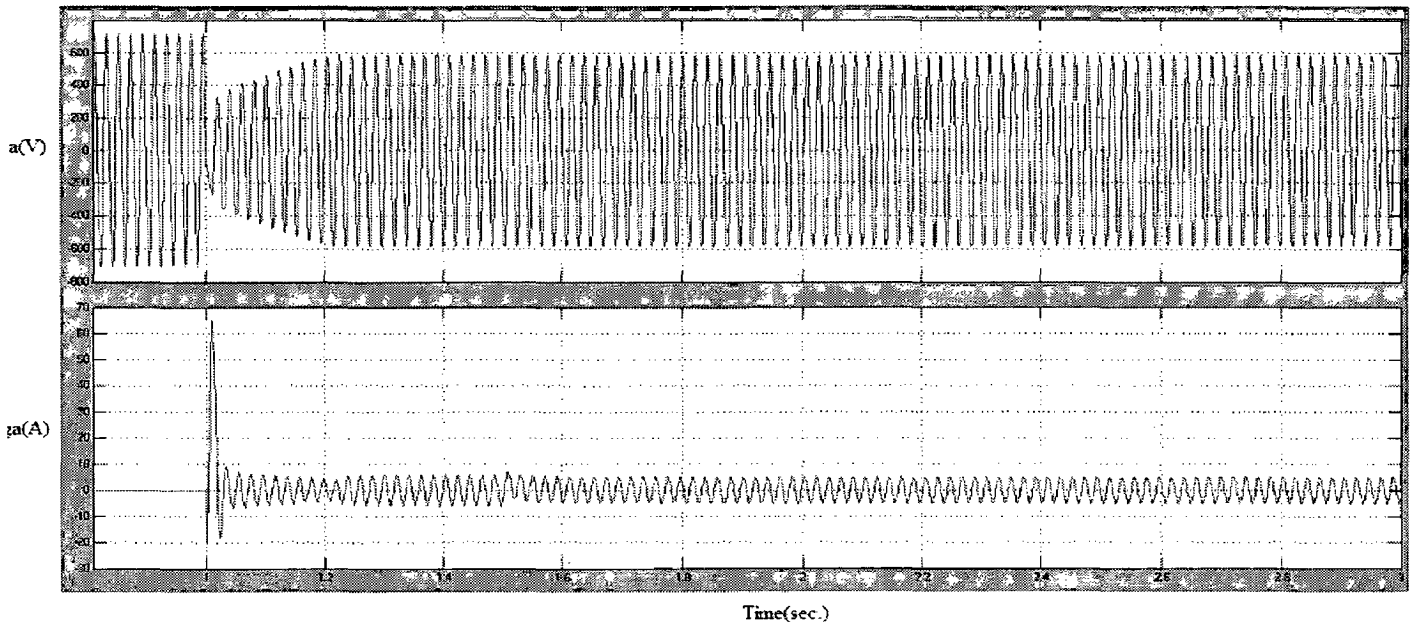
Fig. 4.13: Voltage and current waveforms of line-A at the SEIG terminals due to sudden removal of resistive load
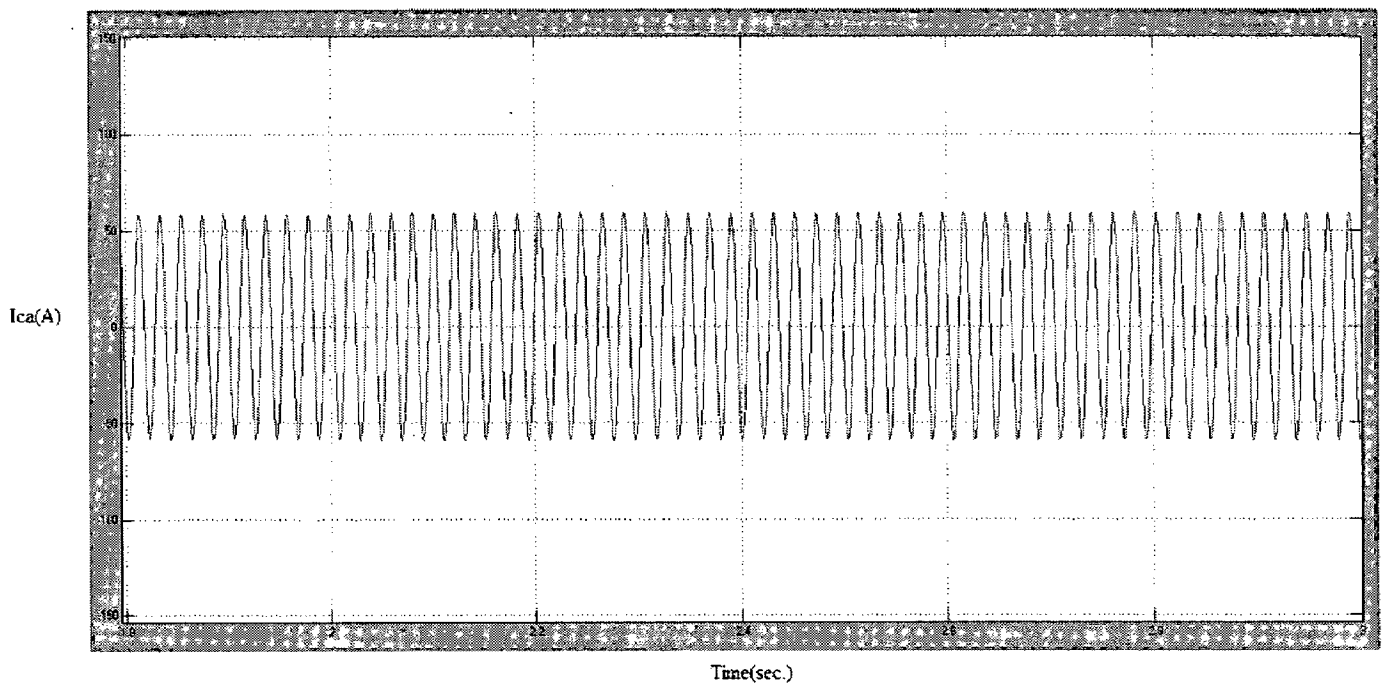
Fig. 4.14: Capacitor current of line-A at due to sudden removal of resistive load
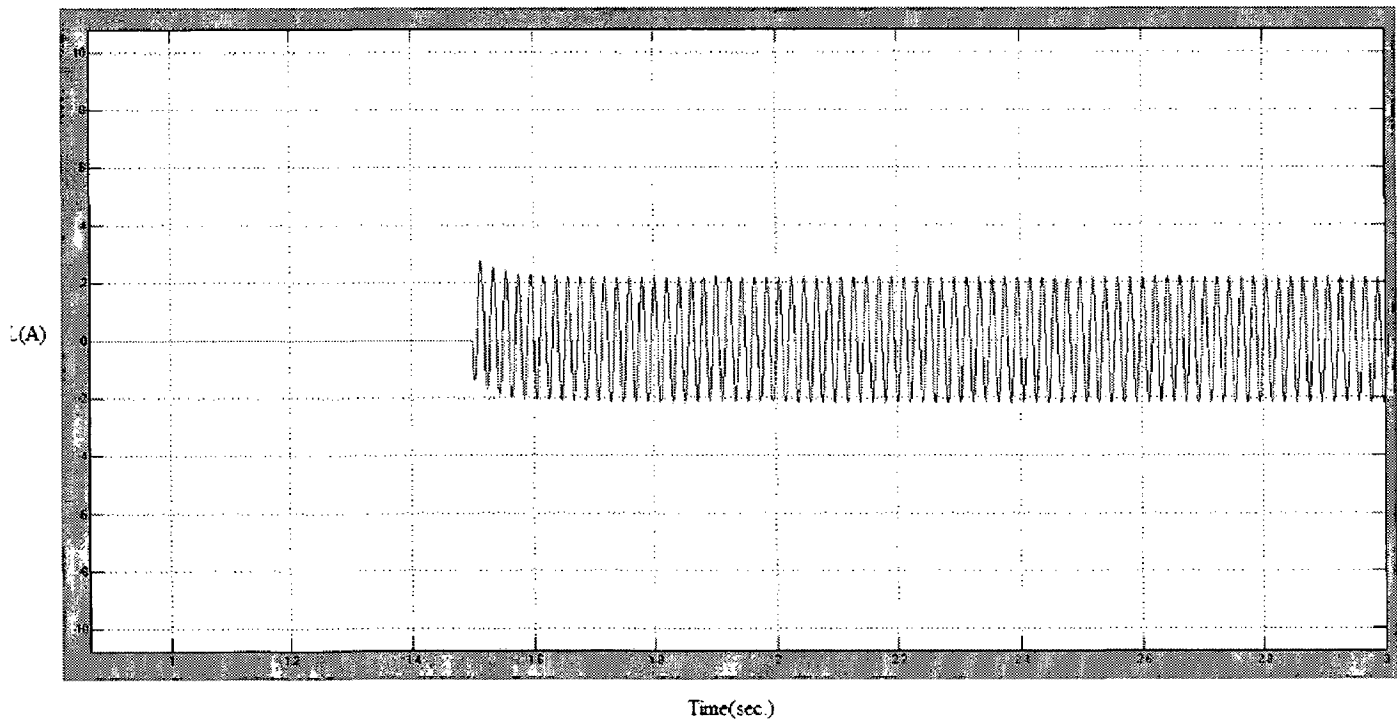
40

Fig. 4.15: Waveforms of main load current of line-A due to sudden removal of resistive load
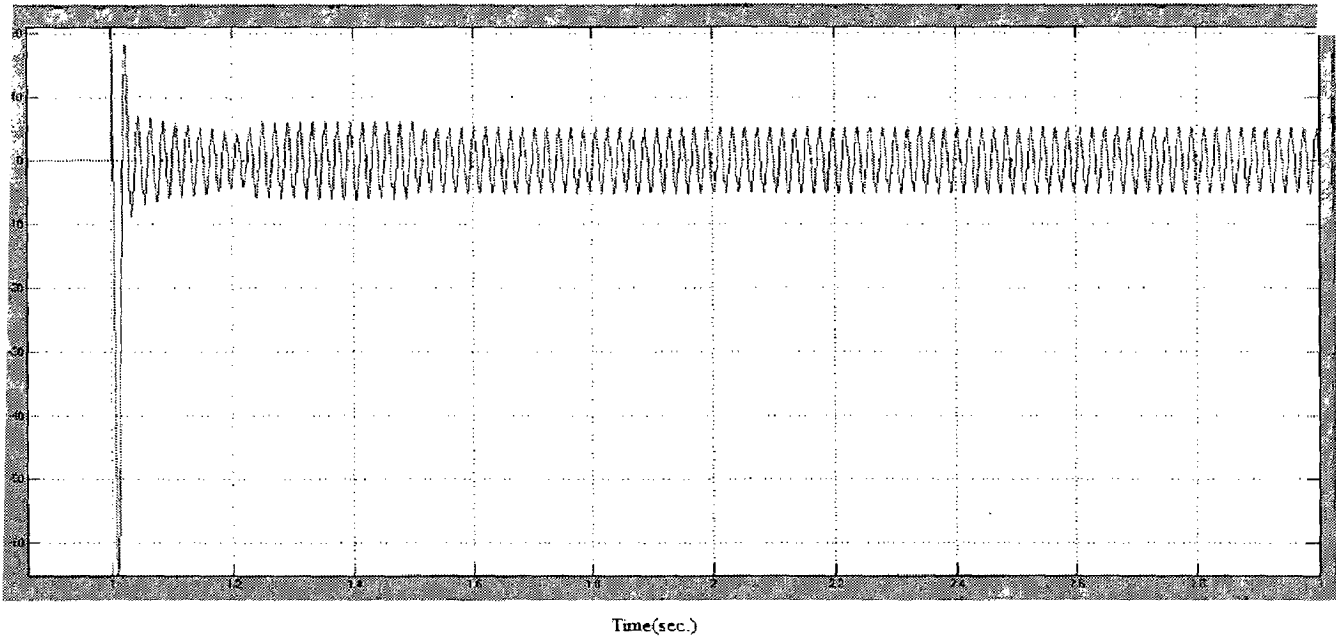

Fig. 4.16: Waveforms of ELC current of line-A due to sudden removal of resistive load

41

Fig. 4.17: Electromagnetic torque and rotor speed in SEIG due to sudden removal of resistive load

Time(sec.)

Fig. 4.18: Frequency of generated voltage due to sudden removal of resistive load

42

Time(sec.)

Fig. 4.24: Waveforms of ELC current of line-A due to sudden application of IM load

Time(sec.)

**Fig. 4.25: Electromagnetic torque and rotor speed in SEIG due to sudden application of IM load**

46
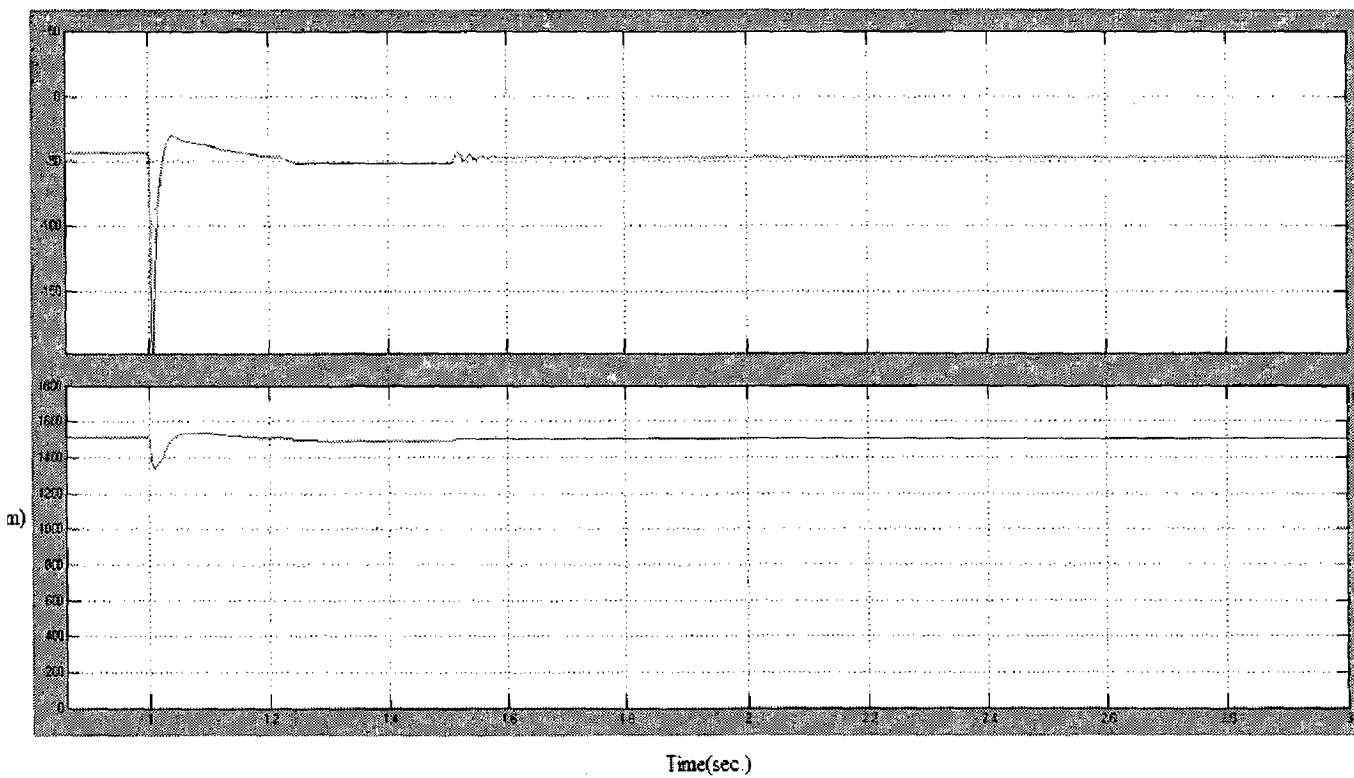
dicating that the power is transferred from dump load to motor load and the total power ipplied by the SEIG remains unchanged.
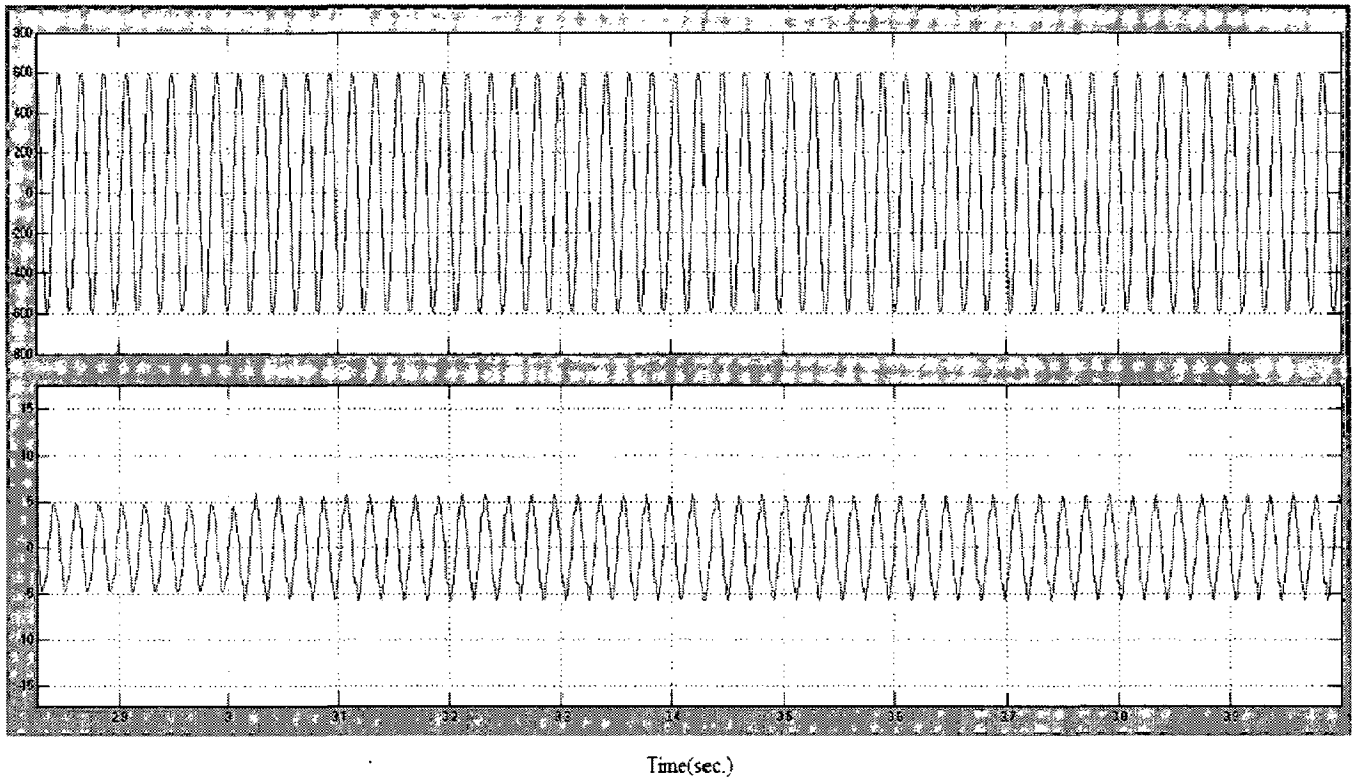

Fig. 4.20: Voltage and current waveforms of line-A at the SEIG terminals due to sudden application of IM load
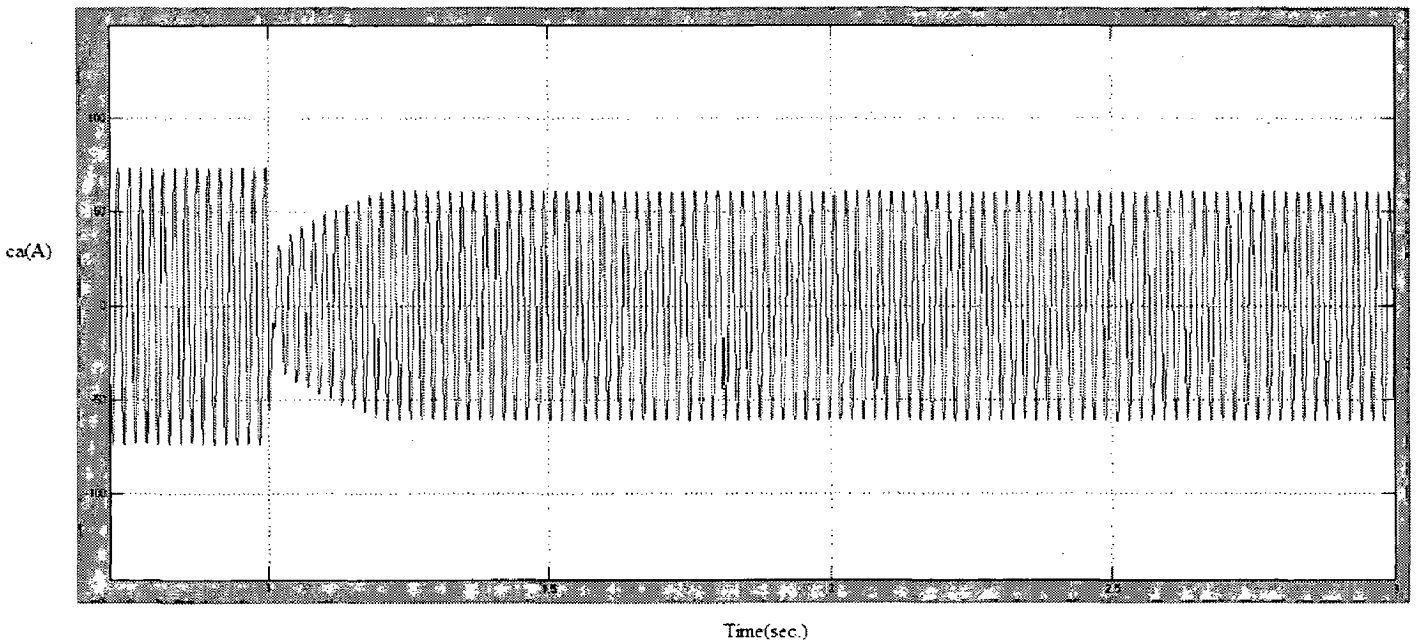
Fig. 4.21: Capacitor current of line-A at due to sudden application of IM load

44
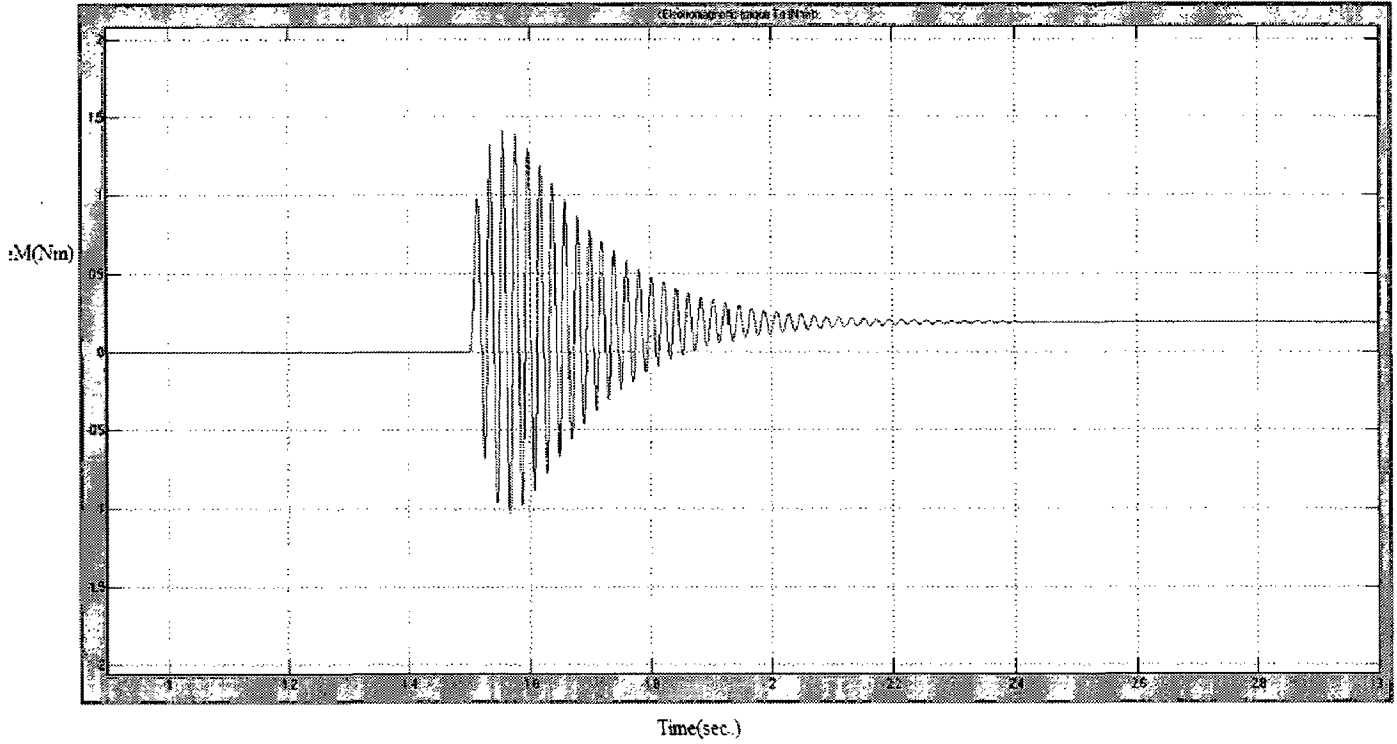
Fig. 4.22: Electromagnetic torque developed in IM load

Fig. 4.23: Waveforms of main load current of line-A due to sudden application of IM load

45

Time(sec.)

Fig. 4.24: Waveforms of ELC current of line-A due to sudden application of IM load

Time(sec.)

Fig. 4.25: Electromagnetic torque and rotor speed in SEIG due to sudden application of IM load

Time(sec.)
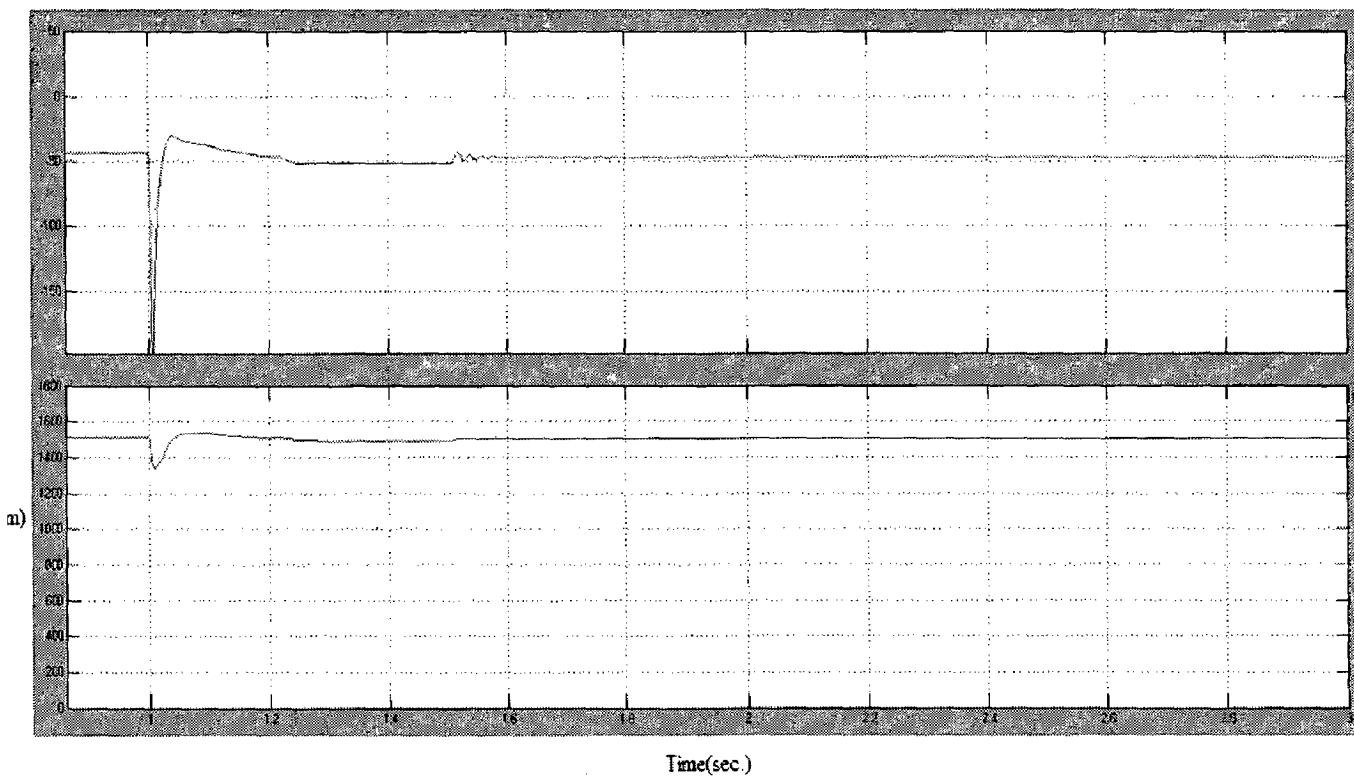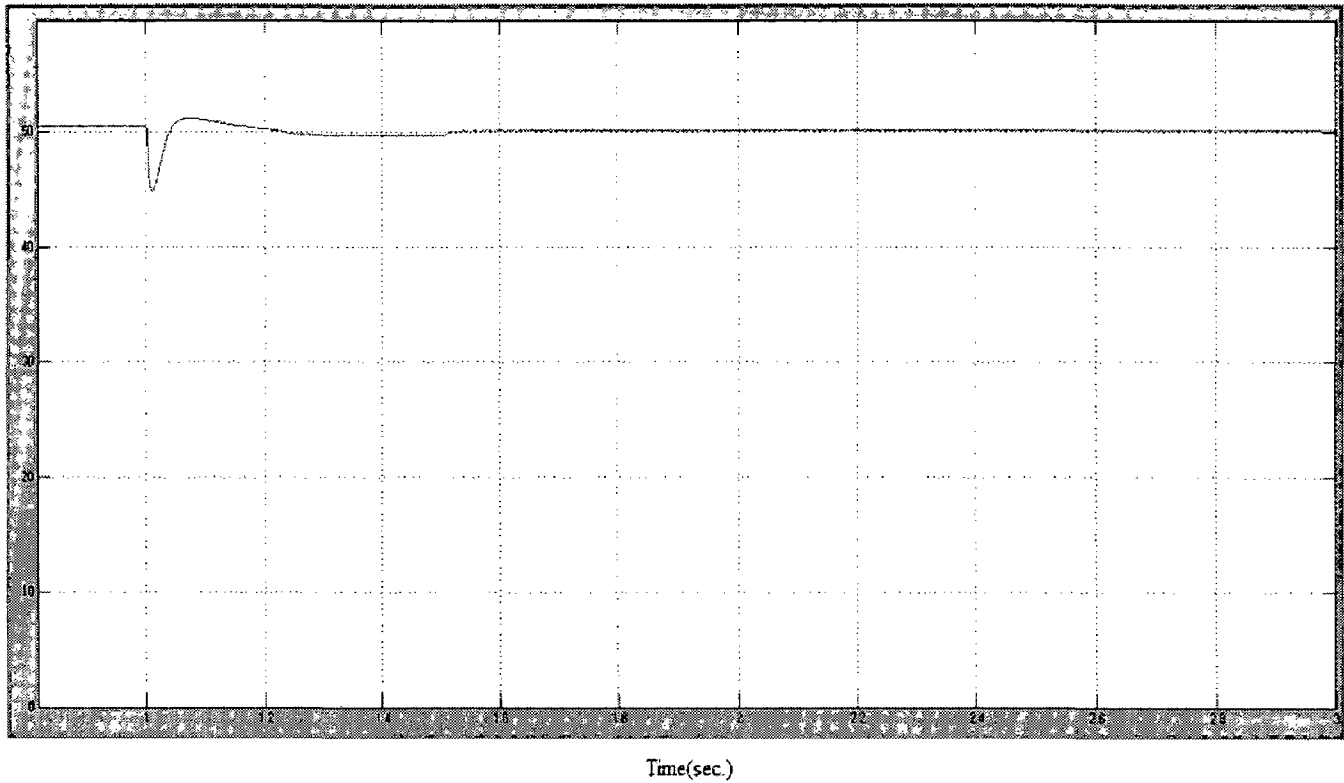
Fig. 4.26: Frequency of generated voltage due to sudden application of IM load

Sudden Removal:

Initially SEIG is feeding IM load. At t =3 sec. IM load is suddenly removed from SEIG terminals. Waveforms corresponding to sudden removal of motor load at t=4 are given in Figs. 4.27 to 4.33.

Fig. 4.27 shows that the voltage at SEIG terminal remains same after removal of ɔr load.

Capacitor current of line-A is shown in the Fig. 4.28 which remain same after the ɔval of dynamic load.

After removal of IM load, ELC current increases which is shown in Fig. 4.31. ll fluctuation in torque, rotor speed and frequency are depicted in Figs. 4.32-4.33.

47

Fig. 4.27: Voltage and current waveforms of line-A at the SEIG terminals due to sudden removal of IM load

Time(sec.)
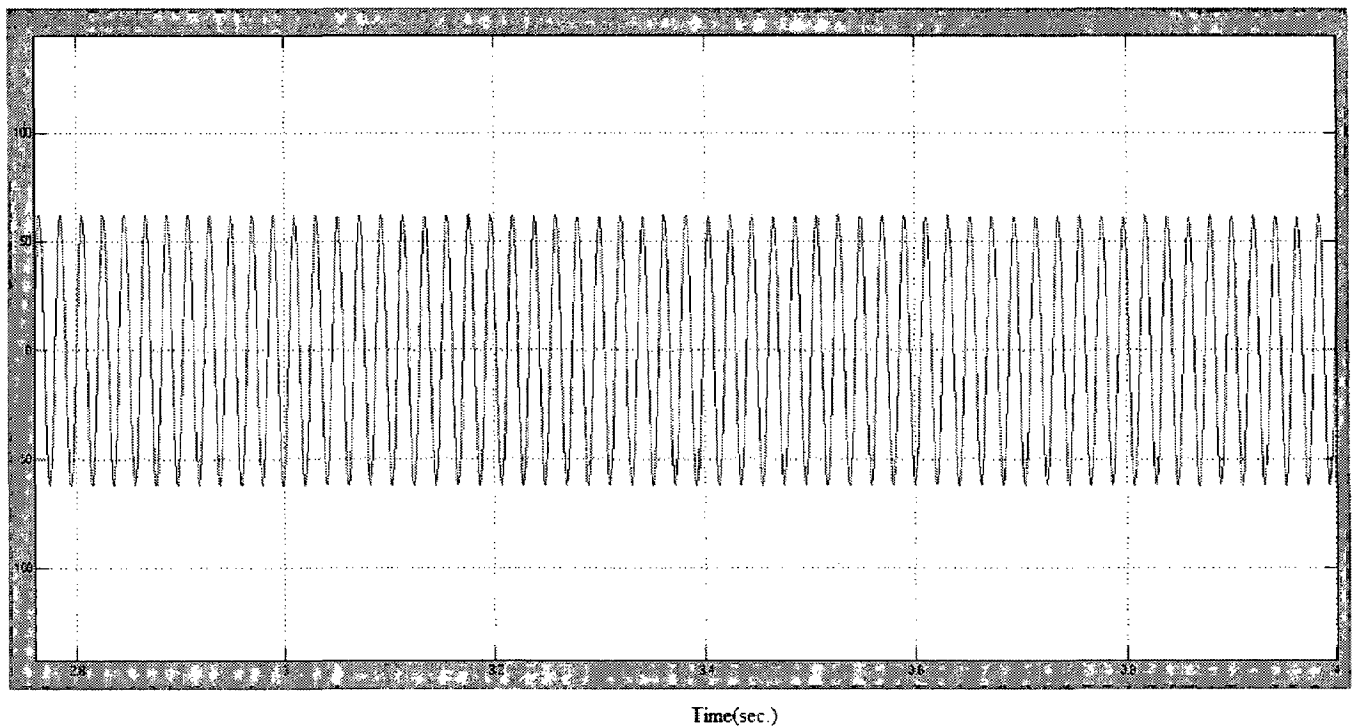
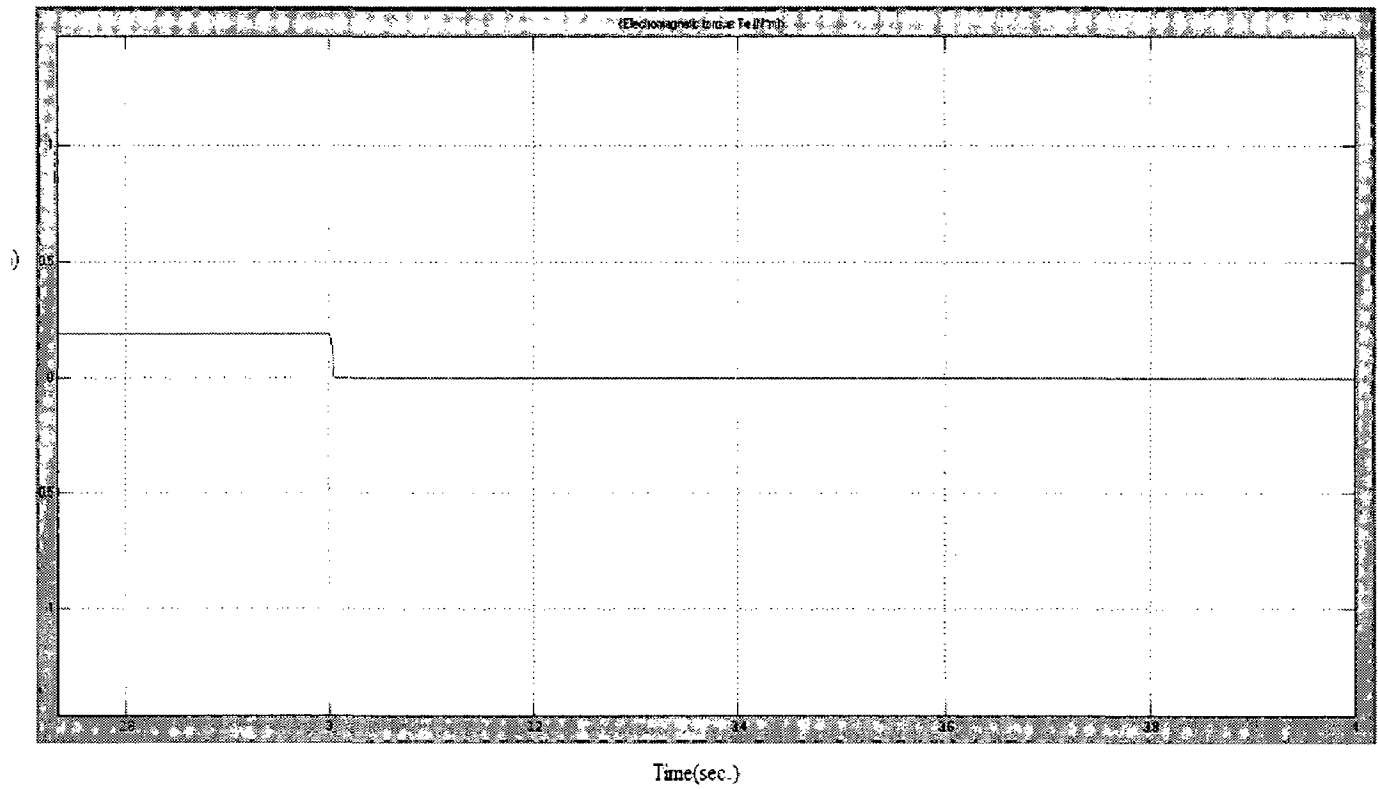**Fig. 4.28: Capacitor current of line-A at due to sudden removal of IM load**

48

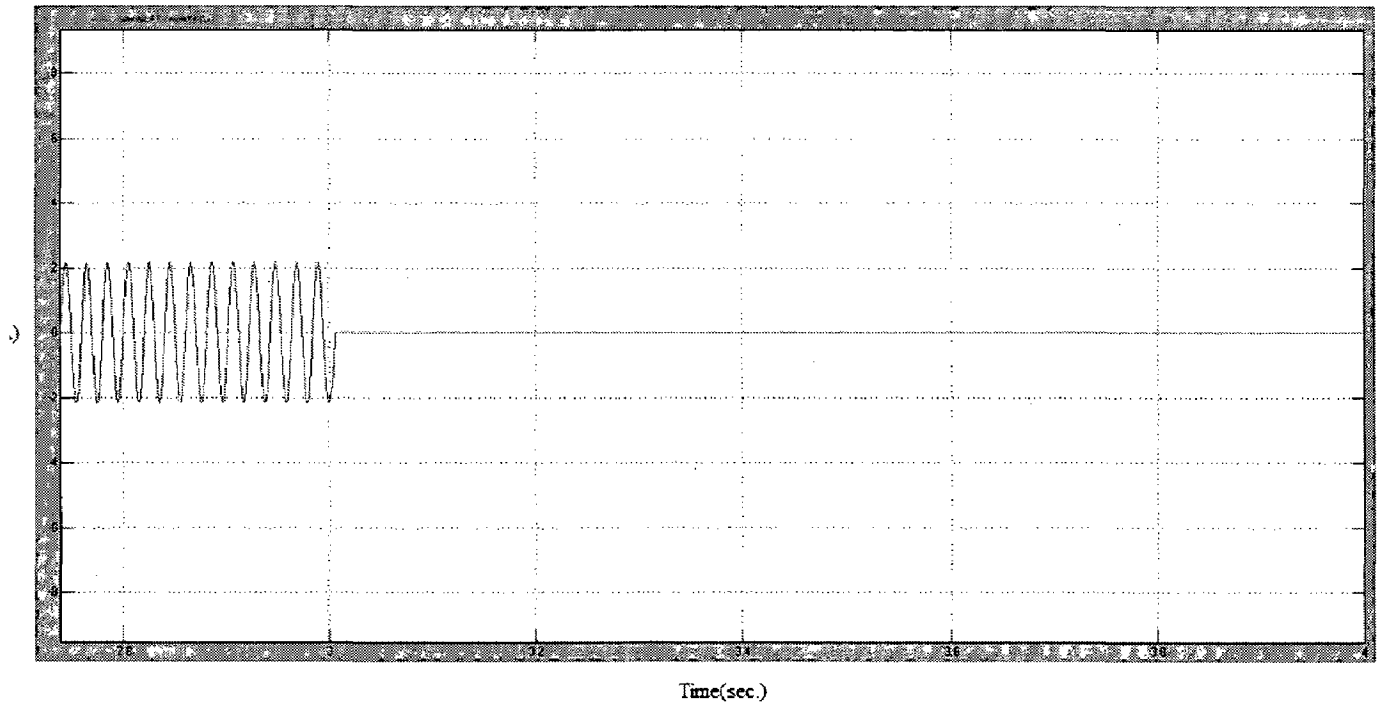**Fig. 4.29: Electromagnetic torque in IM load**

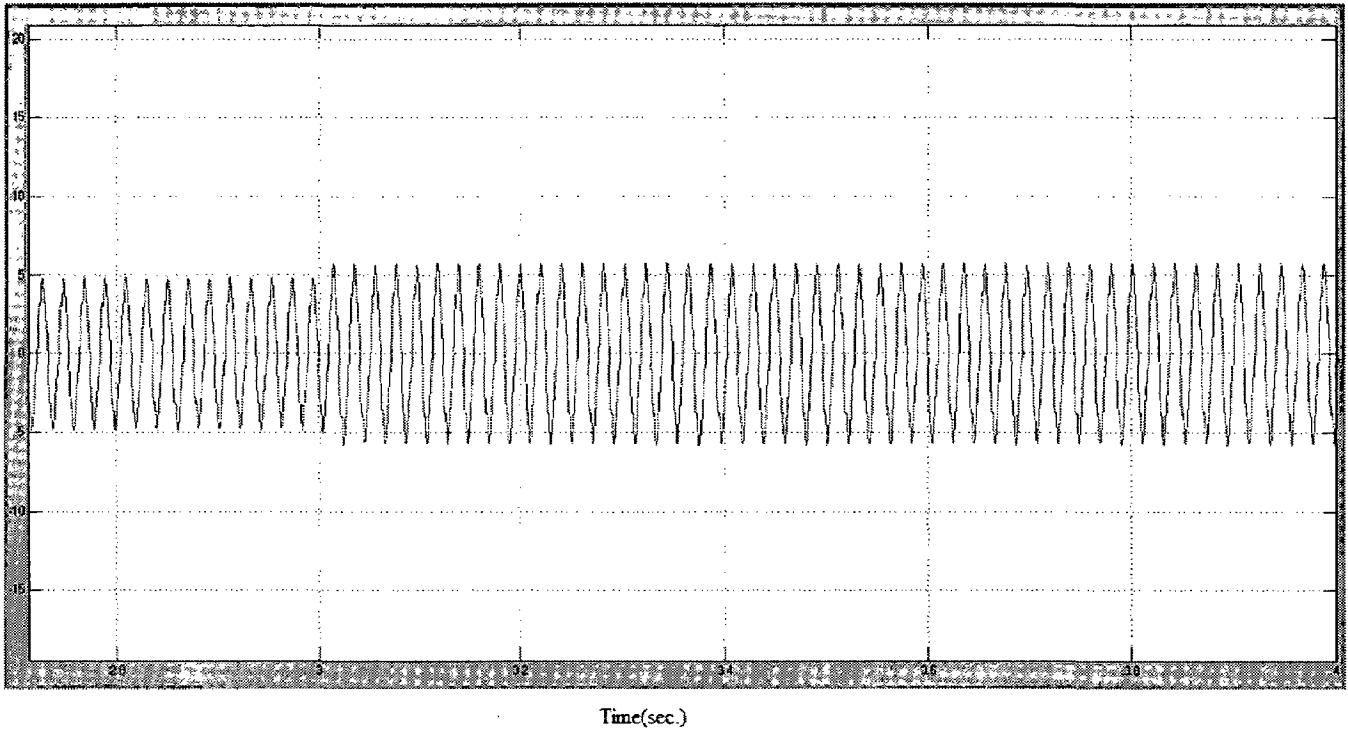**Fig. 4.30: Waveforms of main load current of line-A due to sudden removal of IM load**

49

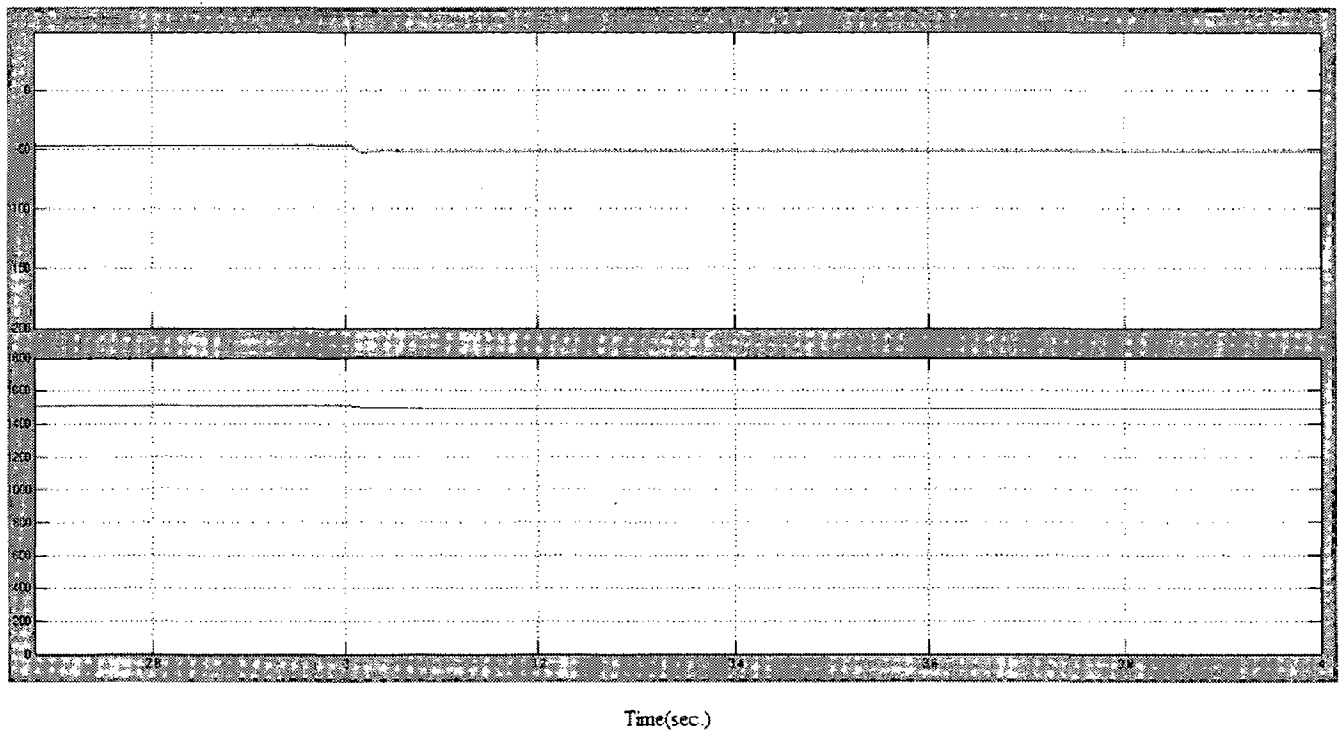**Fig. 4.31: Waveforms of ELC current of line-A due to sudden removal of IM load**

Fig. 4.32: Electromagnetic torque and rotor speed in SEIG due to sudden removal of IM load
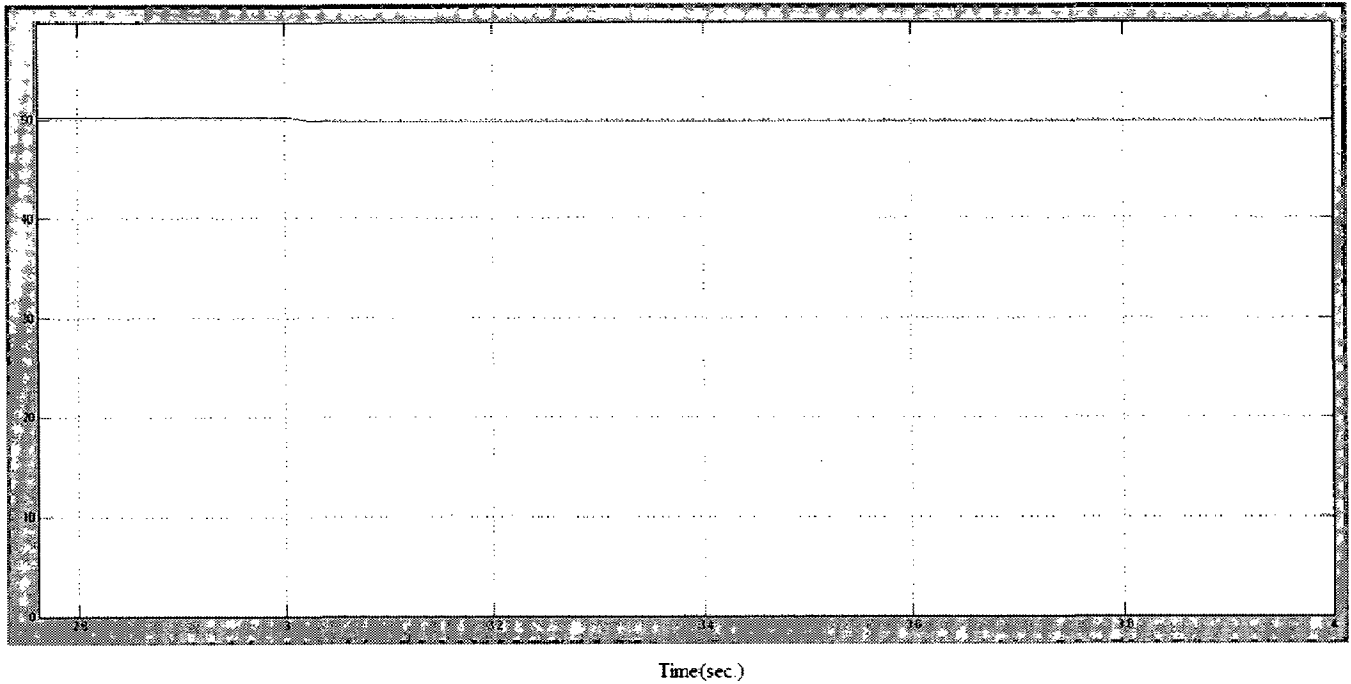
50

Time(sec.)

Fig. 4.33: Frequency of generated voltage due to sudden removal of resistive load

FAULTS:

Transient analysis has been made for three-phase and line-line fault. Simulation ts corresponding to three-phase and line-line faults are discussed as below:

THREE PHASE FAULT:

Initially SEIG is operated with a resistive load of 1500 W. A three phase fault is idered at the load terminals at t=2 sec. Fault is applied for the duration of 0.1 sec. SEIG cannot sustain the short circuit due to failure of excitation and the voltage ipses to zero immediately without any transient as shown in Figs. 4.34-4.35. A ent surge of 7000 A is observed during first cycle of load current as shown in 1.36. This current surge reduces to a very low value due to the voltage collapse. ELC ent reduces to zero during fault and process of voltage build up after the clearance of ., as shown in Fig. 4.37.

51

Voltage rebuild up takes more time due to the weakening of residual magnetism he longer duration fault. Rated voltage is again re-build up at SEIG terminals in nd 0.4 sec after the clearance of fault. Electromagnetic torque, rotor speed and jency increases considerably during three phase fault and depicted in Figs. 4.38-4.39.
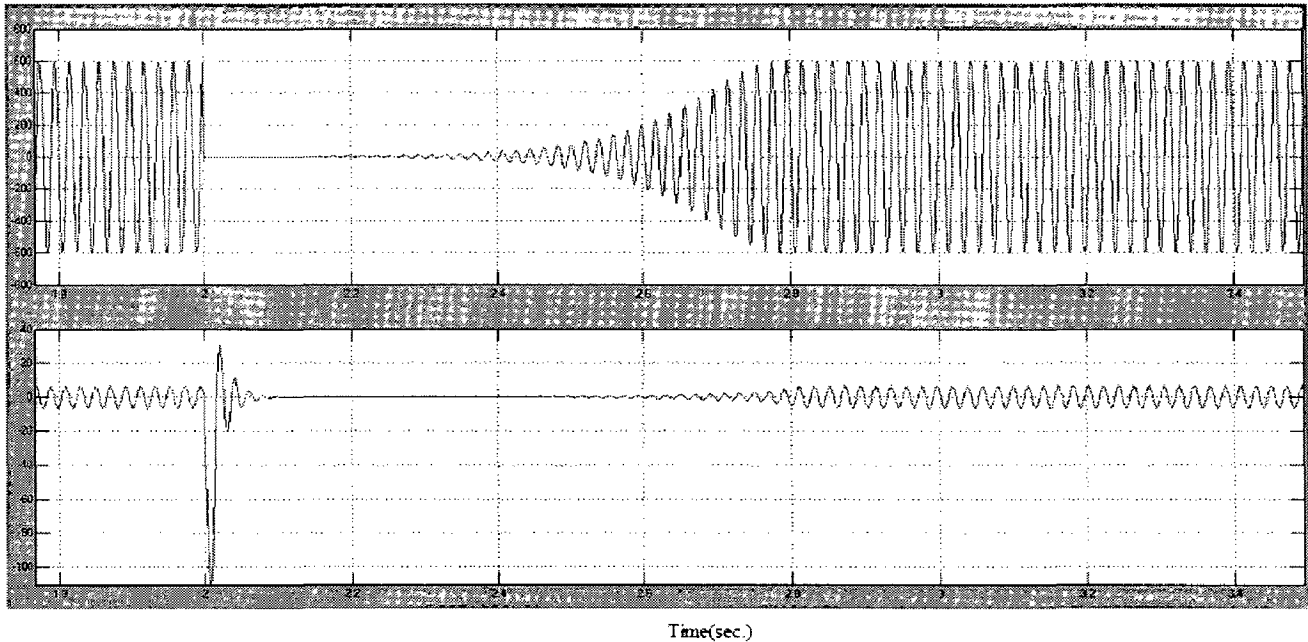

Time(sec.)

Fig.4.34: Voltage and current waveforms of line-A of SEIG due to sudden application and removal of three phase fault
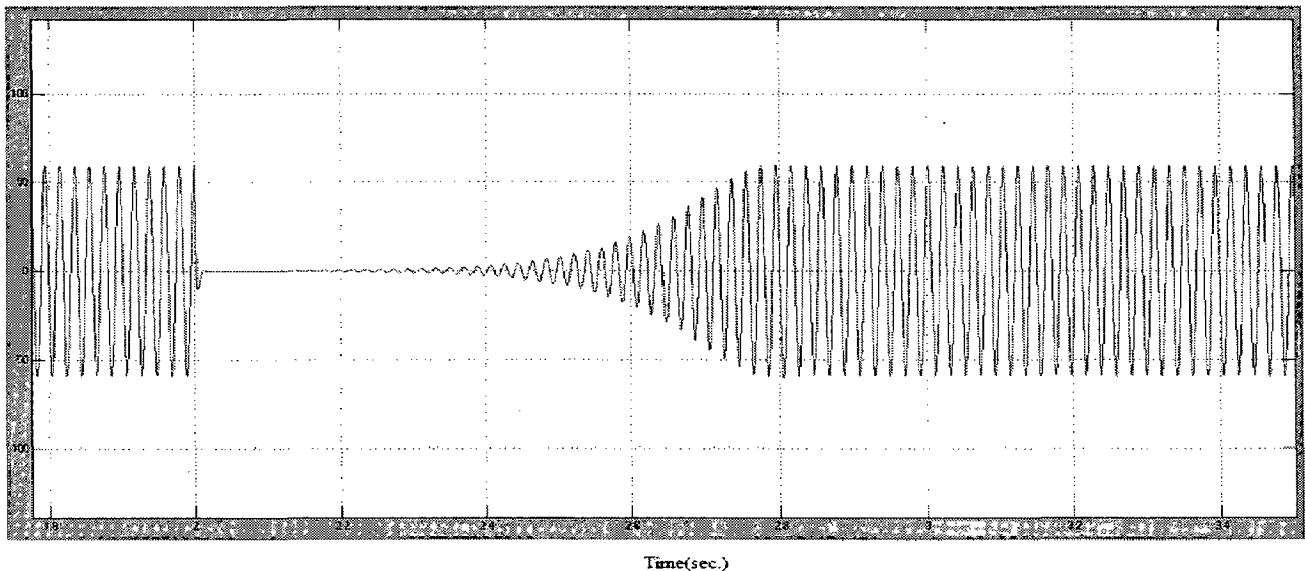

Time(sec.)

Fig.4.35: Capacitor current of line-A due to sudden application and removal of three phase fault
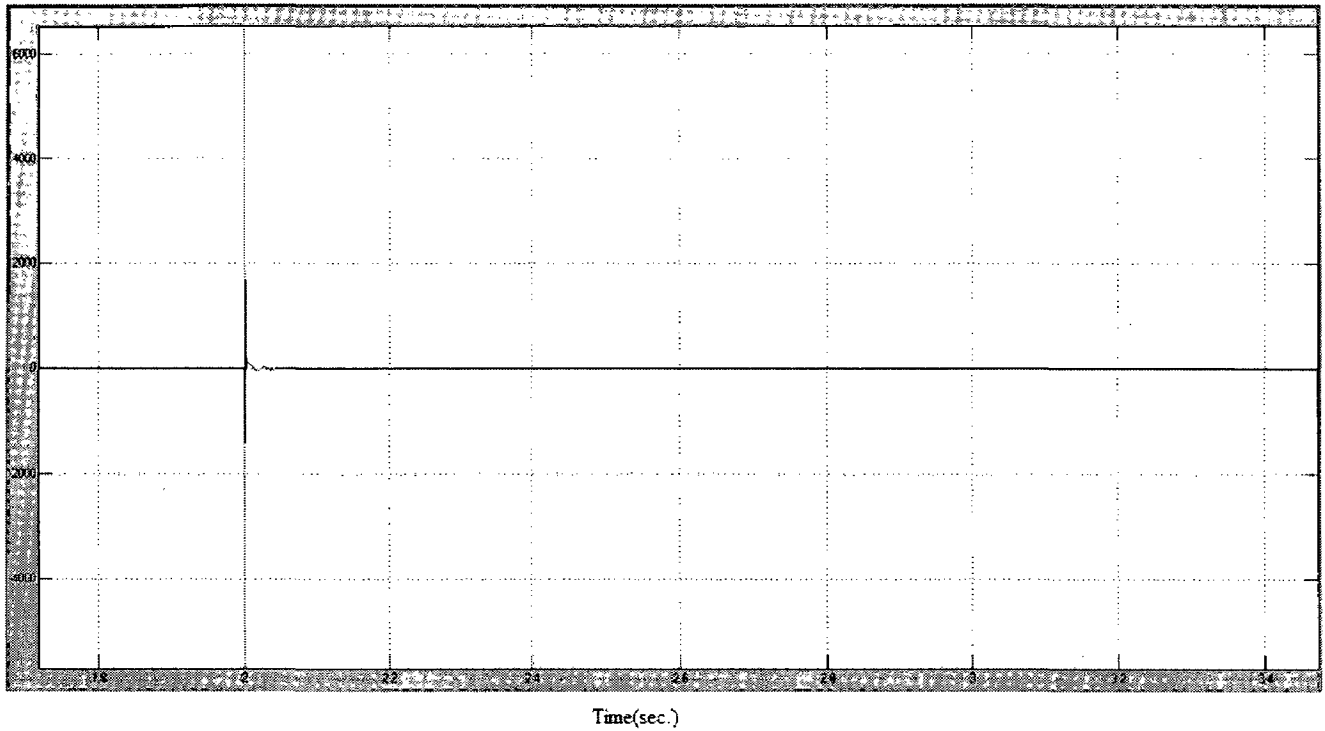
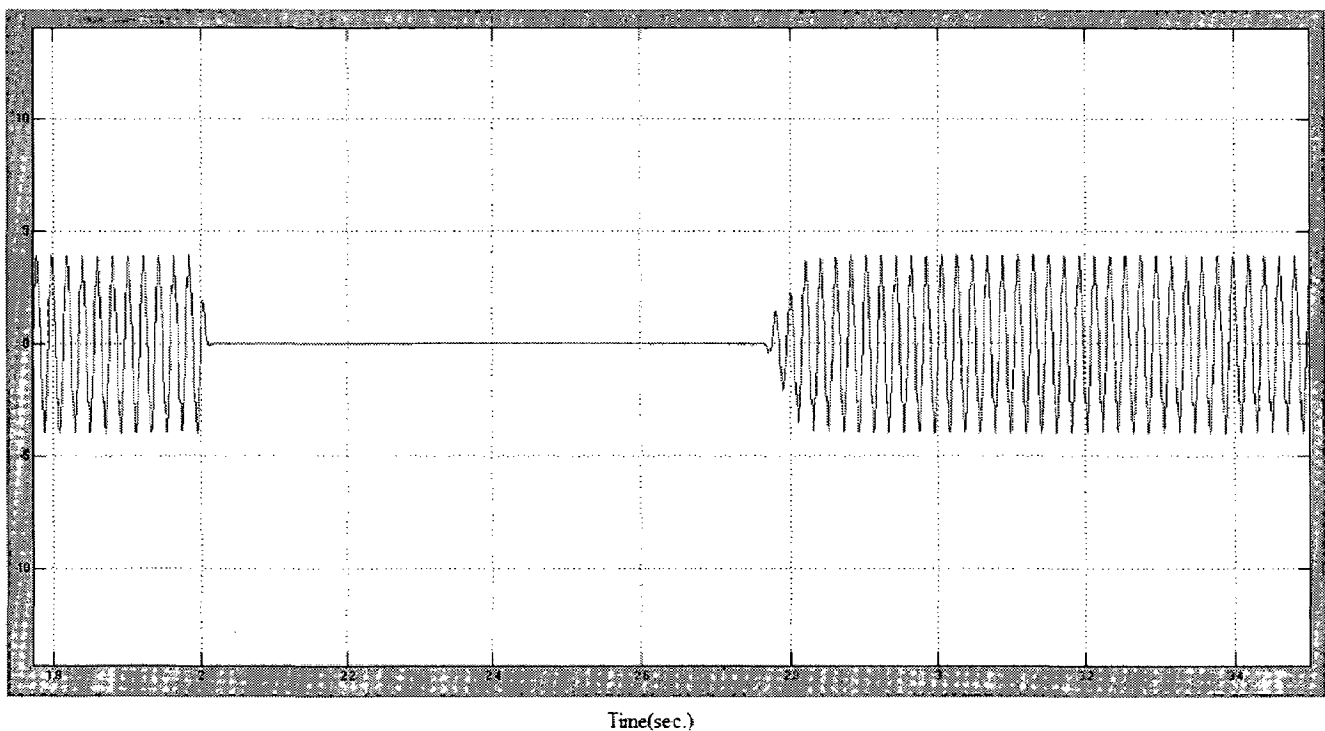**Fig. 4.36: Waveforms of main load current of line-A due to sudden application and removal of three phase fault**

Fig. 4.37: Waveforms of ELC current of line-A due to sudden application and removal of three phase fault
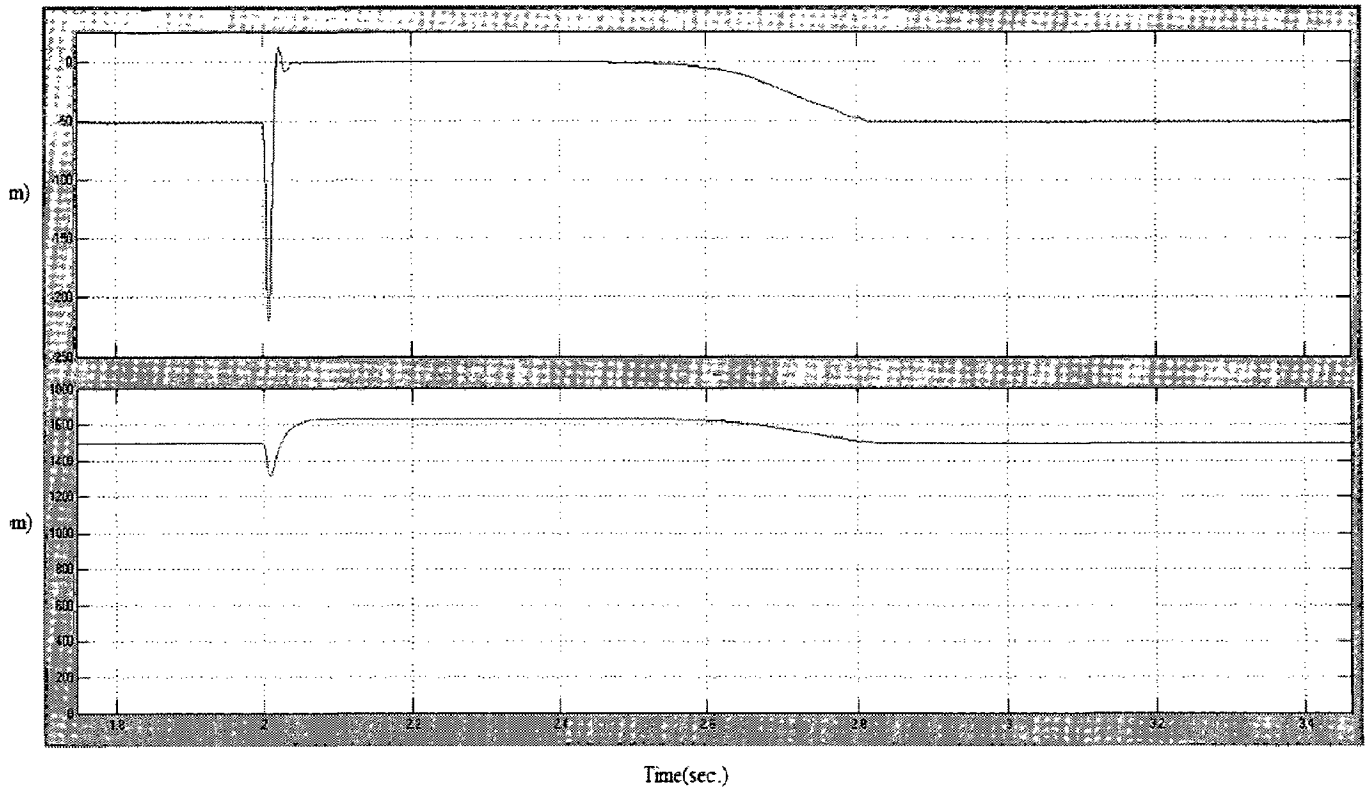
53

Fig. 4.38: Electromagnetic torque and rotor speed in SEIG due to sudden
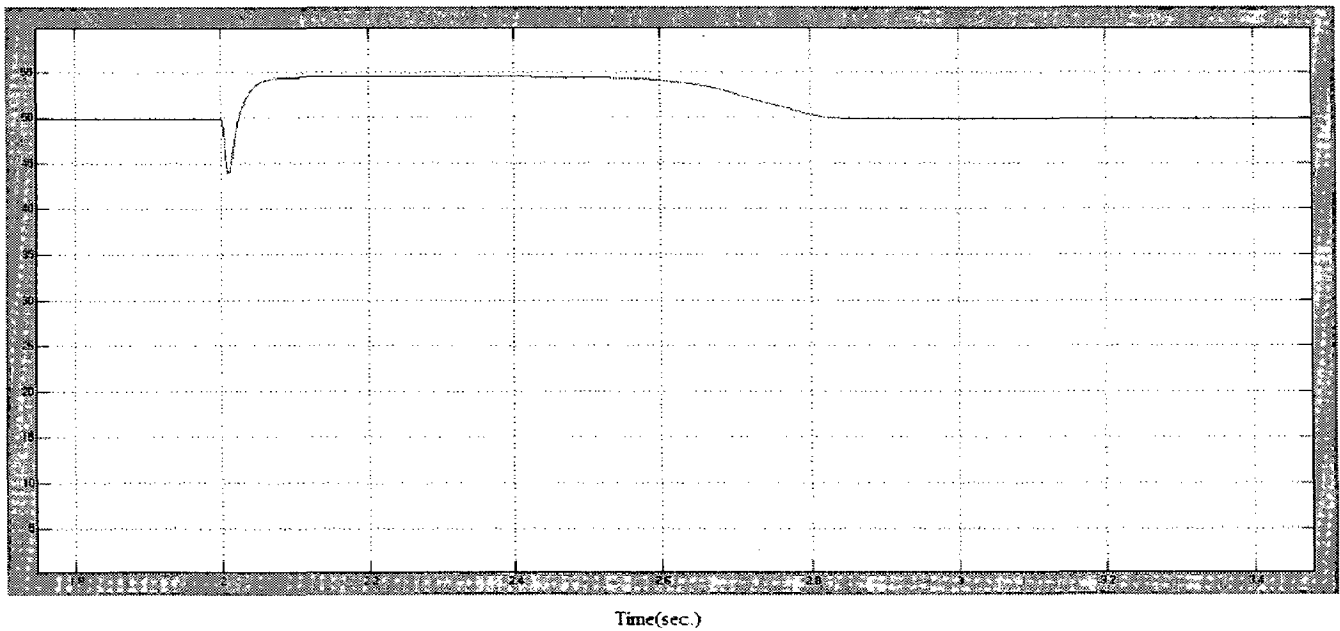application and removal of three phase fault

Fig. 4.39: Frequency of generated voltage due to sudden application and
removal of three phase fault

54

Line to Line Fault:

A line to line short circuit is applied between two lines A and B at the load inals for the duration of 0.1 sec from t = 2 sec. to t = 2.1 sec. The SEIG cannot in the short circuit and the voltage collapses to zero immediately without any ient as shown in the Fig. 4.40.

After the clearance of fault, rated voltage is build up at SEIG terminals in around sec. Capacitor currents also decreases to a small value during line-line fault and /n in the Fig. 4.43.

A current surge of 4500 A is observed during first cycle of load current of line-A line B, which reduces to a very low value due to the voltage collapse and depicted in 4.44. Fig. 4.45 shows the current in the healthy line-C.

Figs. 4.46-4.48 represent the ELC current, electromagnetic torque developed in i, rotor speed and frequency of generated voltage during fault and after the clearance ult.
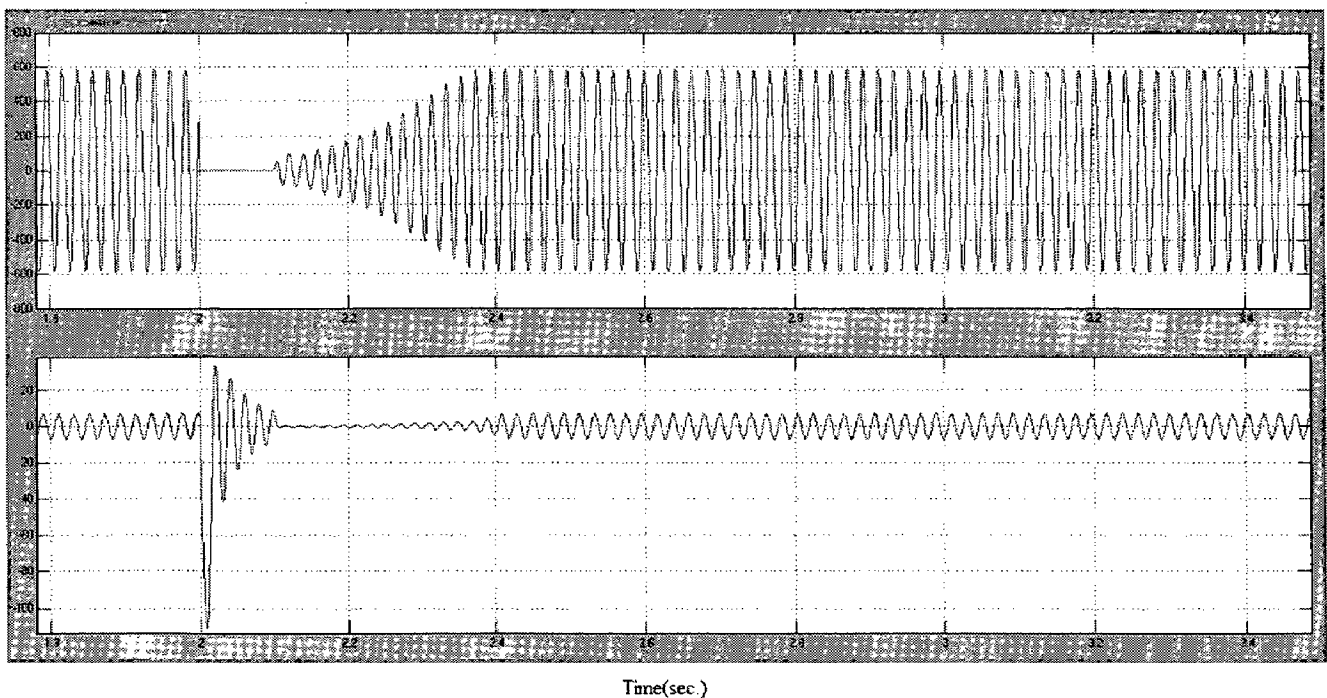

Time(sec.)

Fig.4.40: Voltage and current waveforms of line-A of SEIG due to sudden application and removal of line to line fault
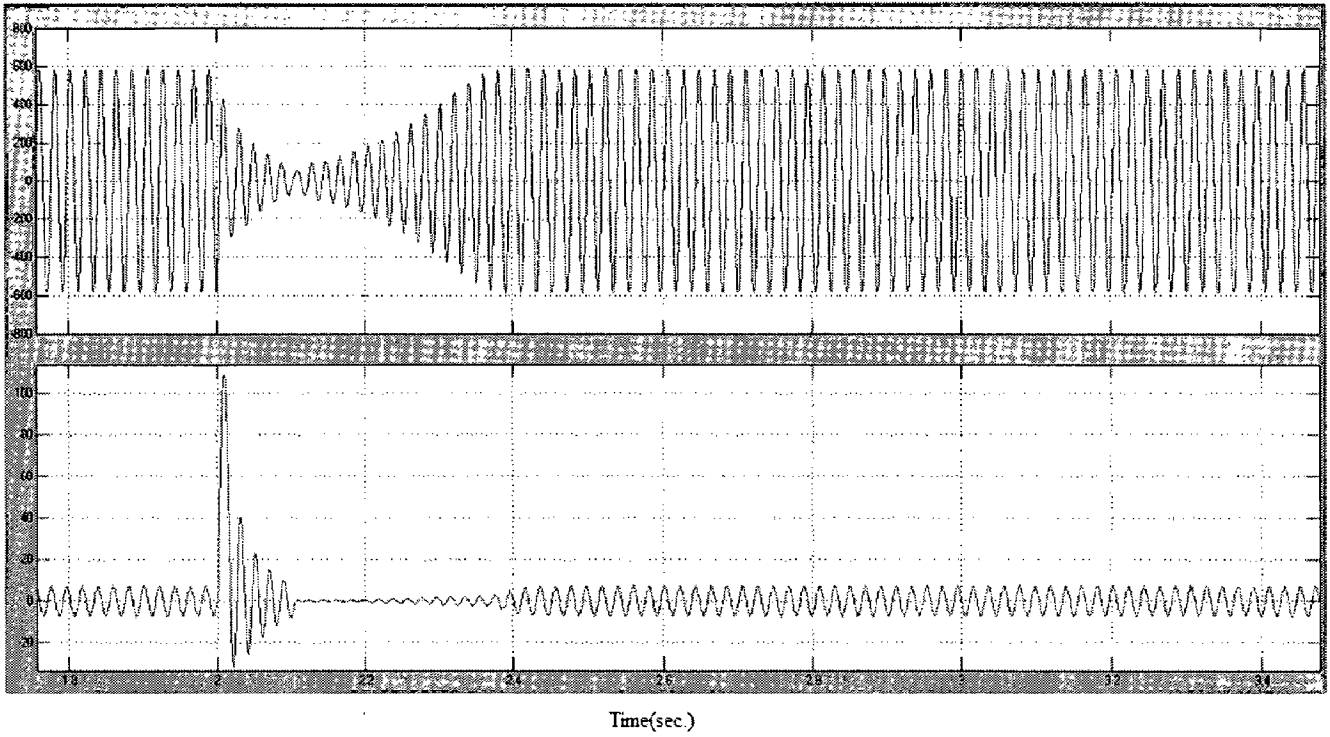
55

Fig 4.41: Voltage and current waveforms of line-B of SEIG due to sudden application and removal of line to line fault
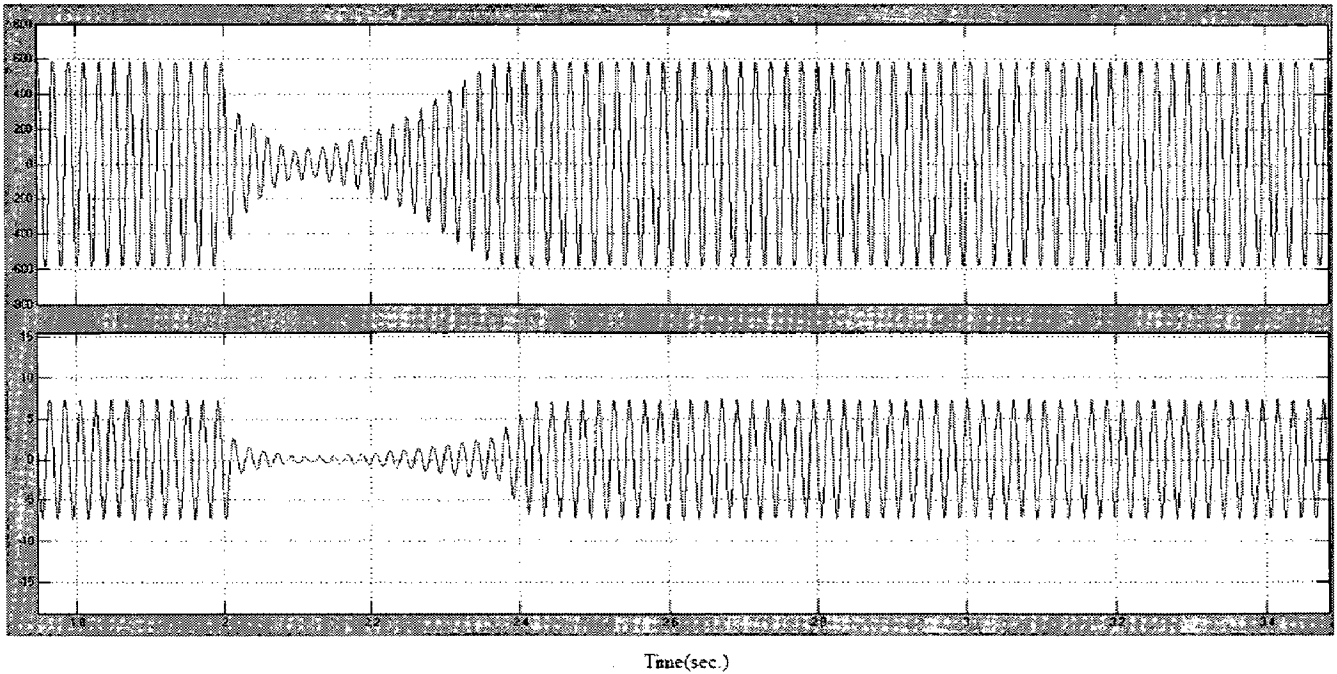

Fig.4.42: Voltage and current waveforms of line-C of SEIG due to sudden application and removal of line to line fault

56
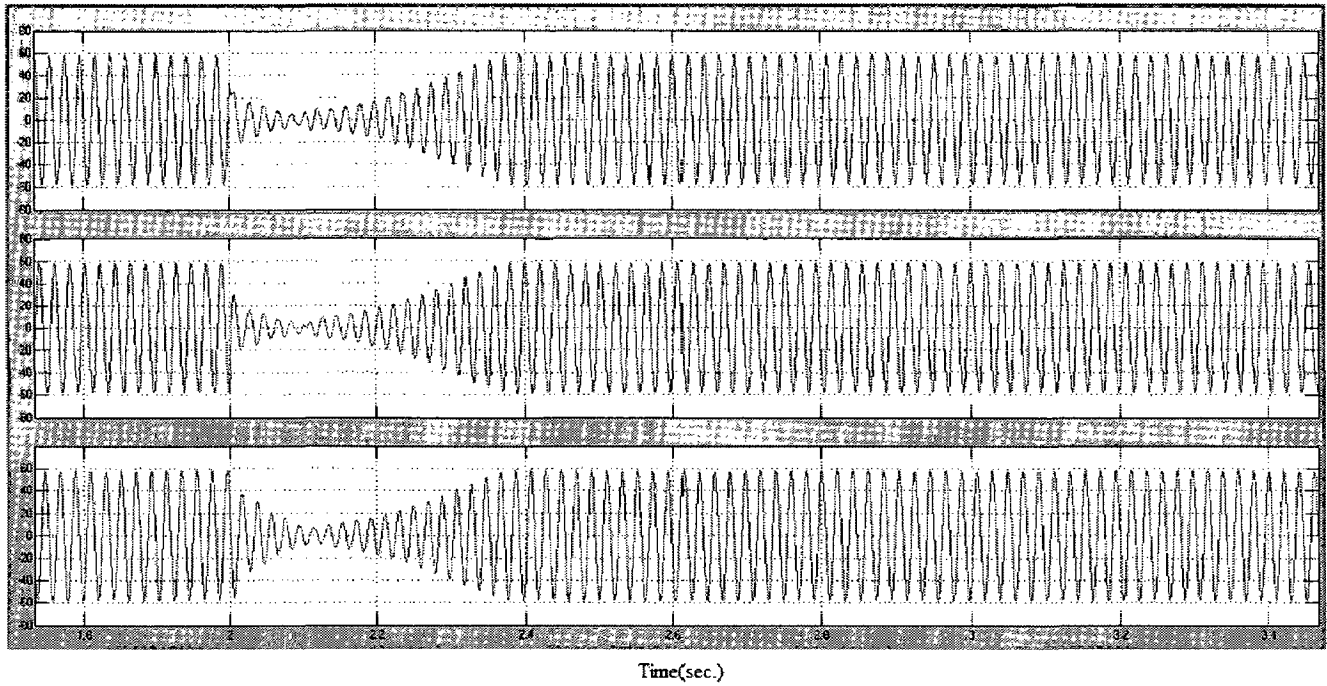
Fig.4.43: Three line Capacitor current due to sudden application and removal of line to line fault

Time(A)
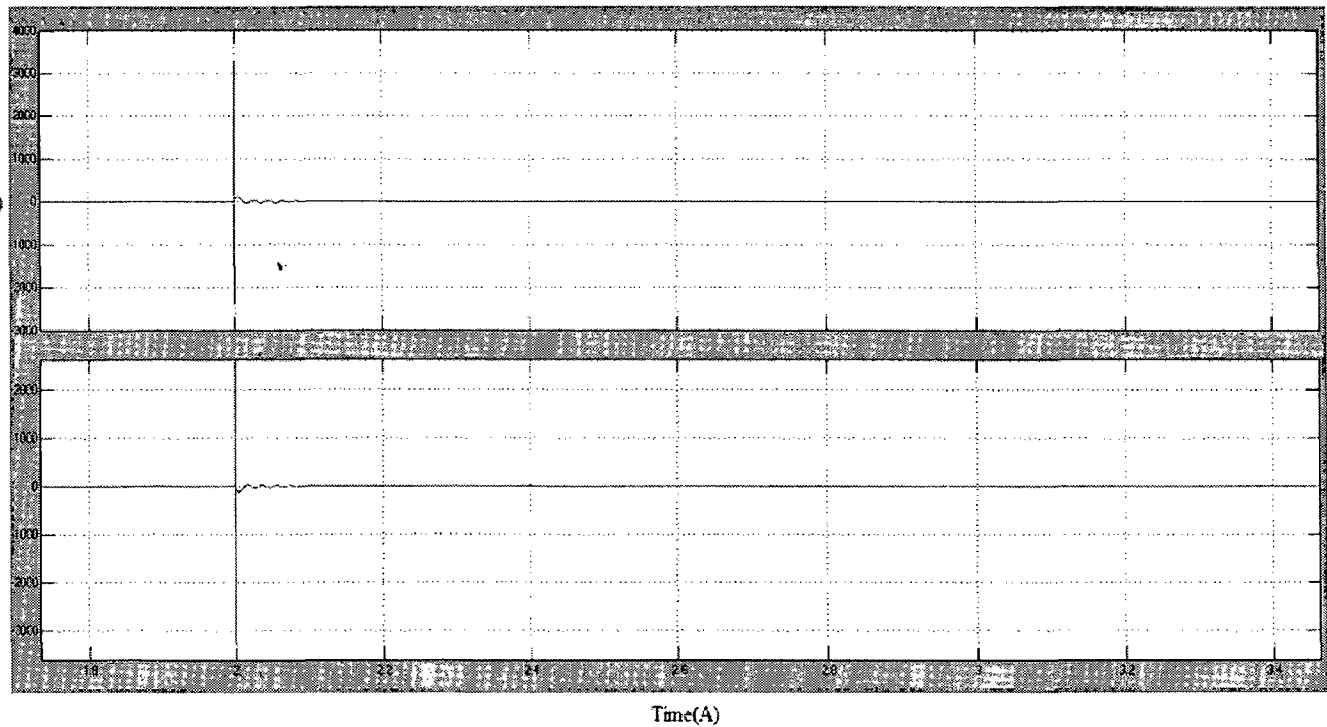
Fig.4.44: Waveforms of main load current of line-A and line-B due to sudden application and removal of line to line fault

57

Time(sec.)

Fig.4.45: Waveforms of main load current of line-C due to sudden application and removal of line to line fault

Time(sec.)

Fig.4.46: Waveforms of ELC current of line-A due to sudden application and removal of line to line fault
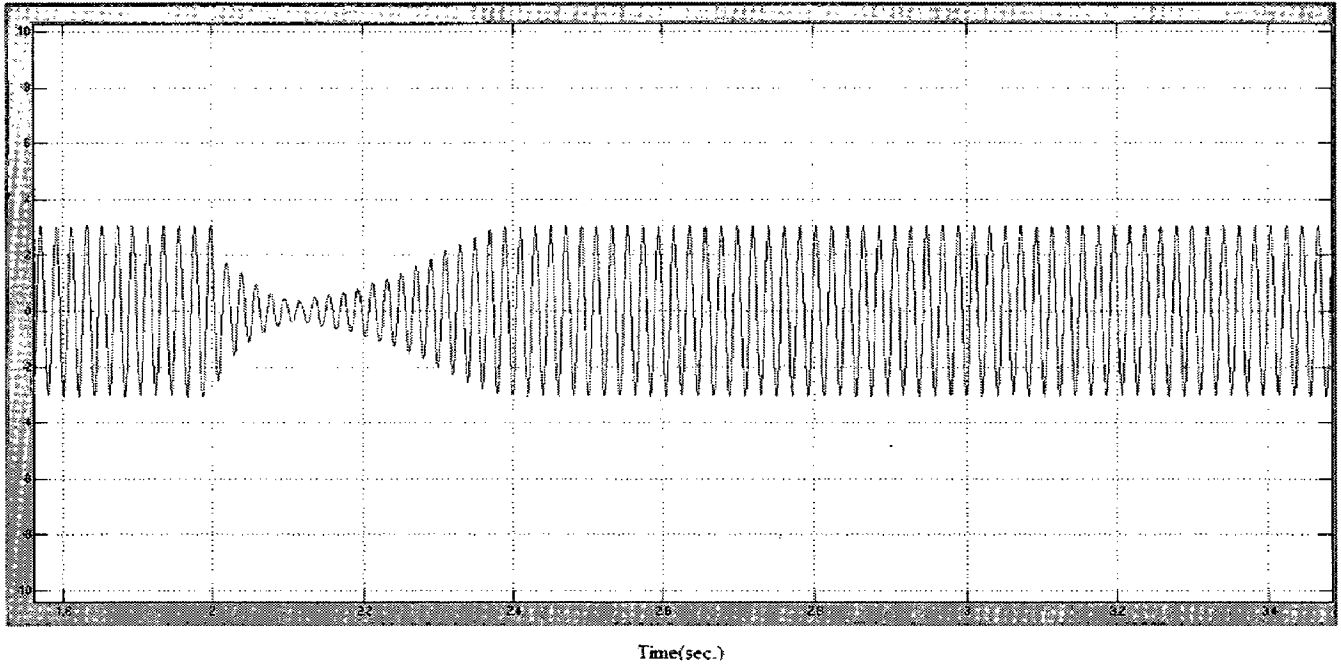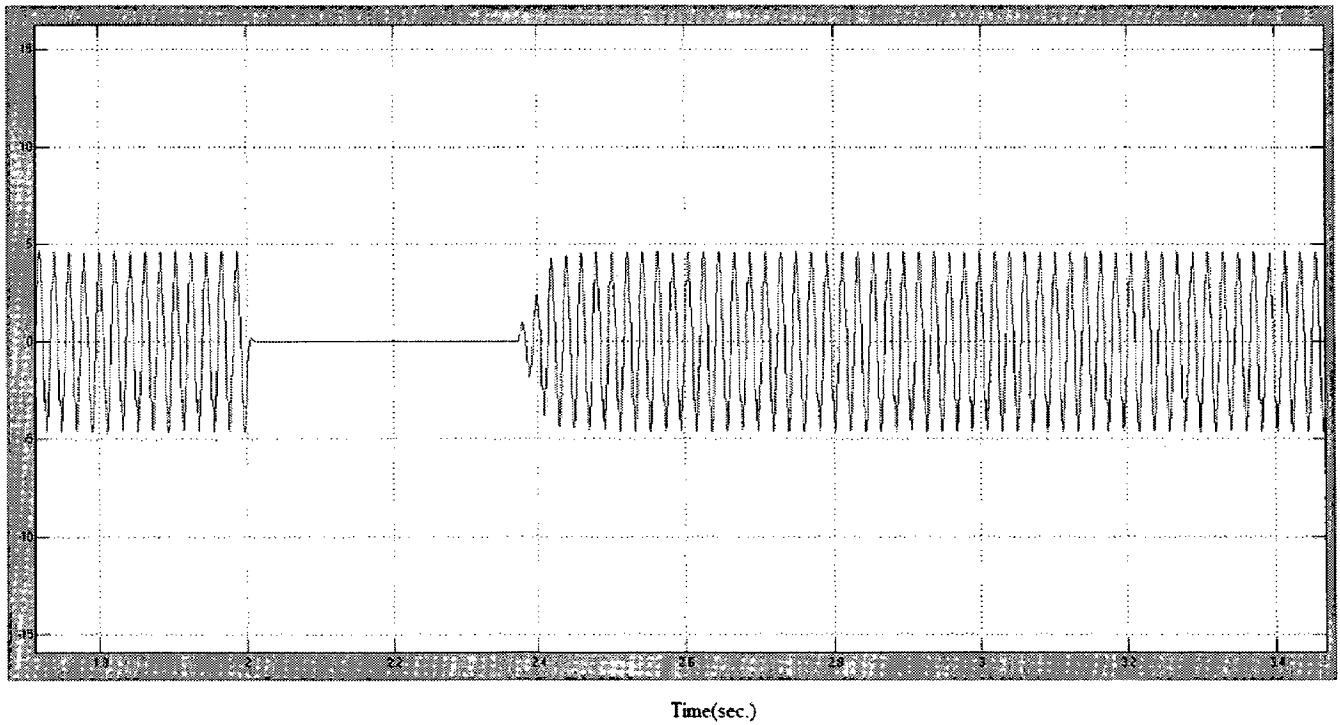
58
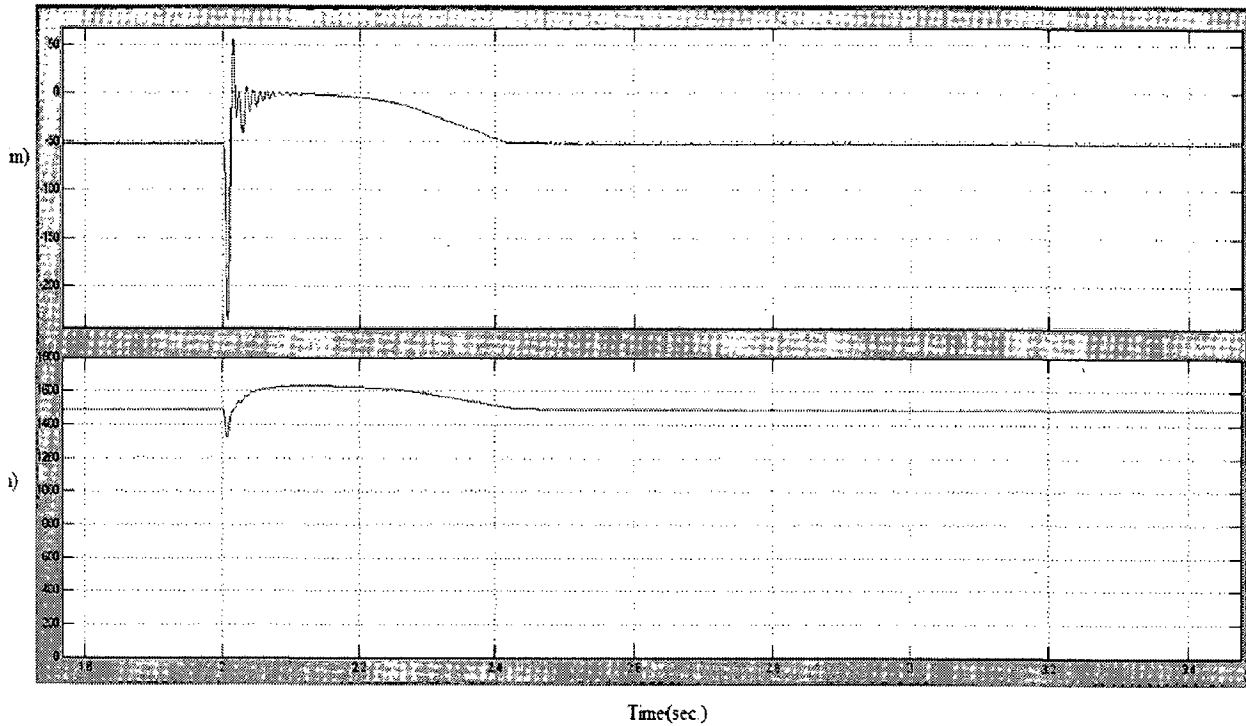
Fig. 4.47: Electromagnetic torque and rotor speed in SEIG due to sudden application and removal of line to line fault
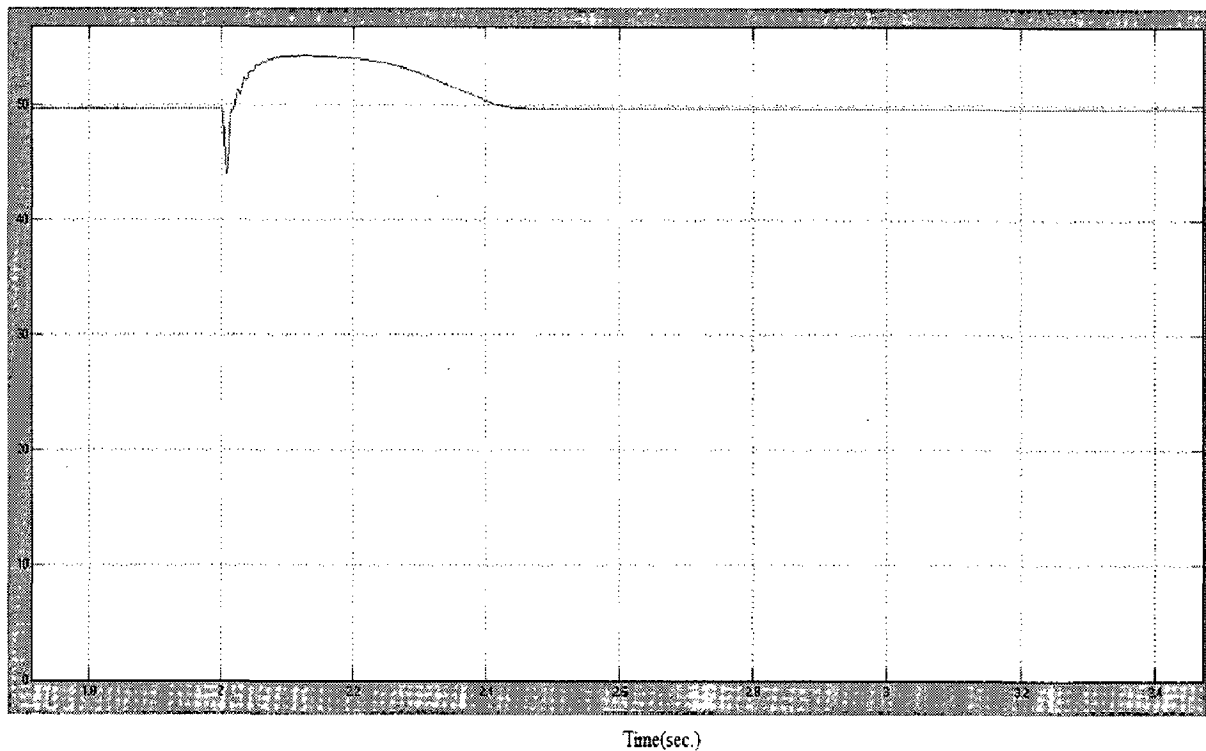
Fig. 4.48: Frequency of generated voltage due to sudden application and removal of line to line fault

59

UNBALANCED LOADING

Initially SEIG-ELC is operated with resistive load of 1500 W. An unbalanced is made by opening of line-A of a three phase resistive load at t = 2 sec. Voltage pse and failure of excitation are not observed in this case as shown in the Fig. 4.49-

Figs. 4.51-4.52 represent the load current of all the three lines. ELC current :ases due to unbalanced loading as shown in Fig. 4.53. Figs. 4.54 to 4.55 show the romagnetic torque, rotor speed and frequency of generated voltage due to opening of A at load.

Due to line-A opening at load, the SEIG is now effectively feeding a load of $R_{lc})R_{lb}/(R_{la}+R_{lb}+R_{lc})$ where R_{la}, R_{lb} and R_{lc} are the values of delta connected three e resistances.

Fig.4.49: Voltage and current waveforms of line-A of SEIG due to opening of line-A at load

60

Fig.4.50: Three line Capacitor current due to opening of line-A at load

Time(sec.)
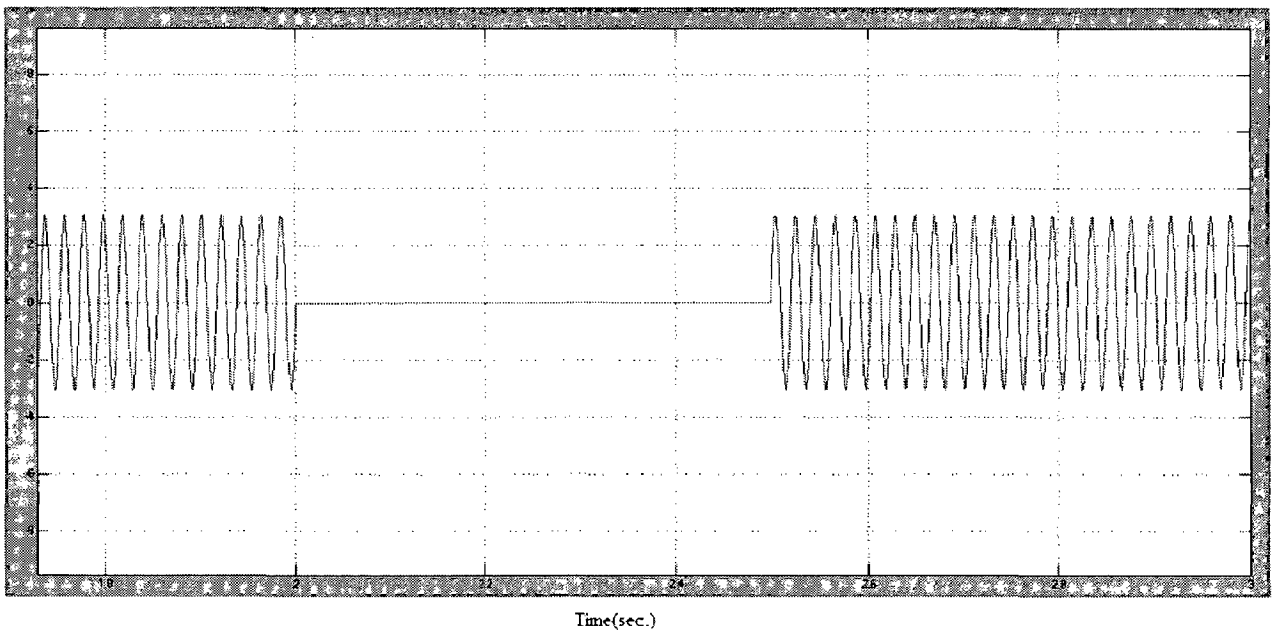
Fig.4.51: Waveforms of main load current of line-A due to opening

of line-A at load

61
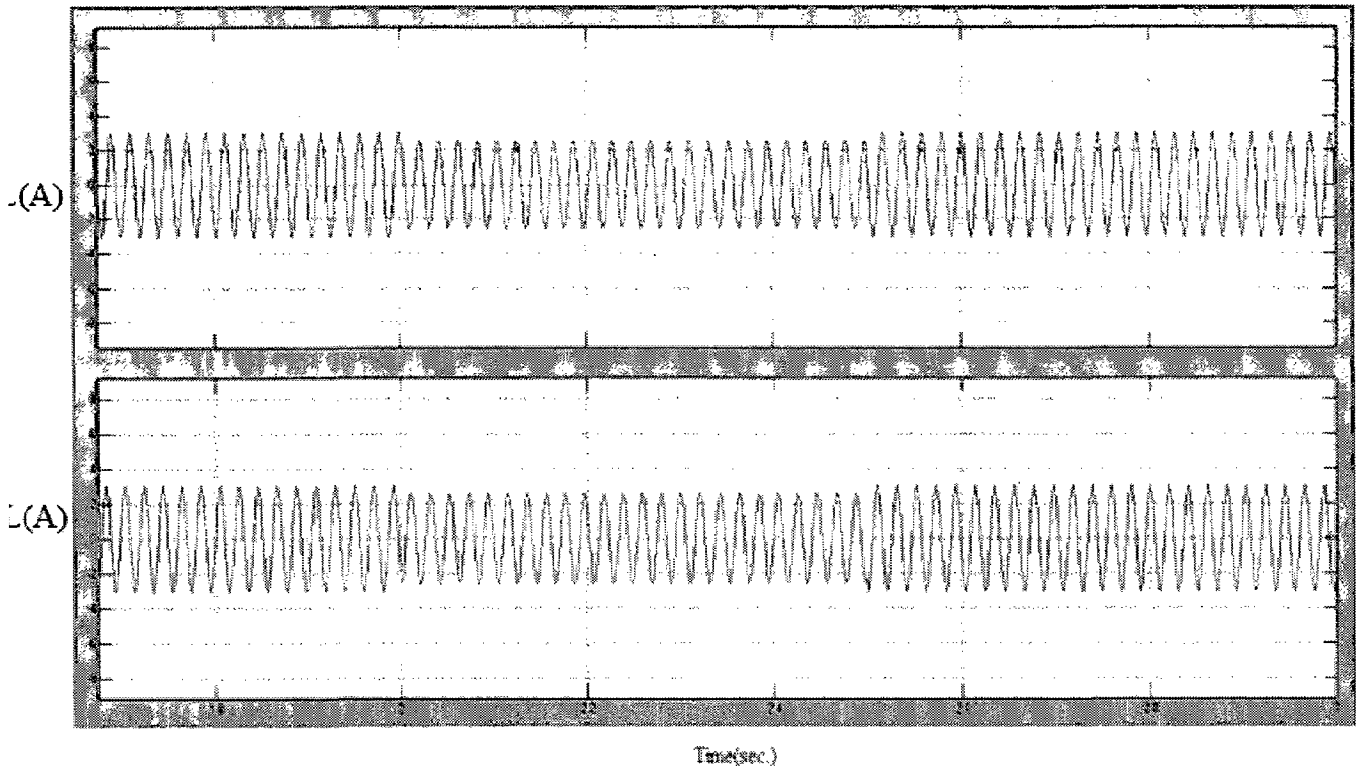
Fig.4.52: Waveforms of main load current of line-B and line-C due to opening of line-A at load
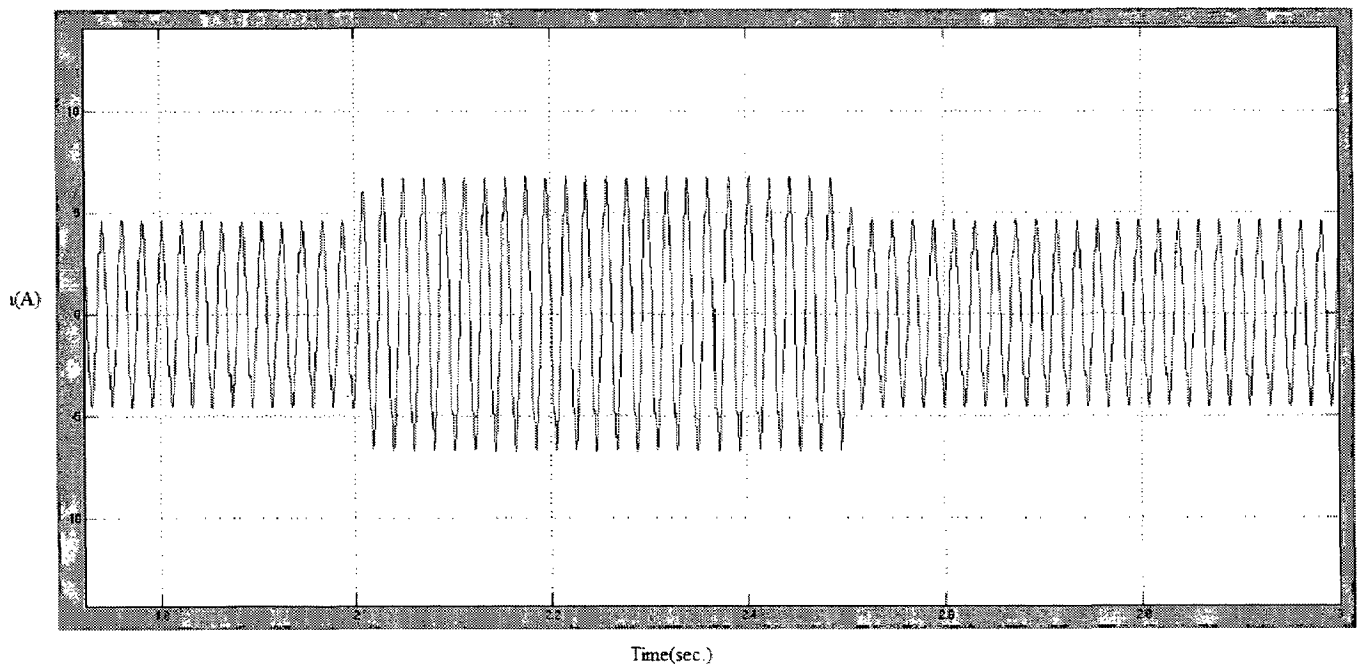
Fig.4.53: Waveforms of ELC current of line-A and line-C due to opening of line-A at load

62

.2.6 UNBALANCED EXCITATION

Initially SEIG is operated with resistive load of 1500 W. A single capacitor ɔtween line-A and line-B opens in capacitor bank at t=2 sec. Transient waveforms due ɩ sudden opening of single capacitor are shown in the figure from Figs. 4.51 to 4.56.

The capacitor opening causes a reduction in net reactive power and SEIG operates a lower saturation level, which decreases stator voltages and currents with time. owever, the exact rate of decay depends on the value of capacitance and load. No ɩrrent surge is observed during capacitor opening.

Figs. 4.51-4.52 shows the voltage and current of line-A and capacitor currents of three lines. Figs. 4.53-4.54 represent the load current of all three lines, ELC current of ɩe-A. Fig.4.55 shows the pulsating electromagnetic torque, rotor speed of SEIG and ɩquency of generated voltage during unbalanced excitation.
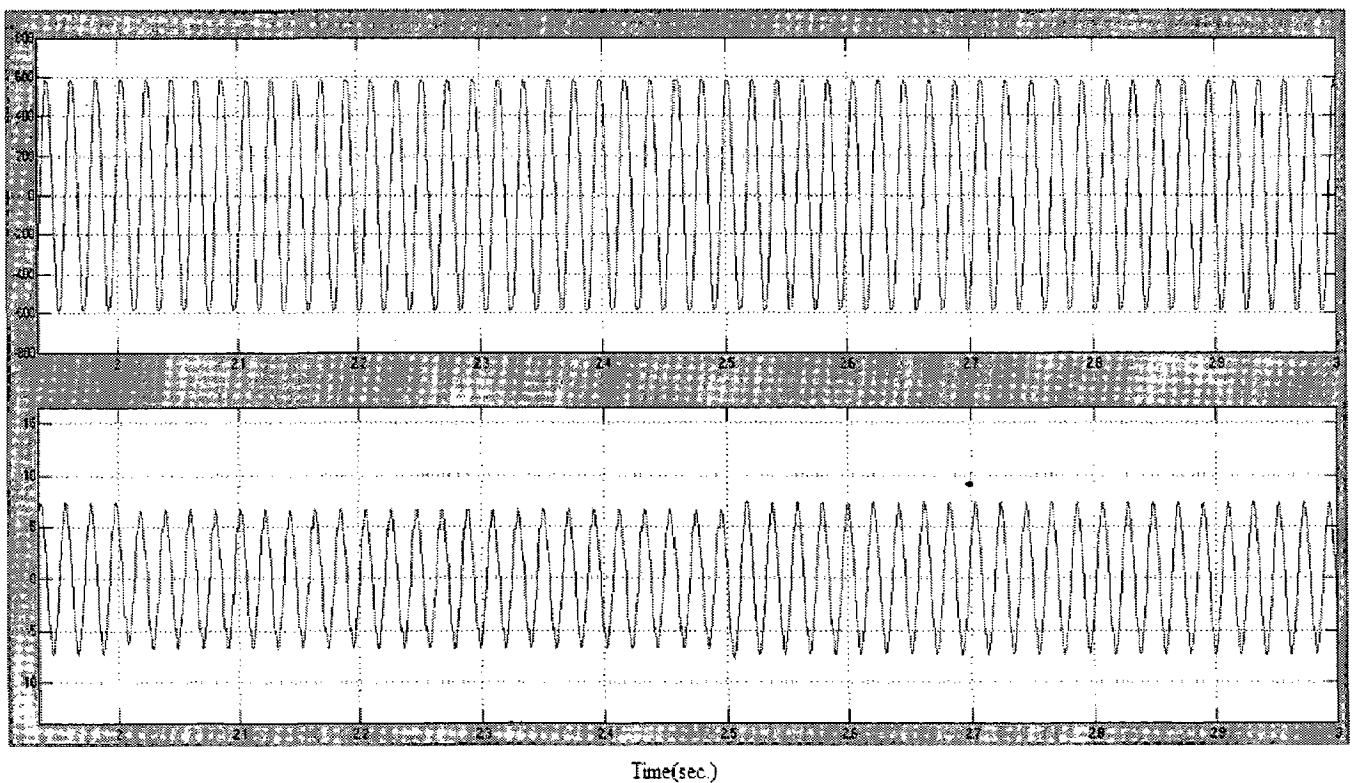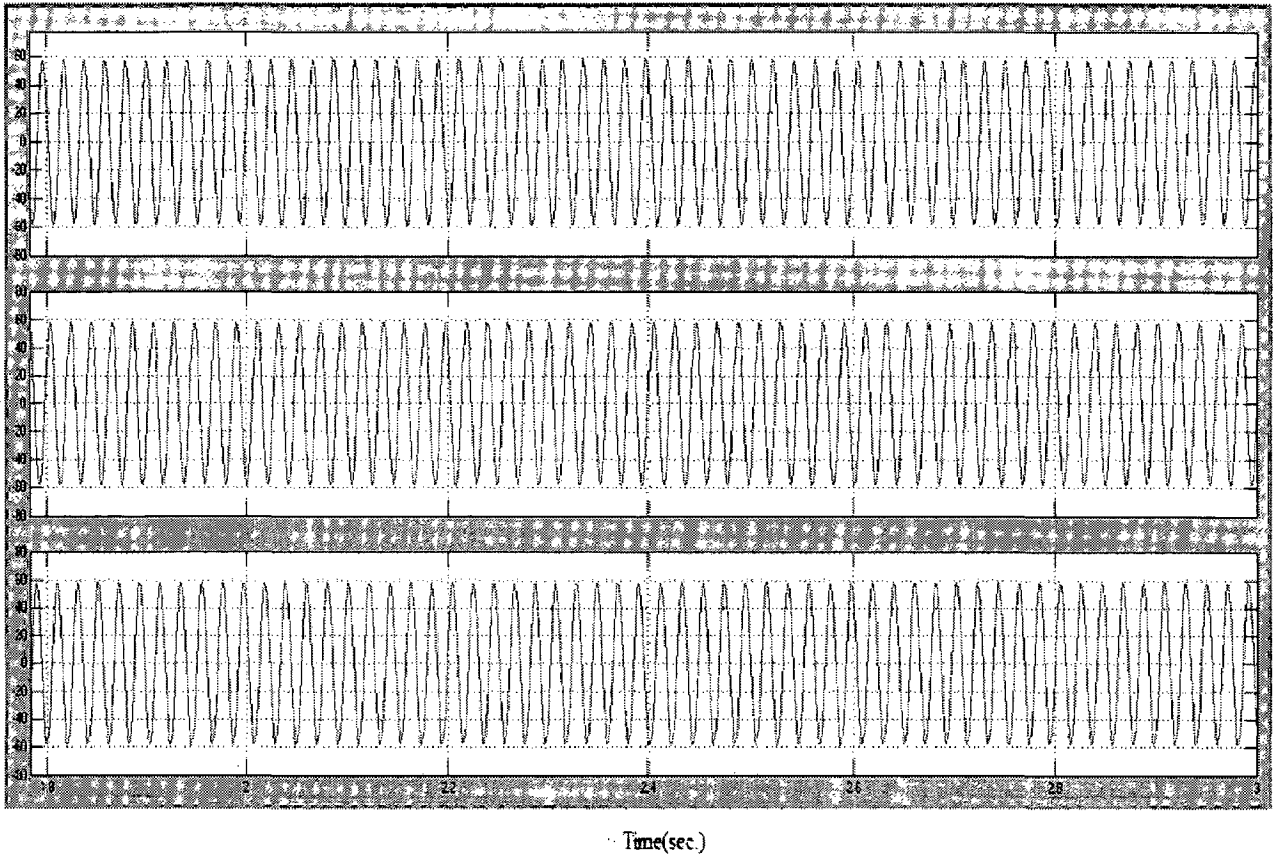

Time(sec.)
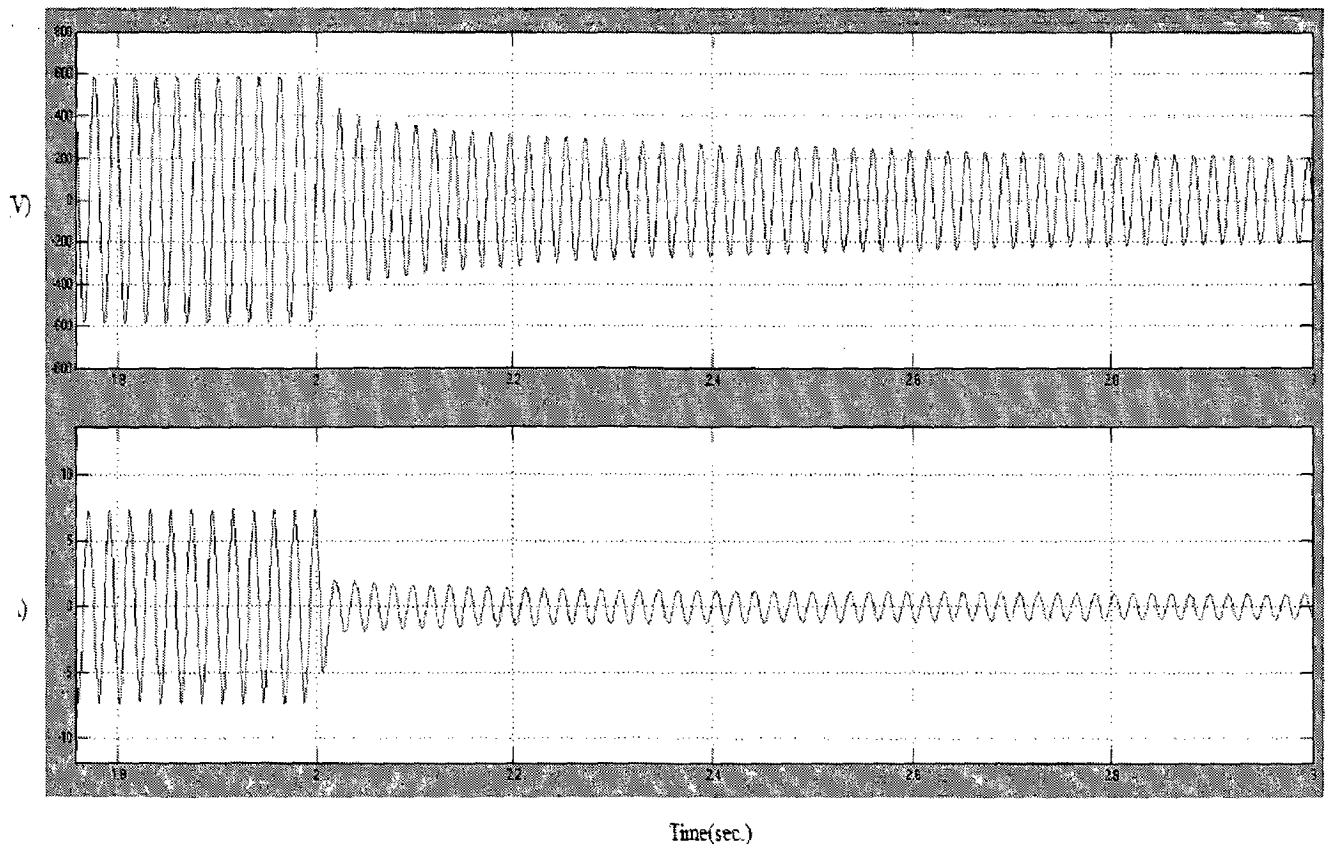
Fig.4.56: Voltage and current waveforms of line-A of SEIG due to opening of single capacitor

64
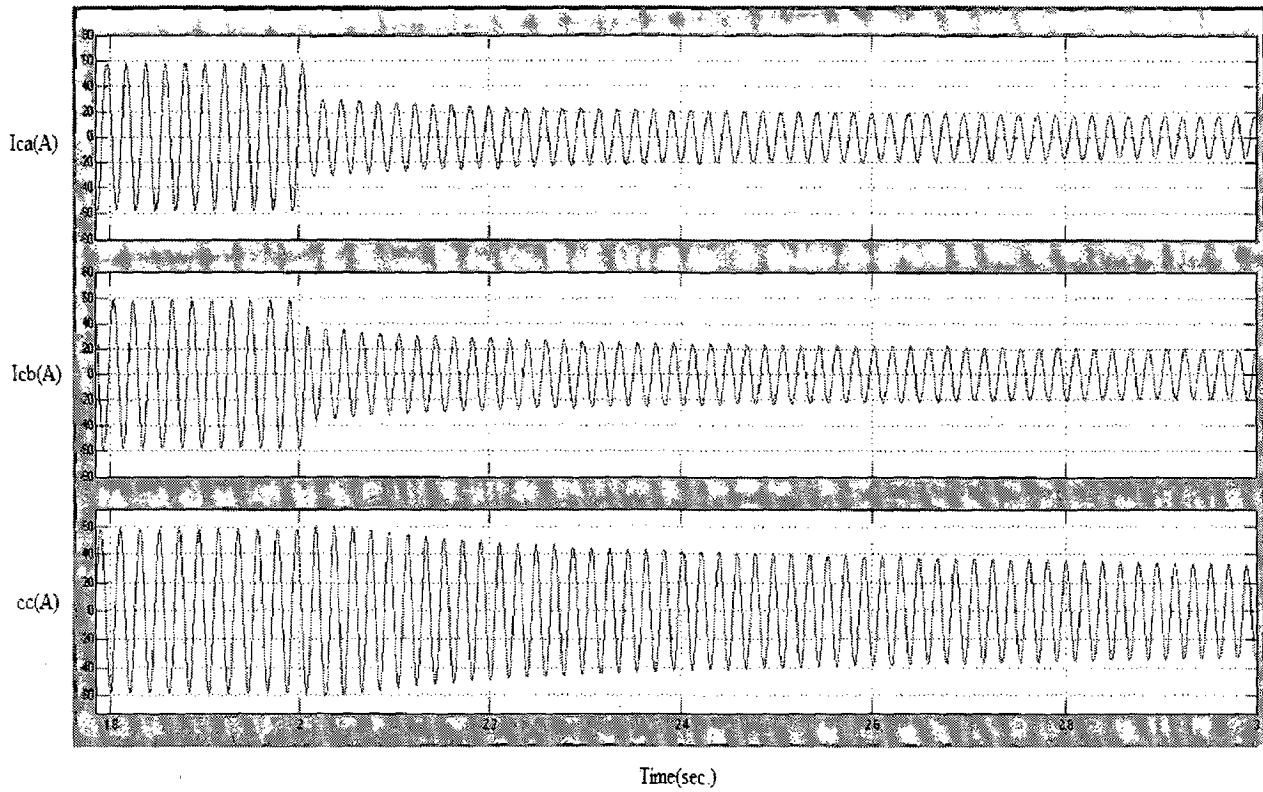
**Fig. 4.57: Three line capacitor current due to opening of single capacitor**
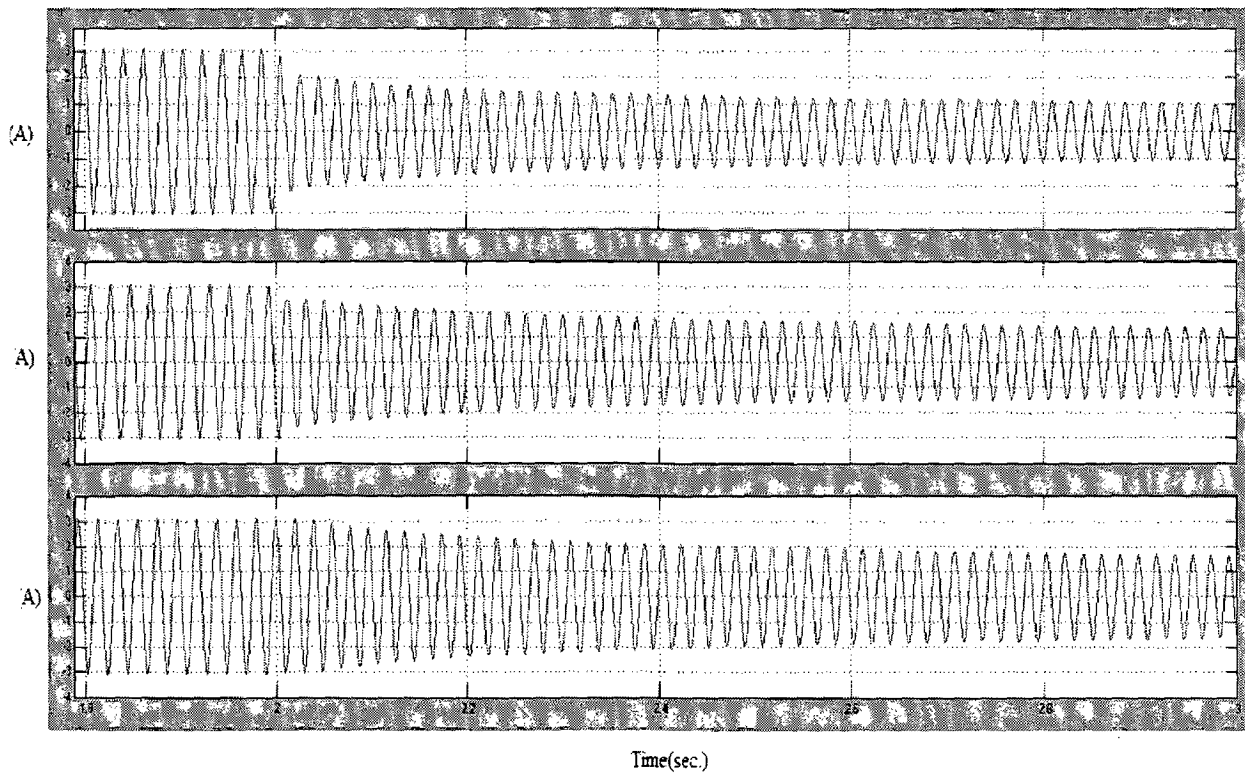
Fig. 4.58: Waveforms of output voltage of the SEIG and line-A load current due to opening of single capacitor

65
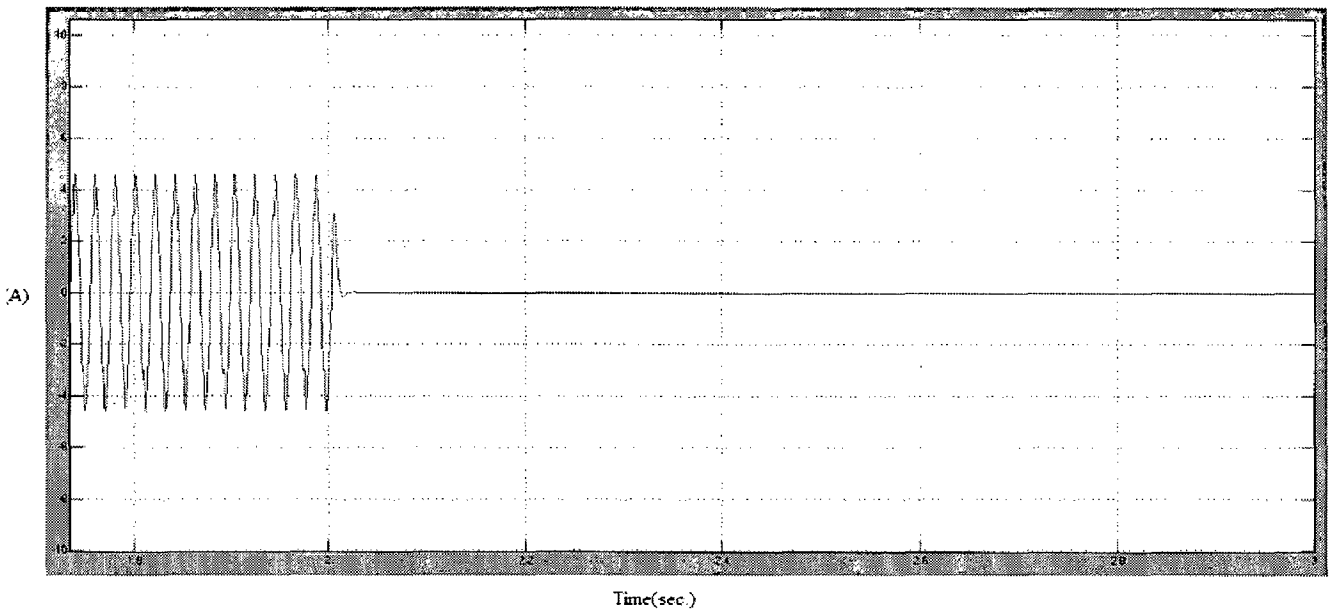
Fig. 4.59: Waveforms of output voltage of the SEIG and line-A current of
ELC due to opening of single capacitor

Time(sec.)
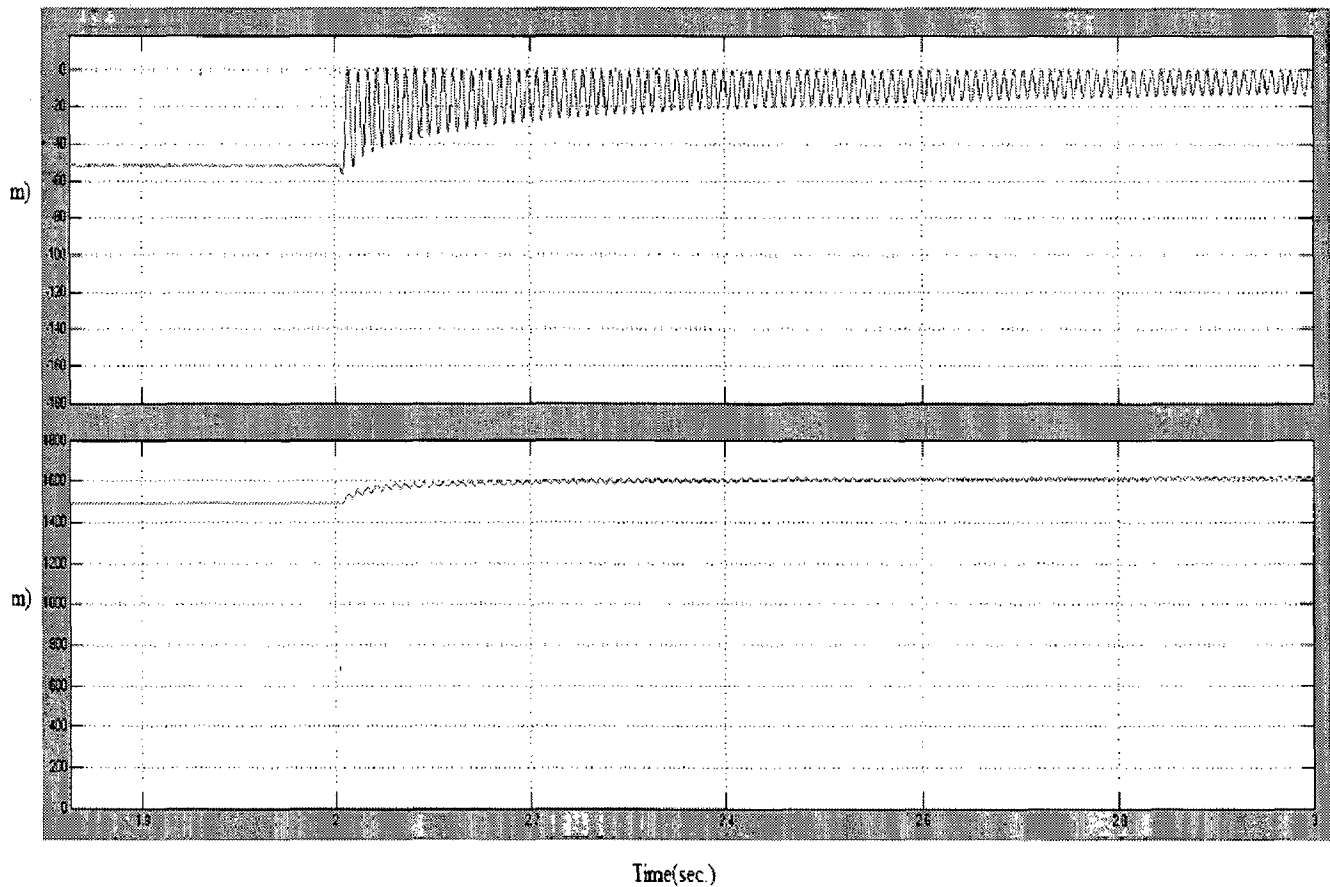
Fig. 4.60: Electromagnetic torque and rotor speed of SEIG due to opening
of single capacitor

66

Time(sec.)
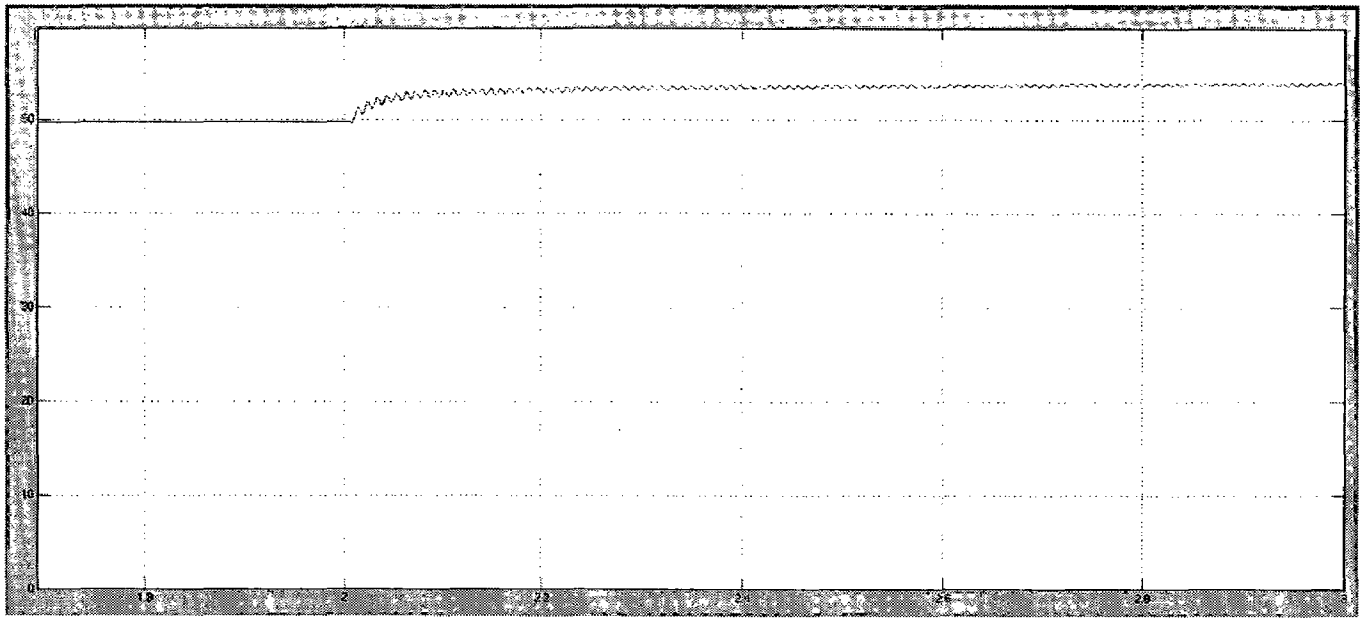
Fig. 4.61: Frequency of generated voltage due to opening of single capacitor

CONCLUSION

In this chapter, conclusion of the thesis work and scope for future work are esented.

1 CONCLUSION:

The simulation of SEIG-ELC based micro hydro power plant system has been rried out in MATLAB/SIMULINK environment. The performance of the SEIG with ad controller has been simulated for transient conditions such as process of self-citation, voltage build up, faults, unbalanced excitation and switching of resistive and namic load. From the simulation results, the following conclusions are drawn:

1. For resistive main load, the stator line voltages of the SEIG remain same before and after application of main load.

2. The induction motor load also can be started up successfully. Using a fixed value of capacitance for excitation, an SEIG can safely feed an induction motor rated upto 50% of its rating. In this case also, the stator line voltages of the SEIG reduce slightly after application of motor load due to increase of VAR demand.

3. In case of application of motor load, it draws heavy inrush current until the steady state condition is reached. During this period, the ELC current i.e. the dump load ac current reduces considerably. When the steady state is reached, the ELC starts dumping power to the dump load.

4. After application of main load, the harmonics contents in the stator phase voltages and currents of the SEIG reduce because the current through the ELC decreases and the effect of ELC on the SEIG is reduced.

5. Three phase fault, line to line fault and unbalanced excitation cause voltage collapse and de-excitation except opening of line-A at load.

6. The excessive high torque during short circuit and the sustained pulsating torque during imbalance may be taken into account with appropriate shaft design.

7. The dynamic model of SEIG can handle any capacitor and/or load configuration while maintaining the integrity and generalized nature of the load.

The dynamic behavior of the SEIG with load controller reveals that this system n be used satisfactorily in constant power applications such as micro-hydro with controlled turbine. This study has practical significance due to enormous small hydro tential in isolated locations in several countries.

2 FUTURE SCOPE OF WORK:

Unbalanced operation of SEIG leads to voltage stresses and over heat in the achine and correspondingly leads inefficient operation due to the voltage and current gative sequence components. To reduce these problems, strategy may be made to inimize the unbalancing by selecting the appropriate size and rating of excitation pacitors. Following works are proposed for future:

(1) Transient analysis can also be made to evaluate the performance and designing of machine parts such as winding and coupling shaft and devising of the protection strategy during unbalanced condition.

(2) In the load controller, the difference of generated power and the consumer load power is dumped to the dumping resistance, which is wastage of power. Alternative arrangement such as that battery charging, water heating, space heating, cooking, baking etc. may be developed to improve the efficiency.

(3) Digital signal processor (DSP) based controller may be developed to study the comparative performance of the SEIG-ELC system.

REFERENCES

R. C. Bansal, "Three-Phase Self-Excited Induction Generators: An Overview", IEEE Transactions on Energy Conversion, Vol. 20, No. 2, pp.292-299, Jun. 2005.

Padmanaban S, "Triggering Market for Energy Efficiency in India", Renewable Energy India, Vol. 1, No. 1, pp. 17-18, Jan. 2005.

International Course on "Small Hydropower Development", AHEC, IIT Roorkee, Feb. 2004.

G.K. Singh, "Self-Excited Induction Generator Research-a survey", Electric Power Systems Research, Vol. 69, No. 1, pp. 107-114, Aug. 2003.

T. Ahmed, O. Noro, K. Matzuo, Y. Shindo and M. Nakaoka, "Minimum Excitation Capacitance Requirements for Wind Turbine Coupled Stand-alone Self-excited Induction Generator with Voltage Regulation based on SVC", IEEE Transactions on Industrial Applications, Vol. 1, No. 1, pp. 396-403, Oct. 2003.

D. Seyoum, C. Grantham and M. F. Rahman, "The Dynamic Characteristics of an Isolated Self-excited Induction Generator Driven by a Wind Turbine", IEEE Transactions on Industrial Applications, Vol. 39, No. 4, pp. 936-944, Aug. 2003.

N. H. Malik and A. A. Mazi, "Capacitance Requirements For Isolated Self Excited Induction Generators", IEEE Transactions on Energy Conversion, Vol. EC-2, No. 1, pp.62-69, Mar. 1987.

Li Wang and Jian-Yi Su, "Determination of Minimum and Maximum Capacitances of an Isolated SEIG using Eigen Value Sensitivity Approach", IEEE Proceedings of International Conference on Power Electronics , Vol. 1, No. 1, pp. 610-614, Aug. 1998.

G. K. Singh, "Modeling and Experimental Analysis of a Self-excited Six-phase Induction Generator for Stand-alone Renewable Energy Generation", Renewable Energy, Vol. 33, No. 7, pp. 1605-1621, Jul. 2008.

J. L. Bhattacharya and J. L. Woodward, "Excitation Balancing of a Self-excited Induction Generator for Maximum Power Output", IEE Proc. Inst. Elect. Eng., Gener., Transm. Distrib., Vol. 135, No. 2, pp. 88 – 97, Mar. 1988.

A.M. Eltamaly, "New Formula to Determine the Minimum Capacitance Required for Self-Excited Induction Generator", IEEE Transactions on Energy Conversion, Vol. 1, No. 1, pp. 106-110, Jun. 2002.

Li Wang and Ruey-Yong Deng, "Transient Performance of an Isolated Induction Generator under Unbalanced Excitation Capacitors", IEEE Transactions on Energy Conversion, Vol. 14, No. 1, pp. 887-893, Dec. 1999.

S. N. Mahato, M. P. Sharma, and S. P. Singh, "Transient Analysis of a Single-Phase self-regulated self-Excited Induction Generator using a Three-Phase Machine", Electric Power Systems Research, Vol. 77, No. 7, pp. 839-850 May 2007.

S. K. Jain, J. D. Sharma and S. P. Singh, "Transient Performance of Three-phase Self-Excited Induction Generator during Balanced and Unbalanced Faults", IEE Proceeding on Generation, Transmission and Distribution, Vol. 149, No. 1, pp. 50-57, Jan. 2002.

L. Shridhar, B. Singh, C. S. Jha and B. P. Singh, "Analysis of Self-Excited Induction Generator Feeding Induction Motor", IEEE Transactions on Energy Conversion, Vol. 9, No. 2, pp. 390-396, Jun. 1994.

Bhim Singh, Gaurav Kumar Kasal and Sanjay Gairola, "Power Quality Improvement in Conventional Electronic Load Controller for an Isolated Power Generation", IEEE Transactions on Energy Conversion, Vol. 23, No. 3, pp. 764-773, Sep. 2008.

L. Wang and C. H. Lee, "Long-shunt and Short shunt Connections on a Dynamic Performance of a SEIG feeding an Induction Motor Load", IEEE Transactions on Energy Conversion, Vol. 15, No. 1, pp. 1-7, Mar. 2000.

L.Wang and J. Y. Su, "Dynamic Performances of an Isolated Self-Excited Induction Generator Under Various Loading Conditions", IEEE Transactions on Energy Conversion, Vol. 14, No. 1, pp. 93-100, Mar. 1999.

Gaurav Kumar Kasal and Bhim Singh, "Decoupled Voltage and Frequency Controller for Isolated Asynchronous Generators Feeding Three-Phase Four-Wire Loads", IEEE Transactions on Power Delivery, Vol. 23, No. 2, pp.966-973, Apr. 2008.

L. Shridhar, B. Singh, C. S. Jha, and B. P. Singh, "Analysis of Self-Excited Induction Generator Feeding Induction Motor Conditions", IEEE Transactions on Energy Conversion, Vol. 9, No. 1, pp. 390-396, June 1994.

T. F. Chan, "A Novel Single-Phase Self-Regulated Self-Excited Induction Generator Using a Three-Phase Machine", IEEE Transactions on Energy Conversion, Vol. 16, No. 2, pp. 204-208, Jun. 2001.

A.L. Alolah and M.A. Alkanhal, "Optimization-based Steady State Analysis of Three Phase Self-Excited Induction Generator", IEEE Transactions on Energy Conversion, Vol. 15, No. 1, pp. 61-65, Mar. 2000.

Bhim Singh, S. S. Murthy and Sushma Gupta, "Analysis and Design of Electronic Load Controller for Self-Excited Induction Generators", IEEE Transactions on Energy Conversion, Vol. 21, No. 1, pp. 285-293, Mar. 2006

T.Ahmed, O.Noro, E.Hiraki and M.Nakaoka, "Terminal Voltage Regulation Characteristics by Static Var Compensator for a Three-phase Self-Excited Induction Generator", IEEE Transactions on Industrial Applications, Vol. 40, No. 1, pp. 978- 988, Jul. 2004.

Oleg Chtchetinine, "Voltage Stabilization System for Induction Generator in Stand Alone Mode", IEEE Transactions on Energy Conversion, Vol. 14, No. 3, pp. 298-303, Sep. 1999.

B. Singh, S. S. Murthy, Madhusudan, M. Goel, and A. K. Tandon, "A Steady State Analysis on Voltage and Frequency Control of Self-Excited Induction Generator in Micro-Hydro System", IEEE Transactions on Industrial Applications, Vol. 1, No. 1, pp. 1-6, Dec. 2006.

D. Joshi, K. S. Sandhu, and M. K. Soni, "Constant Voltage Constant Frequency Operation for a Self-Excited Induction Generator", IEEE Transactions on Energy Conversion, Vol. 21, No. 1, pp. 228-234, Mar. 2006.

S. P. Singh, S. K. Jain, and J. Sharma, "**Voltage Regulation Optimization of Compensated Self-Excited Induction Generator with Dynamic Load**", IEEE Transactions on Energy Conversion, Vol. 19, No. 1, pp. 724-732, Dec. 2004.

D. K. Palwalia and S. P. Singh, "**New Load Controller for Single-phase Self-excited Induction Generator**", Electric Power Components and Systems, Vol.37, No.1, pp.658-671, Apr. 2009.

C. Chakraborty, S. N. Bhadra, and A. K. Chattopadhyay, "**Analysis of parallel Operated Self- Excited Induction Generators**", IEEE Transactions on Energy Conversion, Vol. 14, No. 1, pp. 209-216, June 1999.

Li.Wang and Lee Ching-Huei, "**A Novel Analysis of Parallel Operated Self-Excited Induction Generators**", IEEE Transactions on Energy Conversion, Vol. 13, No. 1, pp. 117-123, Jun. 1998.

A.H. Al-Bahrani, and N. H. Malik, "**Voltage Control of Parallel Operated Self-Excited Induction Generators**", IEEE Transactions on Energy Conversion, Vol. 8, No.1, pp. 236 -242, Jun. 1993.

P.C. Krause and C. H. Thomas, "**Simulation of Symmetrical Induction Machinery**", IEEE Transactions on Power Apparatus and Systems, Vol. 84, No. 11, pp. 1038-105, Nov. 1965

P.C.Krause, "**Analysis of Electrical Machinery**", McGraw-Hill Book Company, 1986.

Bhim Singh, S. S. Murthy and Sushma Gupta, "**Transient Analysis of Self-Excited Induction Generator with Electronic Load Controller (ELC) Supplying Static and Dynamic Loads**", IEEE Transactions on Industrial Applications, Vol. 41, No. 5, pp. 1194-1204, Sep. 2005.

B. Singh, S.S. Murthy and S. Gupta,"**Analysis and Implementation of an Electronic Load Controller for a Self-Excited Induction Generator**", IEE Proc.-Gener. Transm. Distrib., Vol. 151, No. 1, pp. 51-60, Jan. 2004.

M. H. Rashid, "**Power Electronics, Circuits, Devices, and Applications**", 2nd ed. New Delhi, India: Prentice Hall of India Private Limited, 1996.

APPENDIX - A

This Appendix presents the developed SIMULINK MODEL of SEIG-ELC 'stem supplying three phase resistive load.
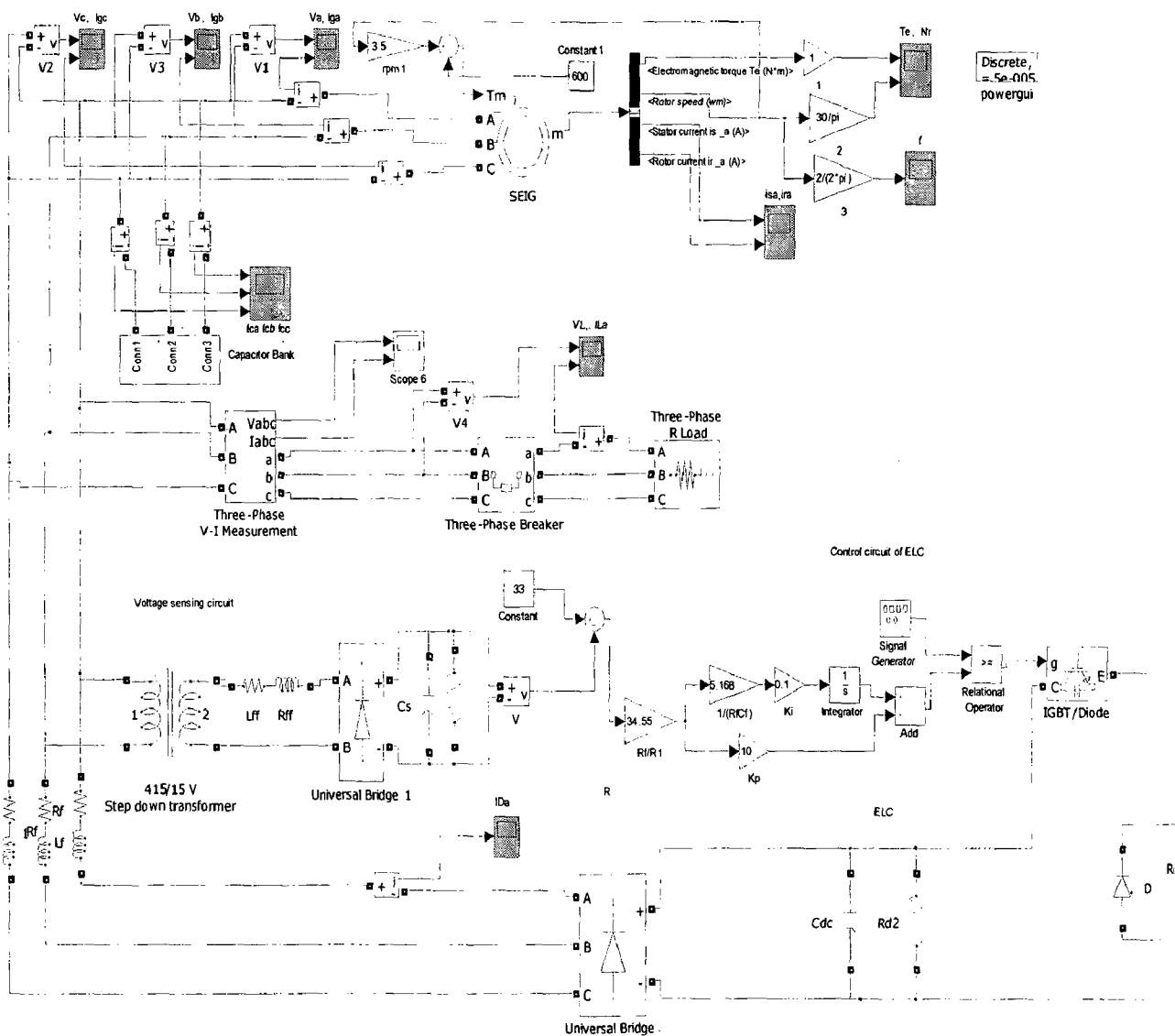
.1 SIMULINK Model of SEIG-ELC system:

Fig. A.1: SIMULINK Model of SEIG-ELC system

APPENDIX – B

This appendix presents the design of three phase ELC for 3.7 kW SEIG.

B.1 Design of Three Phase ELC [23]:

The voltage and current rating of the SEIG decides the component rating of ELC because in the constant power operation, SEIG always operates at the rated power. The voltage rating of the uncontrolled rectifier and chopper switch will be the same and dependent on the rms ac input voltage and average value of the output dc voltage. The dc voltage is calculated as [37]

$$V_{dc} = \frac{3\sqrt{2}\,V_{LL}}{\pi} = (1.35\ V_{LL})$$
(B.1)

where V_{LL} is the root-mean-square (rms) value of the line-to-line voltage of SEIG. For the 3.7 kW SEIG, the line voltage is 415 V and

$$V_{dc} = (1.35\ ) \times 415 = 560.25\ V$$

An overvoltage of 10% of the rated voltage is considered for transient conditions and hence, the rms ac input voltage will be (456.5 V) with a peak value

$$V_{peak} = (\sqrt{2}\ ) \times 456.5\ V = 645.58\ V$$

This peak voltage will appear across the components of ELC. The current rating of the uncontrolled rectifier and chopper switch is decided by the active component of input ac current and calculated as

$$I_{AC} = \frac{P}{(\sqrt{3}V_{LL})}$$
(B.2)

where V_{LL} is the rms value of the SEIG terminal voltage and is the power rating of SEIG. The active current of SEIG may be calculated as

$$I_{AC} = \frac{3700}{(\sqrt{3} \times 415)} = 5.14\ A$$

$$\times \ \{(1 + 1/(\sqrt{2} \times 0.05)\} = 297.49 \ \mu F$$

The nearest commercially available value of 380 μF is selected.

Table B.1 Three Phase ELC Parameters for 3.7 kW SEIG

Power Rating (3.7 kW)	Voltage Rating of rectifier and chopper switch (V)	Current Rating of rectifier and chopper switch (A)	Rating of Dump load (Ω)	Rating of DC filtering capacitor (μF)
Selected	900	15	84	380

The three-phase uncontrolled rectifier draws approximately quasi–square current with the distortion factor of (3/ π=0.955). The input ac current of ELC may be obtained as

$$I_{DAC} = \frac{I_{AC}}{(0.955)} = 5.39 \text{ A} \tag{B.3}$$

The crest factor (CF) of the ac current drawn by an uncontrolled rectifier with a capacitive filter varies from [1.4 to 2.0] so the ac input peak current may be calculated as

$$I_{peak} = 2I_{DAC} = 2 \times 5.39 = 10.78 \text{A} \tag{B.4}$$

From these calculations, it is observed that the maximum voltage may be 645.58 V and peak current may be 10.48 A in the uncontrolled rectifier. The commercially available rating of an uncontrolled rectifier and chopper switch is 900 V and 15 A higher than 645.58 V and 10.48 A, respectively.

Therefore rating of the uncontrolled rectifier and chopper switch has been decided to be 900 V and 15 A for three-phase ELC. The rating of dump load resistance is calculated by

$$R_D = (V_{dc})^2 / P_{rated} \tag{B.5}$$

From this relation, the value of R_D is computed as

$$R_D = (560.25)^2 / 3700 = 84.83 \, \Omega$$

The value of dc-link capacitance of the ELC is selected on the basis of the ripple factor. The relation between the value of dc-link capacitance and ripple factor (RF) for a three-phase uncontrolled rectifier is [12]

$$C = \{1/(12fR_D)\} \{(1 + 1/(\sqrt{2}RF)\} \tag{B.6}$$

If 5% ripple factor is considered in the dc bus voltage of ELC, then the capacitance is calculated as

$$C = \{1/(12 \times 50 \times 84.83)\}$$

76

$\times$ $\{(1 + 1/(\sqrt{2} \times 0.05))\}=297.49 \ \mu F$

The nearest commercially available value of 380 μF is selected.

Table B.1 Three Phase ELC Parameters for 3.7 kW SEIG

Power Rating (3.7 kW)	Voltage Rating of rectifier and chopper switch (V)	Current Rating of rectifier and chopper switch (A)	Rating of Dump load (Ω)	Rating of DC filtering capacitor (μF)
Selected	900	15	84	380